Département de Chimie
Université de Fribourg (Suisse)

Modeling the properties of open d-shell molecules with a multi-determinantal DFT.

THESE

Présentée à la Faculté des Sciences de l'Université de Fribourg (Suisse)
pour l'obtention du grade de Doctor rerum naturalium

Cédrick RAUZY
de
TOULOUSE (FRANCE)

Thèse Nr. 1465

Atelier mécanographique, Université de Fribourg
2005

Acceptée par la Faculté des Sciences de l'Université de Fribourg (Suisse) sur la proposition des membres du jury suivant:

Prof. Thomas Bally, Président du jury, Université de Fribourg

Prof. Claude Auguste Daul, Directeur de thèse, Université de Fribourg
Prof. Jacques Weber, Université de Genève (Suisse)
Prof. Annick Goursot, Université de Montpellier (France)
Prof. Mihail Atanasov, Université de Sofia (Bulgarie)

Fribourg, le 23 mars 2005

Le directeur de thèse:
Prof. Claude Auguste Daul

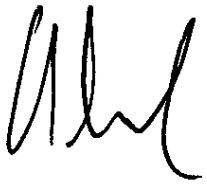

Le Doyen:
Prof. Marco Celio

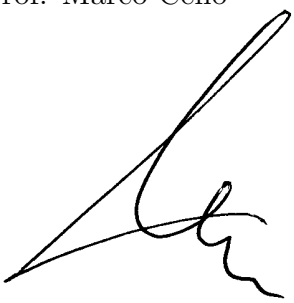

Ce travail a été soutenu par le Fond National Suisse
pour la Recherche Scientifique.

Acknowledgements

This work was accomplished under the direction of Prof. Dr. Claude A. Daul at the Departement of Chemistry of the University of Fribourg, from April 2001 until December 2004. I would like to express my sincere gratitude to him, firstly for accepting me in his research group and also for his support and invaluable guidance throughout this work.

I wish to thank Prof. Dr. Mihail Atanasov, Prof. Dr. Annick Goursot and Prof. Dr. Jacques Weber for accepting to evaluate my thesis and to be members of the jury.

I would like also to thank the president of the jury: Prof. Dr. Thomas Bally.

I would like to thank again Prof. Dr. Mihail Atanasov for the long and nice scientific discussions we had.

I would like to thank Prof. Dr. Carl-Wilhelm Schläpfer and Prof. Dr. Svetozar Niketic for the interesting dicussions and the good advices they gave during the weekly seminars.

I thank Prof. Dr. Franzpeter Emmenegger, Prof. Dr. Peter Belser and Prof. Dr. Thomas Bally for the nice challenges they proposed me in web design.

I would like to thank all my colleagues: Fabio, Valéry, Pio, Mohamed, Sahnoun, Tamil, Emmanuel.

To all the institute staff, a big thank you! And in particular to: Emerith, Hubert, Michel and Philippe.

J'aimerais aussi dédier ce travail à toute ma famille, mes parents : Danièle et Gérard, mais aussi Jacques, Patricia, Régis, Aurélia, Franck et Geoffray.

And of course, last but not least, I want to thank Cris, the best colleague I had in and outside the institute.

Abstract

Ligand field theory has been used along decades with success to describe ground and excited electronic states originating from d^n transition metals complexes. Experimental chemists use such a theory to interpret spectra. On the opposite side, computational chemists can describe with good accuracy the ground states properties but models to calculate excited states properties are still being developed. The Ligand Field -Density Functional Theory, which is the method presented in this thesis, proposes a link between the density functional theory applied to ground state and the determination of excited states properties through the ligand field theory. To achieve this, we compute within the DFT formalism the energies of all the Slater determinants originating of a d^n configuration taken as reference an average of configuration to satisfy the requirement of the Ligand Field Theory. In a first step, the method is applied to well known compounds to test the ligand field and Racah's parameterization in comparison to values fitted from experimental UV-Vis spectra. Then we use a Ligand field program to predict the multiplet structure. Next, extension of the method is proposed to determine ESR parameters and relativistic effect within the same formalism.

At each step, the results are compared to data which are well known for many decades by the chemists. We will also show the ability of the method to give more informations than usually expected.

Résumé

La théorie du champ des ligands a été utilisée avec succès durant des décennies pour décrire l'état fondamental et les états excités des complexes. Les chimistes utilisent cette théorie afin d'interpréter des spectres UV-Vis essentiellement. D'un autre côté, les chimistes computationels peuvent décrire assez précisément les propriétés correspondant à l'état fondamental mais les modèles permettant de décrire les propriétés des états excités sont encore en voix de développement. La méthode "Champ des Ligands - Théorie de la Fonctionnelle de la Densité", qui est la méthode présentée dans cette thèse, propose un lien entre la Théorie de la Fonctionnelle de la Densité (TFD) appliquée à l'état fondamental et la modélisation des propriétés des états excités par l'intermédiaire de la théorie du champ des ligands. Pour ce faire, nous calculons grâce à la TFD les énergies de tous les déterminants de Slater due à une configuration d^n en référence a un état correspondant à une configuration moyenne (répartition égale des électrons d dans les 5 orbitales moléculaires correspondant aux orbitales d de l'élément de transition) afin de satisfaire aux exigences de la théorie du champ des ligands. Dans un premier temps, la méthode est appliquée à des composés connus afin de tester sa validité. Dans un deuxième temps, le champ d'application de la méthode est étendue à la modélisation des tenseurs g et A. Tout au long de cette thèse, les résultats obtenus sont comparés aux données expérimentales obtenues par les chimistes. Nous montrons aussi que la méthode donne plus d'informations que l'on ne pouvait espérer, en particuliers, lors du traitement des effets relativistes.

Contents

List of Figures

List of Tables

Useful notations

Orbitals labels:
ε: $d_{x^2-y^2}$, θ: d_{z^2} , ξ: d_{yz} , η: d_{xz} , ζ: d_{xy}

1 eV = 8066 cm^{-1}

ADF: Amsterdam Density Functional

AO: Atomic Orbital

AOC: Average Of Configuration

AOM: Angular Overlap Model

CF's: Core Functions

CFT: Crystal Field Theory

CI: Configuration Interaction

DF: Density Functional

DFT: Density Functional Theory

EPR: Electron Paramagnetic Resonance

GGA: Generalized Gradient Approximation

HF: Hartree-Fock

HK: Hohenberg-Kohn

irrep: irreducible representation

JT: Jahn-Teller

KS: Kohn-Sham

LDA: Local Density Approximation

LF: Ligand Field

LFDFT: Ligand Field - Density Functional Theory

LFT: Ligand Field Theory

MCD: Magnetic Circular Dichroism

MO: Molecular Orbital

SCF: Self Consistent Field

SD: Slater Determinant

SFO: Symmetrized Fragment Orbitals

SOC: Spin-Orbit Coupling

TD-DFT: Time Dependent - Density Functional Theory

TF: Thomas-Fermi

TFD: Thomas-Fermi-Dirac

TM: Transition Metal

TZP: Triple-ζ STO basis sets plus one polarization function

ZORA: Zero-Order Regular Approximation

Chapter 1

General Introduction

This thesis is about:
Modeling the properties of open *d*-shell molecules with multi-determinantal DFT
where **Modeling** means to propose a model that can explain experimental data with the aim to describe and predict properties of molecular systems. In this thesis I restrict the investigation to **open *d*-shell molecules**, i.e. essentially to complexes with an open *d*-shell transition metal. The model proposed is based on **multi-determinantal DFT** calculation which means that we calculate the energies of Slater determinants (SD) within the Density Functional Theory (DFT) formalism. Finally, these energies are used in a Ligand Field (LF) approach to parameterize the LF matrix and the Racah's parameters. So the main objective of this thesis is to describe the model called LFDFT for Ligand Field - Density Functional Theory.

Why LFT?

The Ligand Field Theory (LFT) has been and still is a useful theory for interpreting optical and magnetic properties of TM complexes. The predominantly ionic picture, based on metal ions perturbed by surrounding ligands provides an adequate description of the optical $d-d$ transition, paramagnetism, magnetic interactions and electronic spin resonance (ESR). LFT is an empirical approach gaining its parameters by comparison with existing experimental data and its justification lies in its ability to reproduce these data. Hence LF approach is a method for interpreting rather than a method for predicting electronic phenomena in TM complexes. The demand for a predictive theory in this respect is mostly tangible for systems, like active sites of enzymes for which no structural and spectroscopic data are known. The need for a model which is *parameter free* on one side but compatible with the usual ligand field formalism on the other side becomes increasingly pronounced in view of the new developments in bio-inorganic chemistry.[1,2]

Why DFT?

On the other hand, in the computational chemistry field, Density Functional Theory is very popular. This popularity comes from the good balance between computational effort and accuracy of the results for both ground state[3] as well as excited states[4–7] properties.

Moreover, it has been shown in previous studies[8–11] that the multiplet theory of TM ions and complexes is compatible with the DFT formalism. In turn, recipes have been proposed (see[12–14]) to link DFT, in the form of SD energies, with the multiplets energies of Transition Metal (TM) ions or complexes.

Why combining DFT and LFT?

The work presented in this thesis can be considered as an extension of these previous works. Originally, the calculation of multiplet energies was based on a multi Slater determinants method approach: the wave function of the multiplet being expressed as a linear combination of Slater determinants. If we restrict our investigation to multiplet arising from an open *d*-shell system and if we use the symmetry,[11] it can be then proven that only a limited numbers of them (named non-redundant) are necessary to express the wave function of all multiplets considered. But we know that within, the Kohn-Sham (KS) formalism, the exchange-correlation term of the Hamiltonian is calculated in an approximated fashion so the spin-density exhibits a lower symmetry than the electronic Hamiltonian for an open shell system: the DFT symmetry dilemma.[15,16] One of the consequences is that SD's redundancy conditions are not verified within the DFT approach. A simple way to cure this problem (in an approximated fashion) is to consider all the SD's originating of an open *d*-shell and then reduce the error due to approximate exchange-correlation in a least square sense (more elaborated methods can be proposed: to use a better functional or to adopt the symmetrized Kohn-Sham approach[17] and its later developments[18]). Then comes the main idea of this work that is to introduce the LFT instead of expressing multiplets as linear combination of SD's as it was done previously.[11,12,19] In doing so we introduce the following approximations:

- the electrons of the valence shell of the TM ions don't interact with the electrons of the ligands, we just consider an electrostatic potential exerted by the ligands on them,

- the bi-electronic part of the Hamiltonian is not treated in agreement with the symmetry of the system but reduced to $\Re^3$ (for example: via symmetry rule we can reduce the number of bi-electronic integrals to 10 for 0_h symmetry, but within the LFT, their numbers is reduced to 2 like in the group of the sphere independently of the symmetry considered),

We can summarize the situation in saying that the mono-electronic part of the Hamiltonian in LFT respects the symmetry of the system whereas the bi-electronic part is treated like in the spherical group. One of the consequences of the introduction of LFT is that we can not treat systems which are too covalent or where Metal to Ligand Charge Transfer (MLCT) or Ligand to Metal Charge Transfer (LMCT) contribute with an appreciable weight to the ground state wavefunction.

Advantages and Inconveniences of the LFDFT method?

In bringing together the DFT and the LFT, we are taking advantages and inconveniences of both methods but nevertheless adding few advantages. The main advantage

lies in the fact that we are making a bridge between two communities: the experimentalists and the theoreticians because we convert DFT data in variables which are familiar to experimentalists. Moreover the values we get are directly comparable to experimental ones. The second main advantage is that we can get from DFT multiplets energies but we get more freedom from LFT by the fact we can modify the Hamiltonian to take into account other smaller perturbations like Spin-Orbit coupling, Zeeman effects and Hyperfine coupling to cite only the ones treated in this thesis. The other advantages come from the fact we can approach virtual systems, we have a model which is parameter free (non-empirical method). On the other side, there is no real inconvenience but we have to be aware that we are doing some approximations. These approximations don't come from the fact we associate DFT and LFT but are intrinsic to each method. From DFT, the approximation is due to the fact that exchange-correlation is not calculated exactly: the consequences are that kinetic term and bi-electronic term are approximated and that the self-interaction is not null. From LFT, the approximations are due to the fact that bi-electronic integrals are considered like in a spherical symmetry and to the fact that we neglect some contributions of the ligands.

This thesis presents the LFDFT method: a general theory applied to transition metal (TM) complexes which is based on DFT calculations of the manifold of all Slater determinants (SD), originating from a given d^n configuration, to parameterize the ligand field parameters. The description of the theories (DFT and LFT) lying under this method are presented as well as the method by itself (including source code of the programs) and also the tools developed to help along the procedure.

The thesis is structured in the following way. The next chapter consists in an introduction to the theories lying under the LFDFT method; it is dedicated to the presentation of the Ligand Field Theory and to the presentation of the Density Functional Theory. In Chapter 3, a full description of the LFDFT is proposed including: the procedure to run the DFT calculations and extract the data from the output files, all the details of the method, the source code of the LFDFT program, and at the end, the LFDFT method is applied to some examples and compared to values fitted from experimental spectra. Chapter 4 is dedicated to the determination of the multiplet structure once the ligand field matrix and the Racah's parameters are determined by LFDFT. And in Chapter 5, the introduction of relativistic effects in LFDFT is proposed. In Chapter 6, we applied the LFDFT method to calculate the g- and A-tensors to a complex with a Schiff base which is particularly interesting because its ESR parameters present a large anisotropy. In order to test the LFDFT method on this particular aspect, the values are compared with experiments and with values obtaind by other models implemented in the DFT program used. Finally conclusions are summarized in the last chapter along with an outlook for further extensions of the LFDFT model.

Chapter 2

Theoretical Concepts

This chapter gives an introduction to the two theories which are at the basis of the LFDFT method. We can distinguish two parts. Firstly, an introduction to ligand field theory (LFT) is presented over the Crystal Field Theory (CFT[a])[20–23] and the Angular Overlap Model (AOM).[24,25] All the demonstrations are given for a d^n configuration as this work treats only complexes with open d-shell, but has been extended to compounds with open f-shell.[26–28] Secondly, a description of the Density Functional Theory (DFT) is also presented in this chapter.

2.1 The Crystal Field Theory

Within the Crystal Field Theory we treat inorganic complex as an "ionic molecule" where the central atom, generally a transition metal (TM) cation, is subjected to a perturbation due to the surrounding ligands. The ligands can be considered as point charges (overlap between the ligands and the TM orbitals is neglected) which provides a constant electric field having the symmetry of the ligand nuclei arrangement. Thus the crystalline field leads to a lowering of the spherical symmetry of the free ion. Van Vleck,[29] working on the magnetism of complex salts, showed that the Mulliken method's[30] of molecular orbital gives a justification to the above point of view. The Hamiltonian of the system can be written as:

$$\mathscr{H} = \mathscr{H}_F + \mathscr{V} \tag{2.1}$$

where $\mathscr{H}_F$ is the Hamiltonian of the free ion and $\mathscr{V}$, the potential provided by the ligands. $\mathscr{V}$ is considered as a perturbation which influences the motions of the metal electrons. If we decompose the Hamiltonian, we can write it down in terms of various contributions:

$$\mathscr{H} = \underbrace{-\frac{\hbar^2}{2m}\sum_i \nabla_i^2}_{\hat{T}} \underbrace{-\sum_i \frac{Ze^2}{r_i}}_{\hat{V}_{Ne}} + \underbrace{\frac{1}{2}\sum_{i\neq j}\frac{e^2}{r_{ij}}}_{\hat{V}_{ee}} + \underbrace{\sum_i \zeta \cdot l_i \cdot s_i}_{\text{Spin-orbit coupling}} + \mathscr{V} \tag{2.2}$$

where i and j are indices for electrons in the d-shell, $\hat{T}$ represent the kinetic energy term, $\hat{V}_{Ne}$ the nuclear-electron attraction term, $\hat{V}_{ee}$ the inter-electronic repulsion term, Z is

[a] CFT is a particular case of LFT because we just take into account the electric field generated by the ligands and not the polarizability. Within the CFT, the effects of the second sphere of coordination are negligible according to the work of Bethe.

the effective nuclear charge of the TM cation and ζ the spin-orbit constant of the TM. The order of magnitude of $\mathscr{V}$ is different depending on the metal considered and we can distinguish the four following cases:

$$\begin{aligned}
&\zeta(r)l\cdot s < e^2/r_{ij} \approx \mathscr{V} &&: \text{ complexes of the first- and second-transition series}\\
&\zeta(r)l\cdot s \approx e^2/r_{ij} \approx \mathscr{V} &&: \text{ complexes of third transition series}\\
&\mathscr{V} < \zeta(r)l\cdot s \lesssim e^2/r_{ij} &&: \text{ complexes of lanthanides}\\
&\mathscr{V} \approx \zeta(r)l\cdot s \lesssim e^2/r_{ij} &&: \text{ complexes of actinides}
\end{aligned}$$

If $\mathscr{V}$ is less important than the electronic repulsion, the case is called a "weak crystal field" otherwise it is called a "strong crystal field" case. If we focus on $3d$ TM, the spin-orbit coupling term of the Hamiltonian in Eq 2.2 can be neglected in a first approximation. Then to present the CFT in a didactic way, it is useful to consider the strong field case where the interelectronic repulsion ($\hat{V}_{ee}$) contribution is neglected and consider the TM cation as an hydrogen-like atom (one electron system).

2.1.1 A Single d-electron in a Cubic Field

The Hamiltonian of the free-ion with one single electron is equal to:

$$\mathscr{H}_0 = -\frac{\hbar^2}{2m}\nabla^2 - \frac{Ze^2}{r} \tag{2.3}$$

where Z is the effective nuclear charge. If we consider the free-ion (TM cation) surrounded by six ligands in an octahedral environment, the Hamiltonian is then $\mathscr{H} = \mathscr{H}_0 + \mathscr{V}$ with $\mathscr{V}$ being the electrostatic perturbation generated by the six ligands and defined by:

$$\mathscr{V} = -e\int \frac{\rho(R)}{|\vec{R}-\vec{r}|}dR \tag{2.4}$$

where $\vec{R}$ and $\vec{r}$ are defined according to Figure 2.1.

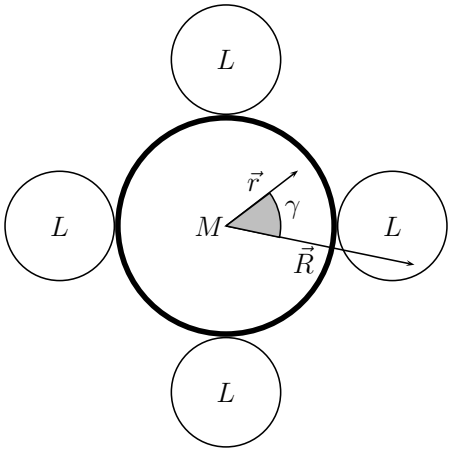

Figure 2.1: *The Metal surrounded by the 4 ligands in the plane.*

2.1.1.1 Expansion of $\mathscr{V}$

The potential $\mathscr{V}$ is expanded in terms of Legendre polynomials (*cf.* Appendix A.1) and reads as Equation 2.5 where $r_<$ and $r_>$ are respectively r and R the metal to ligand distance[b]. ω_i is the angle between $\vec{R}_i$ and $\vec{r}$ where i runs over the point charges.

$$\mathscr{V}_i(r) = \int \rho(R)\sum_k^{\infty}\frac{1}{R}\left(\frac{r}{R}\right)^k P_k(\cos\omega_i)dR \tag{2.5}$$

To proceed, we have to expand $P_k(\cos\omega_i)$ using the spherical harmonic addition theorem (*cf.* Appendix A.3). Moreover it is inconvenient to have complex quantities occurring in

[b]Here we have to make the statement that the electrons of the ions are passive, it means that the energies associated with the electrons of the ligands are low enough compared to the energy of the d-electron of the cations so their role is just to produce a shielding effect of the ligand nuclear charge.

the potential and so we have to replace the complex spherical harmonic, Y_{lm}, by the set of real quantities as it is explained in Appendix A.2. So the spherical harmonic addition theorem reads:

$$P_k(\cos\omega_i) = \left[\frac{4\pi}{2k+1}\right] \sum_{m=-k}^{k} y_{km}(\theta\varphi) y_{km}(\theta_i\varphi_i) \tag{2.6}$$

where $y_{km}(\theta\varphi)$'s are real spherical harmonics and $(r, \theta\varphi)$ and $(a, \theta_i\varphi_i)$ are the polar coordinates of $\vec{r}$ and $\vec{R}_i$, respectively. From Equations 2.5 & 2.6, $\mathscr{V}_i$ (for one point charge) reads:

$$\mathscr{V}_i(r) = \sum_{k=0}^{\infty} \sum_{q=-k}^{k} \frac{-e4\pi}{2k+1} \langle r^k \rangle \int \frac{\rho(R)}{R^{k+1}} y_{kq}(\theta\varphi) y_{kq}(\theta_i\varphi_i) dR \tag{2.7}$$

As we can see we have a summation over k from 0 to ∞. But there is no need to investigate a value of k higher than $2l$, since the integrals with $k > 2l$ of the product of two spherical harmonics of order l must vanish. In the same way, it is not required to calculate the integrals for the odd values of k as a plane of symmetry containing the z-axis is present so the terms cancel. Equation 2.7 can be written as:

$$\mathscr{V}(r) = \sum_{i} \sum_{k=0}^{2l} \sum_{q=-k}^{k} \frac{-e4\pi}{2k+1} \langle r^k \rangle \int \frac{\rho(R)}{R^{k+1}} y_{kq}(\theta\varphi) y_{kq}(\theta_i\varphi_i) dR \tag{2.8}$$

This equation can be generalized by:

$$\mathscr{V}(r) = \sum_{k=0}^{2l} \sum_{q=-k}^{k} h_{kq} y_{kq}(\theta\varphi) \tag{2.9}$$

where h_{kq} is defined by:

$$\begin{aligned} h_{kq} &= -\frac{4\pi e}{2k+1} \langle r^k \rangle \sum_i \int \frac{\rho(R) y_{kq}(\theta_i\varphi_i)}{R^{k+1}} \\ &= \sum_i \sum_{m,m'} (-1)^m (2k+1) \begin{pmatrix} l & l & k \\ -m & m' & q \end{pmatrix} \langle lm|\mathscr{V}|lm'\rangle \end{aligned} \tag{2.10}$$

where $\begin{pmatrix} j_1 & j_2 & j_3 \\ m_1 & m_2 & m_3 \end{pmatrix}$ represents the $3j$-Wigner's symbol (*cf.* Appendix A.4).

2.1.1.2 Evaluation of the Ligand Field Splitting for O_h

As an example, we can consider in a rough approximation ligands as point charges which create an electric field around the central atom (which is a good approximation because d-orbitals of a TM are well contracted around the TM and the mixing with ligands orbitals is small), so equation 2.4 reads if we consider an octahedral environment:

$$\mathscr{V} = \sum_{i=1}^{6} \frac{q_i e}{|\vec{R}_i - \vec{r}|} \tag{2.11}$$

where $\vec{r}$ and $\vec{R}_i$ are respectively the electron position vector and the position vector of the i^{th} point charge (the norm of the $\vec{R}_i$ being equal to a). Equations 2.11 & 2.4 are equivalent since we express $\rho(\vec{R})$ as: $\rho(\vec{R}) = \sum_L q_L \delta(\vec{R} - \vec{R_L})$ where L is an index for the ligands and q_L is the corresponding charge. To determine the ligand field matrix for a cation in an octahedral environment, we solve Equation 2.12 which is equivalent to Equation 2.8:

$$\mathscr{V}(r) = \sum_{i=1}^{6} Ze \sum_{k=0}^{2l} \sum_{q=-k}^{k} \frac{4\pi}{2k+1} \langle r^k \rangle \frac{1}{a^{k+1}} y_{kq}(\theta\varphi) y_{kq}(\theta_i \varphi_i) \tag{2.12}$$

As we are concerned by $3d$-electron ($n = 3$ and $l = 2$), we have to make a sum over $k = \{0, 2, 4\}$. Starting with $k = 0$, the real spherical harmonic y_{00} is well known and is equal to:

$$y_{00} = 2^{-1/2}(2\pi)^{-1/2} \tag{2.13}$$

So the potential $\mathscr{V}_{(i;x,y,z)}$ from $k = 0$ is equal to:

$$\mathscr{V}_{i,k=0} = \frac{Ze}{a} \times (2^{-1/2}(2\pi)^{-1/2})^2 \times \frac{4\pi}{2 \times 0 + 1} = \frac{Ze}{a} \tag{2.14}$$

Since there are six ligands around the central atom, $\mathscr{V}_{(x,y,z)}$ from $k = 0$ is equal to $6Ze/a$. In the same way, the term for $k = 2$ is equal to 0 and the term for $k = 4$ gives:

$$\mathscr{V}_{i,k=4} = \frac{7}{3} \times \sqrt{\pi} \times \left(\frac{Ze\overline{r^4}}{a^5} \right) \left[Y_4^0 + \sqrt{\frac{5}{14}} (Y_4^4 + Y_4^{-4}) \right] \tag{2.15}$$

So the potential $\mathscr{V}$ due to the ligand is equal to the sum: $\mathscr{V}_{k=0} + \mathscr{V}_{k=4}$. To evaluate the energy shift on the orbital due to the ligand field, we have to evaluate the following integrals:

$$\langle \Psi_{nlm} | \mathscr{V} | \Psi_{nlm'} \rangle \tag{2.16}$$

For $\mathscr{V}_{k=0}$ we can write:

$$\begin{aligned} \Delta E = \int \Psi^*_{nlm} (e \times 6Ze/a) \Psi_{nlm'} = 6Ze^2/a \int \Psi^*_{nlm} \Psi_{nlm'} \\ = \begin{cases} 6Ze^2/a & \text{if } m = m' \\ 0 & \text{if } m \neq m' \end{cases} \end{aligned} \tag{2.17}$$

So the energy shift due to $\mathscr{V}_{k=0}$ is independent of the angular momentum of the orbital considered and is equal to: $6Ze^2/a$ (*cf.* Figure 2.2). Doing the same for $\mathscr{V}_{k=4}$, we find the matrix elements equal to:

$$\begin{aligned} \langle \varphi_{nd+2} | e \times \mathscr{V}_{k=4} | \varphi_{nd+2} \rangle &= -4Dq \\ \langle \varphi_{nd-2} | e \times \mathscr{V}_{k=4} | \varphi_{nd-2} \rangle &= 6Dq \\ \langle \varphi_{nd\pm1} | e \times \mathscr{V}_{k=4} | \varphi_{nd\pm1} \rangle &= -4Dq \\ \langle \varphi_{nd0} | e \times \mathscr{V}_{k=4} | \varphi_{nd0} \rangle &= 6Dq \end{aligned} \tag{2.18}$$

where:

$$D = \frac{35Ze^2}{4a^5} \quad \text{and} \quad \mathrm{q} = \frac{2}{105} \langle \mathrm{r}^4 \rangle_{\mathrm{nd}} \tag{2.19}$$

and:

$$\langle r^k \rangle_{nd} = \int dr\, r^{2+k} |R_{nd}(r)|^2 \tag{2.20}$$

We can notice that D depends on the ligands positions and q reflects the properties of the central ion electrons. Now, the perturbed energies of the electrons are given the following secular matrix which is arranged by $m = -2, -1, 0, 1, 2$:

$$\begin{array}{c|ccccc|} xy & \varepsilon_3^0 - 4Dq - \varepsilon & 0 & 0 & 0 & 0 \\ yz & 0 & \varepsilon_3^0 - 4Dq - \varepsilon & 0 & 0 & 0 \\ z^2 & 0 & 0 & \varepsilon_3^0 + 6Dq - \varepsilon & 0 & 0 \\ xz & 0 & 0 & 0 & \varepsilon_3^0 - 4Dq - \varepsilon & 0 \\ x^2 - y^2 & 0 & 0 & 0 & 0 & \varepsilon_3^0 + 6Dq - \varepsilon \\ \end{array} = 0 \tag{2.21}$$

This system has two roots which can be easily determined, the five degenerate orbitals splits into one doubly and one triply degenerate level having for energy ε_{e_g} and $\varepsilon_{t_{2g}}$ defined by:

$$\varepsilon_{e_g} = \varepsilon_3^0 + 6Dq \quad \varepsilon_{t_{2g}} = \varepsilon_3^0 - 4Dq \tag{2.22}$$

We can see from Figure 2.2 that the first term is just elevating the energies of all d-orbitals and the other ones are symmetry dependent; they split the 5 d-orbitals in two levels where $10Dq$ is the amount of energy separating them. But for TM with more than one d-electron, neglecting the interelectronic repulsion, except for a didactic purpose, is not a realistic model.

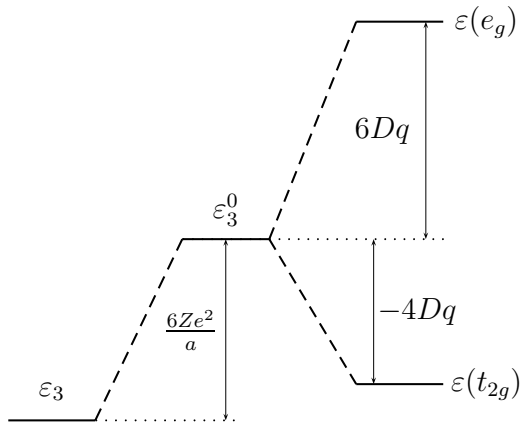

Figure 2.2: *Scheme of the crystal field splitting in an octahedral environment*

2.1.2 Two electrons in a Cubic Field

Neglecting spin-orbit coupling, the Hamiltonian of a system with two d-electrons can be written as:

$$\mathscr{H} = f_1 + f_2 + g_{12} \tag{2.23}$$

where:

$$f_i = -\frac{1}{2}\Delta_i - \frac{Ze^2}{r_i} + \mathscr{V}(r_i) \qquad (\mathrm{i} \in \{1, 2\}) \tag{2.24}$$

is the one-electron operator acting on the i^{th} electron and g_{12}:

$$g_{12} = 1/r_{12} \tag{2.25}$$

is the two-electron operator representing the Coulomb interaction between electrons 1 and 2. It is to note that we can use the same development than in Section 2.1.1.1 to find the matrix elements of g_{12} and a program to determine the matrix elements is presented in Section C.2.1. With the Hamiltonian given in Eq 2.23, the Schrödinger equation is written as:

$$\mathscr{H}\Psi(r_1\sigma_1, r_2\sigma_2) = E\Psi(r_1\sigma_1, r_2\sigma_2) \tag{2.26}$$

where r_i and σ_i are respectively the position and the spin (α or β) of the i^{th} electron. The Hamiltonian can be split into two terms:

$$\mathscr{H} = \mathscr{H}_0 + \mathscr{H}_1 \tag{2.27}$$

where $\mathscr{H}_0$ is the one-electron Hamiltonian ($f_1 + f_2$) and $\mathscr{H}_1$ is the interelectronic repulsion (g_{12}). The eigenfunctions and the eigenvalues of $\mathscr{H}_0$ are already known:

$$\mathscr{H}_0\Psi_0(r_1\sigma_1, r_2\sigma_2) = E_0\Psi_0(r_1\sigma_1, r_2\sigma_2) \tag{2.28}$$

separating f_1 and f_2 and looking for the eigenvalues of the one-electron operator which can be written in a general equation:

$$\varepsilon_k = \langle\chi_k|f|\chi_k\rangle \tag{2.29}$$

where f is a spinless operator and $\chi_k(r\sigma)$ is the product of an orbital function and a spin-function called *spin-orbital*. Then if we define:

$$\Psi_{0kl}(r_1\sigma_1, r_2\sigma_2) = \chi_k(r_1\sigma_1)\chi_l(r_2\sigma_2) \tag{2.30}$$

the energy E_{0kl} is equal to:

$$E_{0kl} = \varepsilon_k + \varepsilon_l \tag{2.31}$$

According to the Pauli principle, wavefunctions for electrons should be antisymmetric with respect to the exchange of electrons. To obey to the antisymmetric condition, the wavefunction can be written as a Slater determinant:

$$\begin{aligned}\Psi_{0kl}(r_1\sigma_1, r_2\sigma_2) &= \frac{1}{\sqrt{2}}\begin{vmatrix}\chi_k(r_1\sigma_1) & \chi_l(r_1\sigma_1)\\ \chi_k(r_2\sigma_2) & \chi_l(r_2\sigma_2)\end{vmatrix}\\ &\equiv |\chi_k\chi_l|\end{aligned} \tag{2.32}$$

If we now consider two electrons confined into the t_{2g} orbitals, there are 15 possibilities to distribute these two electrons over the 6 spin-orbitals. Here we know that orbitals are degenerate so we can conclude that the one electron operator gives the same results for:

$$\langle\zeta|f|\zeta\rangle = \langle\eta|f|\eta\rangle = \langle\xi|f|\xi\rangle = \varepsilon_{t_{2g}} \tag{2.33}$$

The expectation values of the integrals defined in Eq 2.33 are given within the LFDFT method by the energies of the Kohn-Sham orbitals for an Average Of Configuration (AOC) calculation (the calculation details are reported in section 3.1.3). As long as we neglect the coulomb interactions, the fifteen μ-states have the same energies. This high degeneracy is partially removed by the introduction of the interelectronic repulsion. To account for this, we have to calculate the matrix elements of $\mathscr{H}_1$:

$$\sum_{\sigma_1\sigma_2}\int d\tau_1 d\tau_2 |\chi_{l_1m_1s_1}(1)\chi_{l_2m_2s_2}(2)|^* g_{12}|\chi_{l'_1m'_1s'_1}(1)\chi_{l'_2m'_2s'_2}(2)| \tag{2.34}$$

for the chosen example l_i represents the t_{2g} orbitals, m_i its component and s_i the spin function. After the expansion of the single determinants, we get the expression:

$$\langle\chi_{l_1m_1s_1}(1)\chi_{l_2m_2s_2}(2)|g_{12}|\chi_{l'_1m'_1s'_1}(1)\chi_{l'_2m'_2s'_2}(2)\rangle - \langle\chi_{l_1m_1s_1}(1)\chi_{l_2m_2s_2}(2)|g_{12}|\chi_{l'_2m'_2s'_2}(1)\chi_{l'_1m'_1s'_1}(2)\rangle \tag{2.35}$$

Since g_{12} is independent from the spin coordinate, this equation can be expressed in terms of orbital functions $\phi_{lm}(r)$ rather than spin-orbital functions $\chi_{lms}(r\sigma) = \phi_{lm}(r)\theta_{\frac{1}{2}s}(\sigma)$:

$$\begin{aligned}\langle\chi_{l_1m_1s_1}(1)\chi_{l_2m_2s_2}(2)|g_{12}|\chi_{l'_1m'_1s'_1}(1)\chi_{l'_2m'_2s'_2}(2)\rangle \\ = \delta(s_1s'_1)\delta(s_2s'_2)\langle\phi_{l_1m_1}(1)\phi_{l_2m_2}(2)|g_{12}|\phi_{l'_1m'_1}(1)\phi_{l'_2m'_2}(2)\rangle \\ = \delta(s_1s'_1)\delta(s_2s'_2)\langle\phi_{l_1m_1}(1)\phi_{l_2m_2}(2)|\phi_{l'_1m'_1}(1)\phi_{l'_2m'_2}(2)\rangle\end{aligned} \tag{2.36}$$

We use the following notation for the Coulomb integral:

$$\begin{aligned}J(\phi_{l_1m_1}\phi_{l_2m_2}) &= \langle\phi_{l_1m_1}(1)\phi_{l_2m_2}(2)|g_{12}|\phi_{l_1m_1}(1)\phi_{l_2m_2}(2)\rangle \\ &= \langle\phi_{l_1m_1}(1)\phi_{l_2m_2}(2)|\phi_{l_1m_1}(1)\phi_{l_2m_2}(2)\rangle \\ &= [\phi_{l_1m_1}(1)\phi_{l_1m_1}(1)|g_{12}|\phi_{l_2m_2}(2)\phi_{l_2m_2}(2)]\end{aligned} \tag{2.37}$$

and the following for the exchange integral:

$$\begin{aligned}K(\phi_{l_1m_1}\phi_{l_2m_2}) &= \langle\phi_{l_1m_1}(1)\phi_{l_2m_2}(2)|g_{12}|\phi_{l_2m_2}(1)\phi_{l_1m_1}(2)\rangle \\ &= \langle\phi_{l_1m_1}(1)\phi_{l_2m_2}(2)|\phi_{l_2m_2}(1)\phi_{l_1m_1}(2)\rangle \\ &= [\phi_{l_1m_1}(1)\phi_{l_2m_2}(1)|g_{12}|\phi_{l_1m_1}(2)\phi_{l_2m_2}(2)]\end{aligned} \tag{2.38}$$

Then the expression for the diagonal matrix element ($l_1 = l'_1$, $l_2 = l'_2$, $m_1 = m'_1$, $m_2 = m'_2$) of Eq 2.35 can be written as:

$$\begin{aligned}\sum_{\sigma_1\sigma_2}\int d\tau_1 d\tau_2|\chi_{l_1m_1s_1}(1)\chi_{l_2m_2s_2}(2)|^* g_{12}|\chi_{l_1m_1s_1}(1)\chi_{l_2m_2s_2}(2)| \\ = J(\phi_{l_1m_1}\phi_{l_2m_2}) - \delta(s_1s_2)K(\phi_{l_1m_1}\phi_{l_2m_2})\end{aligned} \tag{2.39}$$

2.1.3 Many Electrons in a Cubic Field

For the many electrons cases, the Hamiltonian of the Eq 2.23 can be generalized to:

$$\mathscr{H} = \sum_{i=1}^{n} f_i + \sum_{i>j}^{n} g_{ij} \tag{2.40}$$

then if we define the two wavefunctions Ψ and Ψ' by:

$$\begin{aligned}\Psi &= |\chi_{k_1}\chi_{k_2}\dots\chi_{k_n}| \\ \Psi' &= |\chi_{k'_1}\chi_{k'_2}\dots\chi_{k'_n}|\end{aligned} \tag{2.41}$$

We can calculate separately the matrix elements corresponding to the one-electron Hamiltonian:

$$\langle\Psi|\mathscr{H}_0|\Psi'\rangle = \sum_{i=1}^{N}\sum_{\sigma}\int d\tau|\chi_{k_1}\chi_{k_2}\dots\chi_{k_N}|^* f_i|\chi_{k'_1}\chi_{k'_2}\dots\chi_{k'_N}| \tag{2.42}$$

and the matrix elements corresponding to the two-electron Hamiltonian:

$$\langle\Psi|\mathscr{H}_1|\Psi'\rangle = \sum_{i>j=1}^{N}\sum_{\sigma}\int dt|\chi_{k_1}\chi_{k_2}\dots\chi_{k_n}|^* g|\chi_{k'_1}\chi_{k'_2}\dots\chi_{k'_n}| \tag{2.43}$$

Then if we use Laplace's expansion (*cf.* Appendix A.6), we can demonstrate the Slater's rules which are proposed in Appendix C.3.

2.1.4 Reduced Electrostatic Matrix Elements (Wigner-Eckart)

2.1.4.1 Slater-Condon Parameters

One way to reduce the number of two-electron integrals is to assume a simple angular dependence for the t_{2g} and e_g wavefunctions. As d-electrons in the crystal are relatively localized around the TM cation and the deformation of atomic d-orbitals is not preponderant, it is reasonable to assume, as first approximation, that the t_{2g} and e_g wavefunctions have pure d-characters and if we consider that the radial part is the same for all electrons occupying the d-orbitals, we can then express molecular orbital wavefunction as:

$$\phi_{dm}(r) = R_d(r)Y_{2m}(\theta\phi) \quad m \in \{2, 1, 0, -1, -2\} \tag{2.44}$$

where $Y_{2m}(\theta\phi)$ is a spherical harmonic (*cf.* Appendix A.2). Let us take a two electron integral:

$$\langle\phi_{dm_1}(1)\phi_{dm_2}(2)|\frac{1}{r_{12}}|\phi_{dm'_1}(1)\phi_{dm'_2}(2)\rangle \tag{2.45}$$

Then we can expand $1/r_{12}$ (*cf.* Appendix A.1) and using Eq 2.6:

$$\frac{1}{r_{12}} = \sum_{k=0}^{2l} \frac{r_<^k}{r_>^{k+1}} \left[\frac{4\pi}{2k+1}\right] \sum_{m=-k}^{k} (-1)^m Y_{km}(\theta_1, \phi_1) Y_{km}(\theta_2, \phi_2) \tag{2.46}$$

where (r_1, θ_1, ϕ_1) and (r_2, θ_2, ϕ_2) are the polar coordinates of the electrons 1 and 2 and where $r_<$ and $r_>$ are the lesser and the greater of r_1 and r_2 respectively.
If we use real spherical harmonics as we are concerned by real quantities, Eqs 2.45 & 2.46 read:

$$\begin{aligned}
&\langle\phi_{dm_1}(1)\phi_{dm_2}(2)|\frac{1}{r_{12}}|\phi_{dm'_1}(1)\phi_{dm'_2}(2)\rangle = [\phi_{dm_1}(1)\phi_{dm'_1}(1)|\frac{1}{r_{12}}|\phi_{dm_2}(2)\phi_{dm'_2}(2)] \\
&= \sum_{k=0}^{2l} \left[\frac{4\pi}{2k+1}\right] \sum_{m=-k}^{k} \iint y_{dm_1}(1) y_{dm_2}(2) y_{km}(1) y_{km}(2) y_{dm'_1}(1) y_{dm'_2}(2) d\tau_1 d\tau_2 \times F^k(dd) \\
&= \sum_{k=0}^{2l} \left[\frac{4\pi}{2k+1}\right] \sum_{m=-k}^{k} \int y_{dm_1}(1) y_{km}(1) y_{dm'_1}(1) d\tau_1 \times \int y_{dm_2}(2) y_{km}(2) y_{dm'_2}(2) d\tau_2 \times F^k(dd)
\end{aligned} \tag{2.47}$$

where (1), (2), $d\tau_1$ and $d\tau_2$ mean respectively (θ_1, ϕ_1), (θ_2, ϕ_2), $d\phi_1 d\theta_1 \sin\theta_1$ and $d\phi_2 d\theta_2 \sin\theta_2$ and where:

$$F^k(dd) = \int_0^\infty r_1^2\, dr_1 \int_0^\infty r_2^2\, dr_2\, R_d^2(r_1) R_d^2(r_2) \frac{r_<^k}{r_>^{k+1}} \tag{2.48}$$

To simplify Eq 2.47, we can use Clebsch-Gordan coefficients, $c^k_{m_1,m'_1}$ (*cf.* Appendix A.5), defined as:

$$c^k_{m_1,m'_1} = \int y_{lm_1} y_{km} y_{lm'_1} d\phi d\theta \sin\theta \tag{2.49}$$

Eq 2.47 reads:

$$\begin{aligned}
&\langle\phi_{dm_1}(1)\phi_{dm_2}(2)|\frac{1}{r_{12}}|\phi_{dm'_1}(1)\phi_{dm'_2}(2)\rangle \\
&= \sum_{k=0}^{2l}\sum_{m=-k}^{k}\frac{1}{2k+1}(-1)^k c^k_{m_1,m'_1}c^k_{m_2,m'_2}\times\delta(m+m'_1,m_1)\delta(-m+m'_2,m_2)\times F^k(dd) \\
&= \delta(m_1+m_2,m'_1+m'_2)(-1)^{m_1-m'_1}\sum_{k=0}^{2l}\frac{1}{2k+1}c^k_{m_1,m_2}\times c^k_{m'_1,m'_2}\times F^k(dd)
\end{aligned} \tag{2.50}$$

The Slater integrals or the Slater-Condon parameters, F_k, are often used and are defined as:

$$F_0 = F^0(dd), \qquad F_2 = \frac{1}{49}F^2(dd), \qquad F_4 = \frac{1}{441}F^4(dd) \tag{2.51}$$

2.1.4.2 Racah's Parameters

Another parameterization of the interelectronic repulsion parameters has been proposed by Racah. Eq 2.52 gives the expression of the A, B and C Racah's parameters in terms of the three Slater-Condon parameters:

$$A = F_0 - 49F_4, \quad B = F_2 - 5F_4, \quad C = 35F_4 \tag{2.52}$$

We notice that Racah's parameters are linked linearly to the Slater-Condon parameters so we can use the less physical but more commonly used Racah's parameters for our further studies.

$\langle\zeta\zeta\|\zeta\zeta\rangle$	=	$4B+3C+A$	$\langle\xi\xi\|\xi\xi\rangle$	=	$4B+3C+A$
$\langle\zeta\zeta\|\xi\xi\rangle$	=	$3B+C$	$\langle\xi\varepsilon\|\xi\varepsilon\rangle$	=	$-2B+C+A$
$\langle\zeta\eta\|\zeta\eta\rangle$	=	$-2B+C+A$	$\langle\xi\theta\|\eta\zeta\rangle$	=	$-2\sqrt{3}B$
$\langle\zeta\xi\|\zeta\xi\rangle$	=	$-2B+C+A$	$\langle\xi\theta\|\xi\varepsilon\rangle$	=	$2\sqrt{3}B$
$\langle\zeta\varepsilon\|\zeta\varepsilon\rangle$	=	$4B+C+A$	$\langle\xi\theta\|\xi\theta\rangle$	=	$2B+C+A$
$\langle\zeta\varepsilon\|\xi\eta\rangle$	=	$3B$	$\langle\varepsilon\varepsilon\|\zeta\zeta\rangle$	=	C
$\langle\zeta\theta\|\zeta\theta\rangle$	=	$-4B+C+A$	$\langle\varepsilon\varepsilon\|\eta\eta\rangle$	=	$3B+C$
$\langle\zeta\theta\|\xi\eta\rangle$	=	$\sqrt{3}B$	$\langle\varepsilon\varepsilon\|\xi\xi\rangle$	=	$3B+C$
$\langle\eta\eta\|\zeta\zeta\rangle$	=	$3B+C$	$\langle\varepsilon\varepsilon\|\varepsilon\varepsilon\rangle$	=	$4B+3C+A$
$\langle\eta\eta\|\eta\eta\rangle$	=	$4B+3C+A$	$\langle\varepsilon\theta\|\eta\eta\rangle$	=	$\sqrt{3}B$
$\langle\eta\xi\|\eta\xi\rangle$	=	$-2B+C+A$	$\langle\varepsilon\theta\|\xi\xi\rangle$	=	$-\sqrt{3}B$
$\langle\eta\varepsilon\|\zeta\xi\rangle$	=	$-3B$	$\langle\varepsilon\theta\|\varepsilon\theta\rangle$	=	$-4B+C+A$
$\langle\eta\varepsilon\|\eta\varepsilon\rangle$	=	$-2B+C+A$	$\langle\theta\theta\|\zeta\zeta\rangle$	=	$4B+C$
$\langle\eta\theta\|\zeta\xi\rangle$	=	$\sqrt{3}B$	$\langle\theta\theta\|\eta\eta\rangle$	=	$B+C$
$\langle\eta\theta\|\eta\varepsilon\rangle$	=	$-2\sqrt{3}B$	$\langle\theta\theta\|\xi\xi\rangle$	=	$B+C$
$\langle\eta\theta\|\eta\theta\rangle$	=	$2B+C+A$	$\langle\theta\theta\|\varepsilon\varepsilon\rangle$	=	$4B+C$
$\langle\xi\xi\|\eta\eta\rangle$	=	$3B+C$	$\langle\theta\theta\|\theta\theta\rangle$	=	$4B+3C+A$

Table 2.1: *The non-redundant interelectronic repulsion integrals express in function of the Racah's parameters A, B and C. The adopted notation is: $\langle a(1)b(2)|c(1)d(2)\rangle$.*

Moreover the main advantage of Racah's parameterization is that the differences in energy between multiplets having the same spin multiplicity are expressed only in term of B. The non-redundant interelectronic integrals in spherical symmetry can be expressed as a function of the three Racah's parameters. Table 2.1 gives the linear relation of each non-redundant interelectronic integral as a function of the three parameters. The Slater determinant energies can be easily calculated within the DFT formalism and for a d^2 configuration, we obtain from DFT calculation the 45 energies of all SD. Each of these energies can be expressed in terms of the Racah's parameters A, B and C. The result is an overdetermined system of linear equations which can be solved by least square fit. From those, only B and C can be obtained from the fit, the parameter A being responsible for a shift of all atomic multiplets by the same amount.

2.1.4.3 Griffith's Parameters

A more refined treatment of the two electron term of the Hamiltonian $\mathscr{H}$ is to use Griffith's parameterization.[31] In this case, the number of interelectronic repulsion parameters is not limited to three but to a series of ten since it refers to octahedral symmetry and to MO which includes ligand AO.
The result found by this approach are not given in this thesis but can be found in the article published in *Chem. Phys. Lett.*.[32] However, the details of the Criffith's parameterization are proposed for d-TM in an octahedral environment. If we consider the Eq 2.47, we see that the electrostatic interaction can be expressed a a sum of products of one electron function. In Eq 2.12, we can replace the real spherical harmonic, y_{km}, by linear combinations which are components of bases for irreducible representation:

$$G = \sum f_{i\Gamma M}(1) f_{i\Gamma M}(2) \tag{2.53}$$

where $f_{i\Gamma M}$ is a one electron function which forms the component M of a basis for the irrep Γ and parameter i labels different set of functions forming basis for the same irreducible representation Γ. So the two-electron integrals $\langle ab|G|cd\rangle$ reads:

$$\begin{aligned} \langle ab|G|cd\rangle &= \sum \langle ab|f_{i\Gamma M}(1) f_{i\Gamma M}(2)|cd\rangle \\ &= \sum \langle a|f_{i\Gamma M}(1)|c\rangle \langle b|f_{i\Gamma M}(2)|d\rangle \end{aligned} \tag{2.54}$$

and depends only on the matrix elements of the one electron operator $f_{i\Gamma M}$. If we replace $f_{i\Gamma M}$ by $g_{i\Gamma M}$ where $g_{i\Gamma M}$ has the same matrix elements as $f_{i\Gamma M}$ within the five e and t_2 functions of interest but is equal to zero between these functions and any others and, also, between any other functions. Then G reads:

$$G = \sum_{\kappa<\lambda} G(\kappa\lambda) = \sum_{i\Gamma M} \sum_{\kappa<\lambda} g_{i\Gamma M}(\kappa) g_{i\Gamma M}(\lambda) \tag{2.55}$$

with $g_{i\Gamma M}$ real and having their components correctly connected in phase.
A one electron integral $\langle a|g_{i\Gamma M}|c\rangle$ can only be non-zero if Γ occurs in the product of the representation Γ_1 and Γ_3 to which $|a\rangle$ and $|c\rangle$ belong or, if $\Gamma_1 = \Gamma_3$, to the symmetrized

square of Γ_1. So if we write:

$$\begin{aligned} G &= \sum_{\Gamma} \sum_{i} G_{i\Gamma}(\kappa\lambda) \\ \text{and} \quad G_{i\Gamma}(\kappa\lambda) &= \sum_{M} \sum_{\kappa<\lambda} g_{i\Gamma M}(\kappa) g_{i\Gamma M}(\lambda) \end{aligned} \tag{2.56}$$

The product of the two functions e and t_2 lead to a sum over four contribution for Γ, one from each irreducible representation A_1, E, T_1 and T_2. The derivation of this sum lead to the parameterization of the two-electron integrals in terms of the ten Griffith parameters. In Eq 2.57, the relations between the Racah's and the Griffith's parameters are given if instead of MO, we use pure d-functions:

$$\begin{aligned} a &= e = A + 4B + 3C \\ b &= d = A - 2B + C \\ c &= 2B\sqrt{3} \\ f &= 4B + C \\ g &= B + C \\ h &= i = B\sqrt{3} \\ j &= 3B + C \end{aligned} \tag{2.57}$$

2.1.5 Angular Overlap Model (AOM)

More than forty years ago, the developments of LFT by Jørgensen and Schaeffer[25] give rise to the Angular Overlap Model. In this model, the perturbation of the free ion takes into account the overlap between the metal and the ligands contrary to CFT. For a transition metal with open d-shell surrounded by an octahedral arrangement of ligands, we can distinguish the σ and the π bond (*cf.* Fig. 2.3): an example of σ bond is the overlap between the orbital d_{z^2} of the TM and the orbital p_z from the ligand, π bond is for example the overlap between the orbital d_{xz} of the TM and the p_x orbital from the ligand.
These two interactions can be modeled by two parameters e_σ and e_π. e_σ is generally positive because σ-bond has a strong destabilizing effect (for a given metal to ligand distance, the overlap between orbital of the ligand and orbital of the metal is larger for a σ-bond than for a π-bond) while e_π can be either positive if the ligand is π-donor or negative if the ligand is π-acceptor.

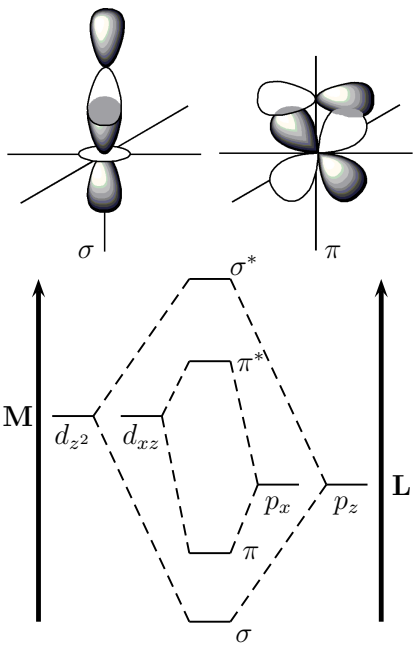

Figure 2.3: *Representation of a σ- and a π-bond and illustration of the resulting MO splitting.*

Ligand		Metal AO				
		d_{z^2}	$d_{x^2-y^2}$	d_{xz}	d_{yz}	d_{xy}
1	σ	1	0	0	0	0
	π	0	0	1	1	0
2	σ	1/4	3/4	0	0	0
	π	0	0	1	0	1
3	σ	1/4	3/4	0	0	0
	π	0	0	0	1	1
4	σ	1/4	3/4	0	0	0
	π	0	0	1	0	1
5	σ	1/4	3/4	0	0	0
	π	0	0	0	1	1
6	σ	1	0	0	0	0
	π	0	0	1	1	0
sum	σ	3	3	0	0	0
	π	0	0	4	4	4

Table 2.2: *Overlap contributions due to each ligand with the five d-orbitals of the TM.*

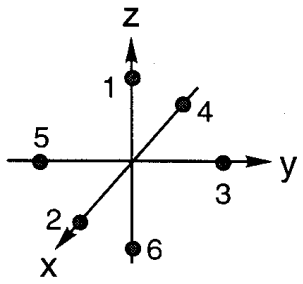

Figure 2.4: *Ligand positions for the demonstrative case.*

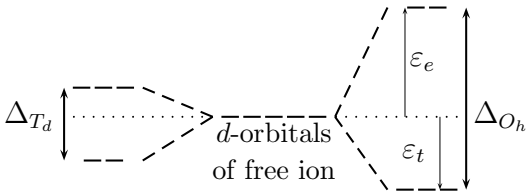

Figure 2.5: *Scheme of the AOM splitting in an octahedral and in a tetrahedral environment.*

Let us take as example an octahedral complex where the ligands are labelled as in the Figure 2.4. The contributions of each ligand to the σ and the π perturbations are listed in the Table 2.2. Then if we do the overall sum, the energy of the MO e_g and t_{2g} are then formulated as $\varepsilon_{e_g} = 3e_\sigma$ and $\varepsilon_{t_{2g}} = 4e_\pi$ leading to a diagonal h_{ab} matrix with $10Dq = 3e_\sigma - 4e_\pi$. The great advantage of using overlap arguments when we parameterize h_{ab} lies in the fact, that overlap energies may be expressed in terms of parameters e_σ and e_π which reflect the strength of the metal-ligand bond. The angular dependence is given by the rotational transformation properties of the d-orbitals since ligand-ligand interaction is neglected. The AOM matrix, h_{ab}, can be expressed in terms of angular factors and the e_σ and e_π parameters. Thus the model has ability to treat systems with little or no symmetry on an equal footing as the higher symmetric ones. Its drawback lies in the large number of model parameters to be determined from experiment for such systems, resulting in a complex parameterization.
We can make two remarks on the AOM theory.

1) Knowing that e_σ is bigger than e_π (in general 4 to 5 times, *cf.* MO diagram in Fig 2.3), the Figure 2.5 can also be explained in a qualitative way if we consider the nature of the bond in a complex, let say if the bond is composed by a σ-interaction or by a π-interaction. From the values of e_σ and e_π, we can say that the MO splitting in an octahedral environment is bigger than the MO splitting in a tetrahedral one.

2) From Table 2.2, we can remark that for each ligand, the sum over σ and the sum over π angular factors are respectively 1 and 2. We can link these numbers to the well known fact that a ligand is linked to the transition metal by one σ (usually p_z) and two π (p_x, p_y) bonds.

2.1.6 Spin-Orbit Coupling

Spin-orbit coupling is an essential constituent to the Hamiltonian for electronic states originating from d^n-configurations of transition metals in ligand fields (LF). It governs the fine structure of the electronic multiplets and, for the ground state it is mainly responsible for the zero-field splitting and the anisotropy affecting the spectroscopic and magnetic behavior of TM compounds with open d-shells.
The ligand field and the interelectronic repulsion dominate over the spin-orbit coupling in complexes of $3d$ transition metal series. This is the reason to neglect the latter thus far. However magnetism, EPR spectroscopy and hyperfine-coupling are largely affected by spin-orbit coupling. Moreover, for 2^{nd} and 3^{rd} row transition metals as well as for the f-elements even qualitative accounts of electronic absorption spectra cannot neglect spin-orbit effects. Similarly, for molecular orbitals calculations in which ligands play an important role, spin-orbit coupling due to ligands like e.g. iodide or bromide must be considered.
The nature and origin of spin-orbit coupling have been discussed in many places.[33] Misetich and Buch[34] have shown that the spin-orbit Hamiltonian of a molecule can be reasonably well approximated as

$$\mathscr{H}_{SO} = \sum_{N,i} \zeta_N \cdot \vec{l}_{i,N} \cdot \vec{s}_i = \sum_i \vec{u}_{i,N} \cdot \vec{s}_i \tag{2.58}$$

where ζ_N, the spin-orbit coupling constant of nucleus N, is incorporated into the molecular operator $\vec{u}_i$ for electron i.
In order to carry out a spin-orbit calculation it is necessary to relate the resultant splitting of many electron states and also the interaction of different states to one-electron spin-orbit coupling matrix elements. This can be done most conveniently in the basis of micro-states (single determinants) as shown in references[11,32,35] for the calculation of multiplets, using Slater's rules.

2.1.7 Qualitative Considerations of LFT

The use of LFT over decades led to the formulation of some general rules. Here, a brief introduction to two of them is presented: the notion of spectro-chemical series and the notion of nephelauxetic effect. In fact, to test our LFDFT method, we will compare quantitatively the values obtained to the ones fitted from experiments but also qualitatively to see if the evolution of the values respects this two rules.

2.1.7.1 The Spectro-chemical Series

Chemists remarked that if we consider one metal, the energy splitting between orbitals change in function of the ligands. Jørgensen[36] studied this effect and classified the ligands in order of their ability to cause orbital separations. This classification is called the spectro-chemical series and in Figure 2.6, a shortened list is given.

Weak Field $\Leftarrow$
$I^- < Br^- < SCN^- \sim Cl^- < F^- < OH^- \sim ONO^- < C2O_4^{2-} < H_2O$
$< NCS^- < EDTA^{4-} < NH_3 \sim$ pyr $\sim$ en $<$ bipy $<$ phen $< CN^- \sim CO$
$\Rightarrow$ **Strong Field**

Figure 2.6: *A shortened spectro-chemical series.*

The negatively charged ligands, such as $I^- < Br^- < Cl^- < F^-$, give rise to smaller $10Dq$ values than neutral molecules, like $H_2O < NH_3$ < pyridine, CN^- and CO being the strongest ligands due to their ability for back bonding (in AOM theory $10Dq = 3e_\sigma - 4e_\pi$, $e_{pi} < 0$).

2.1.7.2 The Nephelauxetic Effect

Using LFT theory many years ago, Schäffer and Jørgensen[37] discovered that the inter-electronic parameters B and C in complexes are smaller than those for the free ions. This phenomenon has been rationalized in terms of the electronic cloud expansion of the d-orbitals when going from free TM ions to complexes and has been called the **nephelauxetic effect**. The more reducing and softer ligands show a stronger reduction than the more oxidizing and harder ones. The nephelauxetic reduction factor is defined by the relation:

$$x_{B_{complex}} = \frac{B_{complex}}{B_0} \tag{2.59}$$

where B_0 is the value of B for the free ion, $B_{complex}$ the value of B for the complex considered and $x_{B_{complex}}$ the nephelauxetic reduction factor of B for the complex considered. Another way to see the nephelauxetic effect is that depending on the ligand, the complex becomes more covalent and the electrons are to some extent spread over the ligands so the d-orbitals are in some way large, we call it "cloud expansion". So the space at the electron disposal is bigger and the electron-electron repulsion is reduced.

2.2 DFT

The DFT which is well described in many text books[38–41] is the method we choose to determine the ligand field parameters. This choice is justified, based on the pragmatic observation, that DFT is computationally less intensive than other methods with similar accuracy. In this section, an introduction to DFT is reported. The main fact in DFT is that the energy of a molecule can be determined from the electron density instead of a wavefunction (Hohenberg and Kohn theorems). From the DFT calculations, in our LFDFT model, we will use the Kohn-Sham (KS) molecular orbitals (MO) to model the h_{ab} ligand field matrix and the energies of Slater determinants to fit the Racah's parameters.

2.2.1 Basic Theory

Within the Born-Oppenheimer approximation, we can separate the electronic Hamiltonian, $\mathscr{H}_{elec}$, from the nuclear part. For a N-electrons and M-nuclei system without

relativistic effects, $\mathscr{H}_{elec}$ is defined by:

$$\mathscr{H}_{elec} = -\frac{1}{2}\sum_{i=1}^{N}\nabla_i^2 + \sum_{i=1}^{N}\sum_{A=1}^{M}\frac{Z_A}{r_{iA}} + \sum_{i=1}^{N}\sum_{j>i}^{N}\frac{1}{r_{ij}} \tag{2.60}$$

or in a short hand notation:

$$\mathscr{H}_{elec} = \hat{T} + \hat{V}_{Ne} + \hat{V}_{ee} \tag{2.61}$$

$\hat{T}$, $\hat{V}_{Ne}$ and $\hat{V}_{ee}$ are the kinetic energy term, the electron-nuclear attraction term and the electron-electron repulsion term, respectively. The total energy of the system can be found by solving the following Schrödinger equation:

$$\mathscr{H}_{elec}\Psi_{elec} = E_{elec}\Psi_{elec} \iff E_{elec} = \langle\Phi_{elec}|\mathscr{H}_{elec}|\Phi_{elec}\rangle \tag{2.62}$$

and then adding the effect of the constant interatomic repulsion potential: $\hat{V}_{NN}$ ($\hat{V}_{NN}$ is constant due to the Born-Oppenheimer approximation):

$$E_{tot} = E_{elec} + E_{nuc} \tag{2.63}$$

where:

$$E_{nuc} = \sum_{A=1}^{M}\sum_{B>A}^{M}\frac{Z_A Z_B}{r_{AB}} \tag{2.64}$$

The attractive potential exerted by the nuclei on the electrons is often called the external potential, $\hat{V}_{ext}$, because it is not limited to the nuclear field but it may include some other perturbations like effects of magnetic or electric fields. The wavefunction Ψ is not an observable and a physical interpretation is relevant only if we consider the square of the wavefunction:

$$|\Psi(\vec{x_1}, \vec{x_2}, \ldots, \vec{x_N})|^2\, d\vec{x_1}\, d\vec{x_2} \ldots d\vec{x_N} \tag{2.65}$$

which represents the probability that electrons $1, 2, \ldots, N$ are found simultaneously in the volume elements $d\vec{x_1}\, d\vec{x_2} \ldots d\vec{x_N}$. As the electrons are indistinguishable, the following equality can be written:

$$|\Psi(\vec{x_1}, \vec{x_2}, \ldots, \vec{x_i}, \vec{x_j}, \ldots, \vec{x_N})|^2 = |\Psi(\vec{x_1}, \vec{x_2}, \ldots, \vec{x_j}, \vec{x_i}, \ldots, \vec{x_N})|^2 \tag{2.66}$$

Then the electronic density $\rho(\vec{r})$ is easily introduced as:

$$\rho(\vec{r}) = N\int\ldots\int|\Psi(\vec{r}_1, \vec{x}_2, \ldots, \vec{x}_N)|^2\, d\vec{s}_1\, d\vec{x}_2 \ldots d\vec{x}_N \tag{2.67}$$

where $\vec{r}_i = \{x_i, y_i, z_i\}$, $\vec{x}_i = \{x_i, y_i, z_i, s_i\}$ and $\rho(\vec{r})$ determines the probability to find one of the N-electrons within the volume element $d\vec{r_1}$ but with arbitrary spin while the others $N-1$ electrons have arbitrary positions and spin in the state represented by Ψ. We can then make the two following statements:

$$\lim_{r\to\infty}\rho(\vec{r}) = 0 \tag{2.68}$$

$$\int\rho(\vec{r})\, d\vec{r} = N \tag{2.69}$$

This notion of the electron density can then be extended to the notion of the pair density and instead to have the density of probability to find one electron with an arbitrary spin within a particular volume element while other electrons are anywhere, we deal with the probability to find a pair of electrons with spins σ_1 and σ_2 simultaneously within two volume elements $d\vec{r_1}$ and $d\vec{r_2}$. This quantity is defined by the Eq 2.70:

$$\begin{aligned}\rho_2(\vec{r}_1,\vec{r}_2) &= \rho_2(\vec{r}_1\vec{r}_2,\vec{r}_1\vec{r}_2)\\ &= \frac{N(N-1)}{2}\int\dots\int|\Psi(\vec{r}_1\vec{s}_1,\vec{r}_2\vec{s}_2,\vec{x}_3,\dots,\vec{x}_N)|^2 d\vec{s}_1 d\vec{s}_2 d\vec{x}_3\dots d\vec{x}_N\end{aligned} \tag{2.70}$$

It should be easily calculated if the electrons cannot interact with themselves, but the electrons are charged and the movement of one is correlated with the movements of the others. Then $\rho_2(\vec{x_1},\vec{x_2})$ contains electron correlation. To describe ρ_2, we have to introduce the reduced density matrix γ_2:

$$\gamma_2(\vec{r}_1\vec{r}_2,\vec{r_1}'\vec{r_2}') = N(N-1)\int\dots\int\Psi(\vec{r}_1\vec{s}_1,\vec{r}_2\vec{s}_2,\vec{x}_3,\dots,\vec{x}_N)\Psi(\vec{r_1}'\vec{s}_1,\vec{r_2}'\vec{s}_2,\vec{x}_3,\dots,\vec{x}_N)d\vec{x_3}\dots d\vec{x_N} \tag{2.71}$$

γ_2 is called the second order density matrix. The first order density matrix can be defined in the same way as:

$$\gamma_1(\vec{r}_1,\vec{r_1}') = N\int\dots\int\Psi(\vec{r}_1\vec{s}_1,\vec{x}_2,\dots,\vec{x}_N)\Psi(\vec{r_1}'\vec{s}_1,\vec{x}_2,\dots,\vec{x}_N)d\vec{x}_2\dots d\vec{x}_N \tag{2.72}$$

If we consider in Eq 2.70 the case where $\vec{r}_1 = \vec{r}_2$ then:

$$\rho_2(\vec{r}_1,\vec{r}_1) = -\rho_2(\vec{r}_1,\vec{r}_1) \tag{2.73}$$

This means that the quantity previously defined is 0, this implies that the probability to find two electrons at the same place vanishies according to the Pauli's principle.
If we integrate upon the spin component, we thus get the density $\rho(r)$ whose eigenvectors are called *natural orbitals*.
All the interactions described by the Hamiltonian are either one- or two-particle interactions. Therefore just 1^{st} and 2^{nd} order density matrices (often called *geminal functions*) are necessary to describe a system of N interacting electrons. An equivalent formulation of the Hamiltonian of Eq 2.60 in term of density matrices is:

$$\langle\Psi|\mathscr{H}|\Psi\rangle = \int\left[-\frac{1}{2}\nabla_1^2\rho_1(r_1,r_2)\right]_{r_1=r_2}dr_1 + \int V_{ext}\rho(r)dr + \int\frac{1}{r_{12}}\rho_2(r_1,r_2)dr_1dr_2 \tag{2.74}$$

where:

$$\begin{aligned}\rho_1(\vec{r_1}',\vec{r}_1) &= N\int\dots\int\Psi^*(\vec{r_1}'\vec{s}_1,\vec{x}_2,\dots,\vec{x}_N)\Psi(\vec{r}_1\vec{s}_1,\vec{x}_2,\dots,\vec{x}_N)d\sigma_1 d\vec{x}_2\dots d\vec{x}_N\\ \rho_2(\vec{r}_1,\vec{r}_2) &= \frac{N(N-1)}{2}\int\dots\int|\phi(\vec{r}_1\vec{s}_1,\vec{r}_2\vec{s}_2,\vec{x}_3,\dots,\vec{x}_N)|^2 d\vec{s}_1 d\vec{s}_2 d\vec{x}_3\dots d\vec{x}_N\end{aligned} \tag{2.75}$$

Thomas and Fermi were the first to use the density as a variable to describe the ground state with the Thomas-Fermi model.

2.2.2 The Thomas-Fermi Model

Thomas and Fermi,[42–44] before the development of the DFT due to Hohenberg and Kohn,[45] introduced a model close to density functional formalism where the energy is expressed in function of ρ:

$$E[\rho] = \langle\phi|\hat{H}|\phi\rangle = \int \rho(r)V(r)\,dr + T[\rho] + V_{ee}[\rho] \tag{2.76}$$

and they proposed to substitute the kinetic energy function with the one derived for a uniform electron gas T_{TF}:

$$T_{TF}[\rho(\vec{r})] = \frac{3}{10}(3\pi^2)^{2/3}\int \rho^{5/3}(\vec{r})d\vec{r} \tag{2.77}$$

while solving the two other terms in a classical way so Eq 2.76 reads:

$$E_{TF}[\rho(\vec{r})] = \frac{3}{10}(3\pi^2)^{2/3}\int \rho^{5/3}(\vec{r})d\vec{r} - Z\int \frac{\rho(\vec{r})}{r}d\vec{r} + \frac{1}{2}\iint \frac{\rho(\vec{r_1})\rho(\vec{r_2})}{r_{12}}d\vec{r_1}d\vec{r_2} \tag{2.78}$$

This equation was the first to introduce the density rather than the wavefunction in order to solve the Hamiltonian. But the importance of this equation is more historical because it cannot really calculate the energy of an atom, this is due to the fact that Eq 2.78 completely neglects the exchange and correlation effect. The only part of the interelectronic interaction taken into account is the Coulomb repulsion, therefore the chemical bonds cannot be well described.[46] Dirac proposed the Thomas-Fermi-Dirac (TFD) model[47] that corrects the TF model by the introduction of exchange of electron gas but TFD model does not constitute a great improvement. A successive correction was given by Weizsacker[48] who proposed a correction of the kinetic energy term with the introduction of T_{TF} which takes into account the inhomogeneity of the density:

$$T_W[\rho] = \frac{1}{8}\int \frac{|\nabla\rho(r)|^2}{\rho(r)}dr \tag{2.79}$$

which leads to the total energy of the $TFD-\lambda W$ model:

$$E_{TFD-\lambda W} = T_{TF}[\rho] - \lambda T_W[\rho] + \int \rho(r)V(r)\,dr + J[\rho] + E_D^x[\rho] \tag{2.80}$$

where $E_D^x[\rho]$ is the Dirac correction:

$$E_D^x[\rho] = \frac{3}{4}\left(\frac{3}{\pi}\right)^{1/3}\int \rho(r)^{4/3}dr \tag{2.81}$$

In a first time, Weizsacker took $\lambda = 1$ but this value changed in many developments.[49–52] The advantages of the $TFD-\lambda W$ model are that the density is now finite at the nuclei and has a correct asymptotic behavior. Moreover, the $TFD-\lambda W$ model is able to describe the chemical bond. But the real development of DFT comes from the two theorems of Hohenberg and Kohn.

2.2.3 The Hohenberg and Kohn Theorems

2.2.3.1 The First Hohenberg and Kohn Theorem

The first Hohenberg and Kohn theorem[45] states, in case of non degenerate ground state, that the density $\rho(\vec{r})$ completely determines the external potential V_{ext}. The proof is given by *reductio ab absurdum* supposing the existence of two different external potentials V_{ext} and V'_{ext} being part of two different Hamiltonians: $\mathscr{H} = \hat{T} + \hat{V}_{ee} + \hat{V}_{ext}$ and $\mathscr{H}' = \hat{T} + \hat{V}_{ee} + \hat{V}'_{ext}$. Then the two Hamiltonians belong to two different ground state wavefunctions Ψ and Ψ' corresponding to two ground state energies E_0 and E'_0.
If we assume that the two wavefunctions give rise to the same electron density and if we define $E_0 = \langle\Psi|\mathscr{H}|\Psi\rangle$ then:

$$E_0 < \langle\Psi'|\mathscr{H}|\Psi'\rangle = \langle\Psi'|\mathscr{H}'|\Psi'\rangle + \langle\Psi'|\mathscr{H} - \mathscr{H}'|\Psi'\rangle \tag{2.82}$$

$\mathscr{H}$ and $\mathscr{H}'$ just differ by the external potential so:

$$\begin{aligned} E_0 &< E'_0 + \langle\Psi'|\hat{T} + \hat{V}_{ee} + \hat{V}_{ext} - \hat{T}' - \hat{V}'_{ee} - \hat{V}'_{ext}|\Psi'\rangle \\ \Leftrightarrow E_0 &< E'_0 + \int \rho(\vec{r})\,\{V_{ext} - V'_{ext}\} \end{aligned} \tag{2.83}$$

If we proceed in the same manner with interchanging the unprimed and the primed quantities we obtain:

$$E'_0 < E_0 + \int \rho(\vec{r})\,\{V_{ext} - V'_{ext}\} \tag{2.84}$$

Eq 2.83 & Eq 2.84 give the absurd result:

$$E_0 + E'_0 < E'_0 + E_0 \tag{2.85}$$

This is the proof that two different external potentials, V_{ext} and V'_{ext}, can not yield to the same ground state electron density.

2.2.3.2 The Second Hohenberg and Kohn Theorem

The second Hohenberg and Kohn theorem[45] introduces the variational principle in terms of the density. Choosing an arbitrary density $\tilde{\rho}$, the corresponding unique wavefunction $\tilde{\Phi}$ leads using the variational principle to:

$$\langle\tilde{\Phi}|\hat{H}|\tilde{\Phi}\rangle = \int \tilde{\rho}V_{ext}\,dr + T[\tilde{\rho}] + V_{ee}[\tilde{\rho}] = E[\tilde{\rho}] > E[\rho] \tag{2.86}$$

where ρ is the true ground state density. Then the variational principle requires that the ground-state density satisfy the stationary principle:

$$\delta E[\rho] - \mu\delta\left[\int \rho(r)dr - N\right] = 0 \tag{2.87}$$

where the integration of the density is imposed to be equal to N. Then using Euler-Lagrange equation:

$$\mu = \frac{\delta E[\rho]}{\delta\rho(r)} = V_{ext}(r) + \frac{\delta F[\rho]}{\delta\rho[r]} \tag{2.88}$$

where $F[\rho] = T[\rho] + V_{ee}[\rho]$ is called the universal functional and is independent of the system. The latter equation shows that knowing the universal function, the best density can be obtained trough a variational procedure. All properties of the system defined by an external potential V_{ext} are determined by the ground state density.

2.2.4 The Constrained Search Approach

The variational principle applied to a wavefunction Ψ is defined by:

$$E_0 = \min_{\Psi \to N} \langle \Psi | \hat{T} + \hat{V}_{Ne} + \hat{T}_{ee} | \Psi \rangle \tag{2.89}$$

But if we want to connect the variational principle to the DF formalism, we have first to define the v- and N-representability of the density. A density ρ is v-representable if it is associated to the wavefunction of a Hamiltonian defined in Eq 2.61 where the external potential $V_{ext}(r)$ is not necessarily a Coulomb potential. A density is N-representable if it can be obtained by squaring the antisymmetric potential wavefunction. Then the N-representability is a weaker condition than the v-representability. The HK theorems demonstrate a one-to-one correspondence between $\rho_0(r)$ and $\Psi_0(r)$ (the subscript 0 referring to ground state). But we want to determine the wavefunction in terms of a density, this is not trivial because an infinite number of antisymmetric wavefunctions give rise to the same density. How to determine the real wavefunctions Ψ_0 and non Ψ_{ρ_0}? The Levy constrained search[53–55] is the answer because the minimum energy principle gives:

$$\langle \Psi_{\rho_0} | \mathscr{H} | \Psi_{\rho_0} \rangle \geqslant \langle \Psi_0 | \mathscr{H} | \Psi_0 \rangle = E_0 \tag{2.90}$$

So we can write:

$$\begin{aligned} \langle \Psi_{\rho_0} | \mathscr{H} | \Psi_{\rho_0} \rangle &= \langle \Psi_{\rho_0} | \hat{T} + \hat{T}_{ee} | \Psi_{\rho_0} \rangle + \int \rho(r) V_{ext}(r) dr \\ &\geqslant \langle \Psi_0 | \hat{T} + \hat{T}_{ee} | \Psi_0 \rangle + \int \rho(r) V_{ext}(r) dr \end{aligned} \tag{2.91}$$

which is equivalent to:

$$\langle \Psi_{\rho_0} | \hat{T} + \hat{T}_{ee} | \Psi_{\rho_0} \rangle \geqslant \langle \Psi_0 | \hat{T} + \hat{T}_{ee} | \Psi_0 \rangle \tag{2.92}$$

If we rewrite the second HK theorem for a v-representable density we obtain:

$$E[\rho] \equiv F_{HK}[\rho] + \int \rho(r) V_{ext} dr \geqslant E_v[\rho_0] \tag{2.93}$$

Therefore we have:

$$F_{HK}[\rho_0] = \langle \Psi_0 | \hat{T} + \hat{V}_{ee} | \Psi_0 \rangle = \min_{\Psi \to \rho_0} \langle \Psi | \hat{T} + \hat{V}_{ee} | \Psi \rangle \tag{2.94}$$

The definition of the constrained search comes from the fact that only the wavefunctions of ρ_0 density are taken into account. If we look at Eq 2.94, we can notice that we are not obliged to restrict to a v-representable ρ_0 ground state but to any N-representable density. Therefore we can extend the definition of $F_{HK}[\rho_0]$ to any N-representable density:

$$F[\rho] = \min_{\Psi \to \rho} \langle \Psi | \hat{T} + \hat{V}_{ee} | \Psi \rangle \tag{2.95}$$

where $F[\rho] = F_{HK}[\rho_0]$. The minimization procedure can be performed in two steps:

$$F[\rho] = \min_{\rho \to N} \left[\min_{\Psi \to \rho} \left(\langle \Psi | \hat{T} + \hat{V}_{ee} | \Psi \rangle + \int \rho(r) V_{ext} dr \right) \right] \tag{2.96}$$

which can be written in a more compact form as:

$$\begin{aligned} E_0 &= \min_{\rho \to N} \left[F[\rho] + \int \rho(\vec{r}) V_{ext} d\vec{r} \right] \\ &= \min_{\rho \to N} E[\rho] \end{aligned} \tag{2.97}$$

2.2.5 The Kohn-Sham Approach

Kohn and Sham[3] suggested to take into account a system of N non-interacting electrons ($V_{ee} = 0$) moving in an external potential V_{ext}. For this approximation the kinetic energy is well known and corresponds to the kinetic energy, T_S, defined as:

$$T_S = \sum_{i=1}^{N} \langle \chi_i | -\frac{1}{2} \nabla^2 | \chi_i \rangle \tag{2.98}$$

but the true kinetic energy, T, is not equal to T_S. Then Kohn and Sham introduce this difference in the functional thus from Eq 2.88:

$$\mu = V_{ext}(r) + \frac{\delta T[\rho]}{\delta \rho(r)} + \frac{\delta V_{ee}[\rho]}{\delta \rho(r)} = V_{ext}(r) + \frac{\delta T_S[\rho]}{\delta \rho(r)} + V_{eff}(r) \tag{2.99}$$

where $V_{ext}(r)$ is a fictitious external potential which should be applied to the non-interacting system to get the density ρ:

$$V_{ext}(r) = \frac{\delta T[\rho]}{\delta \rho(r)} - \frac{\delta T_S[\rho]}{\delta \rho(r)} + \frac{\delta V_{ee}[\rho]}{\delta \rho(r)} \tag{2.100}$$

Then the total energy is:

$$E[\rho] = T_S[\rho] + J[\rho] + T[\rho] - T_S[\rho] + \int V_{ext} \rho(r) dr + V_{ee}[\rho] - J[\rho] \tag{2.101}$$

where:

$$J[\rho] = \frac{1}{2} \int \frac{\rho(r_1)\rho(r_2)}{|r_1 - r_2|} dr_1 dr_2 \tag{2.102}$$

If we set:

$$E_{XC}[\rho] = (T[\rho] - T_S[\rho]) + (V_{ee}[\rho] - J[\rho]) \tag{2.103}$$

then the energy of the system can be expressed as:

$$E[\rho] = T_S[\rho] + J[\rho] + E_{XC}[\rho] + \int V_{ext} \rho(r) dr \tag{2.104}$$

where E_{XC} is called the exchange-correlation energy. The exchange-correlation energy functional can be derived with respect to the density to define the exchange-correlation potential $V_{XC}[\rho]$:

$$V_{XC}[\rho] = \frac{\delta E_{XC}[\rho]}{\delta \rho(r)} \tag{2.105}$$

From Eq 2.101, the KS equations can be derived:

$$\left[-\frac{1}{2}\nabla^2 + \frac{\rho(r')}{|r-r'|} + V_{ext}(r) + V_{XC}(r)\right]\chi_i = \varepsilon_i\chi_i \tag{2.106}$$

where:

$$\rho(r) = \sum_{i=1}^{N}\sum_{\sigma}|\chi_i(r,\sigma)|^2 \tag{2.107}$$

and the total energy is equal to:

$$E = \sum_{i=1}^{N}\varepsilon_i - \frac{1}{2}\int\frac{\rho(r)\rho(r')}{|r-r'|}\,dr\,dr' + E_{XC}[\rho] - \int V_{XC}(r)\rho(r)dr \tag{2.108}$$

We can underline that E_{XC} does not contain only the exchange and correlation energy but also the correction of the kinetic energy: correlation kinetic energy. The main advantage of the DFT approach is the substitution of the non-local non-multiplicative HF term by a local and multiplicative exchange and correlation term. On the other hand, the functional form of E_{XC} is unknown. Therefore all DFT applications are based on an approximate E_{XC} (*cf.* next sections).
As underlined before, V_{ext} can not only consider the potential of the nuclei but can also take into account, for example, a magnetic field which acts only on the spin of the electrons. For this case the total density $\rho(r)$ and the $\alpha-\beta$ electron density $(\rho(r)^\alpha, \rho(r)^\beta)$ should be consider as variables. The Hamiltonian in presence of an external field, $B(r)$, reads:

$$\mathscr{H}_{elec} = -\frac{1}{2}\sum_{i=1}^{N}\nabla_i^2 + \sum_{i=1}^{N}\sum_{A=1}^{M}\frac{Z_A}{r_{iA}} + \sum_{i=1}^{N}\sum_{j>i}^{N}\frac{1}{r_{ij}} + 2\cdot\beta_e\sum_{i=1}^{N}B(r)\cdot S_i \tag{2.109}$$

where $\beta_e = e\hbar/2mc$ and the interaction of orbital angular momentum of electron with the magnetic field has been neglected. It can be shown[38] that the constrained search formulation can be rewritten as:

$$F\left[\rho^\alpha,\rho^\beta\right] = \min_{\Psi\to\rho^\alpha,\rho^\beta}\langle\Psi|\hat{T}+\hat{V}_{ee}|\Psi\rangle \tag{2.110}$$

Therefore following the KS method we obtain:

$$F\left[\rho^\alpha,\rho^\beta\right] = T_S\left[\rho^\alpha,\rho^\beta\right] + J\left[\rho^\alpha,\rho^\beta\right] + E_{XC}\left[\rho^\alpha,\rho^\beta\right] \tag{2.111}$$

and finally, we obtain the spin-polarized set of KS equations:

$$\begin{aligned}\hat{h}^\alpha_{eff} &= \left[-\frac{1}{2}\nabla_i^2 + V^\alpha_{eff}(r)\right]\Psi_{i\alpha}(r) = \varepsilon_{i\alpha}\Psi_{i\alpha}(r)\\ \hat{h}^\beta_{eff} &= \left[-\frac{1}{2}\nabla_i^2 + V^\beta_{eff}(r)\right]\Psi_{i\beta}(r) = \varepsilon_{i\beta}\Psi_{i\beta}(r)\end{aligned} \tag{2.112}$$

and:

$$\begin{aligned}V^\alpha_{eff}(r) &= V_{ext}(r) + \beta_e b(r) + \frac{\rho(r')}{|r-r'|}dr' + \frac{\delta E_{XC}[\rho^\alpha,\rho^\beta]}{\delta\rho^\alpha(r)}\\ V^\beta_{eff}(r) &= V_{ext}(r) + \beta_e b(r) + \frac{\rho(r')}{|r-r'|}dr' + \frac{\delta E_{XC}[\rho^\alpha,\rho^\beta]}{\delta\rho^\beta(r)}\end{aligned} \tag{2.113}$$

where $b(r)$ is the magnetic field in the z direction.
Actually, the spin-polarized extension can also be applied in absence of an external field to give a better description of the E_{XC} for open shell systems and to allow different spins to have different densities. The latter point is equivalent to the concept of Unrestricted-HF and should account for molecules at the near dissociation limit and for processes of spontaneous localization/magnetisation.

2.2.6 Hole Functions

From the Eq 2.74, we can formulate the Hamiltonian in terms of first and second order density matrices and express the energy as:

$$\langle\Psi|\mathscr{H}|\Psi\rangle = \int \left[-\frac{1}{2}\nabla_r^2\rho_1(r,r')\right]_{r=r'} dr + \int V_{ext}\rho_1(r)dr + \int \frac{1}{r_{12}}\rho_2(r_1,r_2)dr_1dr_2 \quad (2.114)$$

In the case we have independent electrons:

$$\rho_2(r_1,r_2)dr_1dr_2 = \frac{1}{2}\rho(r_1)\rho(r_2) \quad (2.115)$$

In the case we have interacting electrons:

$$\rho_2(r_1,r_2)dr_1dr_2 = \frac{1}{2}\rho(r_1)\rho(r_2)\left[1+h(r_1r_2)\right] \quad (2.116)$$

where the last terms incorporates all the interaction between the electrons. If we now recall that:

$$\rho(r_1) = \frac{2}{N-1}\int \rho_2(r_1,r_2)dr_2 \quad (2.117)$$

We can define the *exchange-correlation hole* as:

$$\rho_{xc}(r_1,r_2) = \rho(r_2)h(r_1,r_2) \quad (2.118)$$

From Eq 2.116 & 2.117 we can write:

$$\frac{2}{N-1}\rho(r_1) = \frac{N}{2}\rho(r_1) + \frac{1}{2}\rho(r_1)\int \rho_{xc}(r_1,r_2)dr_2 \quad (2.119)$$

and:

$$\int \rho_{xc}(r_1,r_2)dr_2 = \int \rho(r_2)h(r_1,r_2)dr_2 = -1 \quad (2.120)$$

Therefore from Eq 2.114, we derive:

$$\begin{aligned} V_{ee} &= \int \frac{1}{r_{12}}\rho(r_1,r_2)dr_1dr_2 \\ &= \frac{1}{2}\int \rho(r_1)\rho(r_2)dr_1dr_2 + \frac{1}{2}\int \frac{\rho(r_1)\rho_{xc}(r_1,r_2)}{r_{12}}dr_1dr_2 \\ &= J[\rho] + E_{xc}[\rho] \end{aligned} \quad (2.121)$$

If now we separate the spin-like pairs of electrons from the opposite spins pairs, we have:

$$E_{xc}[\rho] = \frac{1}{2}\int \frac{\rho^\sigma(r_1)\rho_x^{\sigma\sigma}(r_1,r_2)}{r_{12}}dr_1dr_2 + \frac{1}{2}\int \frac{\rho^\sigma(r_1)\rho_c^{\sigma\sigma'}(r_1,r_2)}{r_{12}}dr_1dr_2 \quad (2.122)$$

where $\rho_x^{\sigma\sigma}(r_1 r_2)$ is the *Exchange Hole or Fermi Hole* and it contains both the exchange contribution to the total energy and the correlation of electrons of the same spin, and $\rho_c^{\sigma\sigma'}(r_1 r_2)$ is the *Correlation Hole or Coulomb Hole* and it describes the correlation energy for electrons of opposite spin. The general condition for the exchange-correlation hole function can be rewritten in terms of Exchange and Correlation Hole functions as:

$$\begin{aligned} \int \rho_x^{\sigma\sigma}(r_1, r_2) r_{12} dr_1 dr_2 &= -1 \\ \int \rho_c^{\sigma\sigma}(r_1, r_2) r_{12} dr_1 dr_2 &= 0 \end{aligned} \tag{2.123}$$

Let us consider the exchange correlation hole. Defining the position of electron 2 as a function of the position of electron 1 ($r_2 = r_1 + s$), we have:

$$\lim_{s \to 0} \rho_x^{\sigma\sigma}(r_1, r_1 + s) = \rho^{\alpha}(r_1) \tag{2.124}$$

This condition is equivalent to Pauli principle and it exactly compensates the self interaction energy contained in the $J[\rho]$.

2.2.7 Exchange and Correlation Functional

With the aim to find functionals which can give a better description of chemical systems, several classes of E_{XC} have been proposed. Unfortunately, a straightforward way in which the functional can be improved does not exist. Nevertheless two main routes have been followed: the first is to start from a model for which an exact solution can be found and try to design functionals which satisfy the theoretical conditions; the second is, starting from a given functional form, to fit a number of parameters in order to reproduce the chemical properties of a bunch of compounds taken as reference. The last approach can yield better results but it introduces a lack of generality in the E_{XC} and therefore this concept of a functional optimized for a given set of molecules certainly drives DFT towards the semi-empirical approaches.
Although the number of functional is constantly increasing, we can recast most of the current functionals into three different classes: the Local, the Gradient Corrected and the Hybrid ones. It is important to stress that all the functionals are local, even if sometimes the generalized gradient approximation was misleadingly referred as non-local approximation, since they depend only upon the density or gradient of density at the given position. Finally a short overview of the so-called *meta*-GGA is given in section 2.2.7.4.

2.2.7.1 Local Density Approximation

A simple reference model for which an exact solution can be found is the uniform electron gas. A uniform electron gas can be thought as a system of N electrons in a cube of volume $V = a^3$ where a uniform charge has been spread out in order to maintain the overall system neutral, when $N \to \infty$, $V \to \infty$ while the density remains constant $\rho = \frac{N}{V}$. In this case the ground state energy reads:

$$E[\rho] = T_S[\rho] + \int \rho(r) V_{ext}(r) dr + J[\rho] + E_{XC}[\rho] + E_b \tag{2.125}$$

with E_b being the electrostatic energy of the positive background. This electrostatic energy does compensate the sum of the external potential generated by the electrons and the coulombic interaction between electrons. Therefore the second, third and fifth terms of Equation 2.125 add to zero. In this case, we can thus write:

$$\begin{aligned} E[\rho] &= T_S[\rho] + E_{XC}[\rho] \\ &= T_S[\rho] + E_X[\rho] + E_C[\rho] \end{aligned} \tag{2.126}$$

It can be shown that, using plane waves, the first order spinless density matrix can be expressed as:

$$\begin{aligned} \rho_1(r_1, r_2) &= 3\rho(r)\frac{\sin t - t\cos t}{t^3} \\ t &= k_F(r)s \\ k_F(r) &= [3\pi^2\rho(r)]^{1/3} \\ s &= r_1 - r_2 \end{aligned} \tag{2.127}$$

Consequently, we have:

$$\begin{aligned} T_S[\rho] &= C_F \int \rho(r)^{5/3} dr \\ E_X[\rho] &= -C_x \int \rho(r)^{4/3} dr \\ C_F &= \frac{3}{10}(3\pi^2)^{2/3} \\ C_x &= \frac{3}{4}\left(\frac{1}{3\pi}\right)^{1/3} \end{aligned} \tag{2.128}$$

From Eq 2.128 the TFD formulation can be recognized. In case of a system with a different number of α and β electrons with the corresponding density ρ^α and ρ^β, the kinetic energy and the exchange energy can be expressed as:

$$\begin{aligned} T_S[\rho^\alpha, \rho^\beta] &= 2^{2/3} C_F \int \left[(\rho^\alpha(r))^{5/3} + (\rho^\beta(r))^{5/3}\right] dr \\ E_X[\rho^\alpha, \rho^\beta] &= -2^{1/3} C_x \int \left[(\rho^\alpha(r))^{4/3} + (\rho^\beta(r))^{4/3}\right] dr \end{aligned} \tag{2.129}$$

The correlation functional for a uniform electron gas, was derived from the numerical Monte-Carlo simulations of Ceperley and Alder,[56] subtracting from the total energy the kinetic and the exchange ones obtained through Eq 2.126. And then Vosko, Wilk and Nusair[57] formulated the correlation energy per particle, ε_c, in an analytical way. If r_s is defined as the radius of a sphere whose volume is the effective volume of an electron:

$$\frac{4}{3}\pi r_s^3 = \frac{1}{\rho} \tag{2.130}$$

The expression of $\varepsilon_c(r_s)$ reads:

$$\begin{aligned} \varepsilon_c(r_s) = \frac{A}{2}\Bigg(&\ln\frac{x^2}{X(x)} + \frac{2b}{Q}\arctan\frac{Q}{2x+b} \\ &- \frac{bx_0}{X(x_0)}\left[\ln\frac{(x-x_0)^2}{X(x)} + \frac{2(b+2x_0)}{Q}\arctan\frac{Q}{2x+b}\right]\Bigg) \end{aligned} \tag{2.131}$$

where $x = r_s^{1/2}$, $X(x) = x^2 + bx + c$, $Q = \sqrt{(4c - b^2)}$ and $A = 0.0621814, 0.0310907$; $x_0 = -0.409286, -0.743294$; $b = 13.0720, 20.1231$; $c = 42.7198, 191.578$ for the non spin-polarized and for the spin-polarized cases respectively. The LDA exchange is often referred as S-VWN to stress the two components of the exchange (Slater-Dirac) and correlation (VWN) parts respectively. Most of the functionals developed contain the LDA exchange and a correction to it. Therefore we expect that for LDA functional, the more inhomogeneous the system is, the worst the description should be. [c]

2.2.7.2 Generalized Gradient Approximation

One of the most striking failure of LDA is its wrong asymptotic behavior. Becke[58] starting from the definition of exchange and correlation hole (Eq 2.118) has defined exchange energy as a function of the exchange energy density ($\varepsilon_x(r_1)$) as:

$$\begin{aligned} E_x &= \int \rho(r_1)\varepsilon(r_1)dr_1 \\ \varepsilon_x(r_1) &= \frac{1}{2}\int \frac{\rho_{xc}(r_1, r_2)}{r_{12}}dr_2 \end{aligned} \tag{2.132}$$

The following asymptotic condition should be fullfilled:

$$\lim_{r_1 \to \infty} \varepsilon(r_1) = -\frac{1}{2r_1} \tag{2.133}$$

In the case of LDA functional, the asymptotic condition is equivalent to:

$$\lim_{r_1 \to \infty} \rho(r) \propto -\exp(-\alpha r) \tag{2.134}$$

so Becke defined the asymptotic condition as:

$$\lim_{r_1 \to \infty} \varepsilon_{x-LDA} \propto -\exp(-\alpha r/3) \tag{2.135}$$

Therefore an additional correction should be added. The one proposed by Becke in order to recover the correct asymptotic behavior contains the gradient of the density and has the following functional form:

$$\begin{aligned} \varepsilon_{x-Becke} &= -\beta\rho^{1/3}\frac{x^2}{1 + 6\beta x \sinh^{-1} x} \\ x &= \frac{\nabla\rho}{\rho^{4/3}} \end{aligned} \tag{2.136}$$

This expression contains one adjustable parameter (β) which was chosen so that the sum of the LDA and Becke exchange terms reproduces the exchange energy of six noble gas atoms ($\beta = 0.0042$). The Becke exchange energy functional has the correct asymptotic behavior but the derived potential not (i.e. it behaves like r^{-2} instead of r^{-1}). On the other hand the introduction of the gradient of the density enables a better treatment

[c] We are, within the LFDFT method, using LDA functional to do geometry optimization if we don't have the experimental structure, especially for small coumpounds with negative charge. Sometimes we use it for all the DFT calculations of the LFDFT procedure.

of inhomogeneous systems such as the molecular systems we are normally dealing with. As a typical example of Gradient corrected correlation functional we can consider the Lee-Yang-Parr correlation potential. Starting from the work of Colle and Salvetti[59] who formulated and approximated expression of the correlation energy of He as a function of second order HF density matrix, Lee, Yang and Parr[60] expressed this formula in term of ρ, its gradient and its Laplacian. After integration by part[61] the Laplacian terms are eliminated and the final expression for a closed shell system reads:

$$E_{c-LYP} = -a \int \frac{\rho}{1 + d\rho^{-1/3}} dr - ab \int w\rho^2 \left[C_F \rho^{8/3} + |\nabla\rho|^2 \left(\frac{5}{12} - \delta \frac{7}{12} \right) \right] - \frac{11}{24} \rho^2 |\nabla\rho|^2 dr \tag{2.137}$$

where

$$\begin{aligned} w &= \frac{\exp(-c\rho^{-1/3})}{1 + d\rho^{-1/3}} \rho^{-11/3} \\ \delta &= c\rho^{-1/3} + \frac{d\rho^{-1/3}}{1 + d\rho^{-1/3}} \end{aligned} \tag{2.138}$$

and $a = 0.04918$, $b = 0.132$, $c = 0.2533$, $d = 0.349$ are the Colle-Salvetti parameters for He.
Contrary to the Becke functional for exchange, the LYP functional is not derived from a uniform electron gas model but from correlated wavefunction for a two electrons system. Several other GGA exchange and correlation functionals have been developed from the late 80's until now.

2.2.7.3 Hybrid Functional

As well as "pure-GGA", an increasing number of exchange and correlation functionals include a percentage of exact exchange. This latter class of functionals recasts the so-called Hybrid-Functionals. We can suppose that a system of density ρ can be described as a sum of fictitious systems, all with density ρ but with different electron-electron interaction. This interaction can be tuned via a parameter λ such that $\lambda = 1$ corresponds to full interacting electrons and $\lambda = 0$ corresponds to non-interacting electrons. Therefore we can write:

$$F_\lambda[\rho] = \min \langle \Psi_\rho^\lambda | \hat{T} + \lambda \hat{V}_{ee} | \Psi_\rho^\lambda \rangle \tag{2.139}$$

where Ψ_ρ^λ minimizes the Hamiltonian $\hat{T} + \lambda \hat{V}_{ee}$ and has an exact density ρ. From the expression of E_{xc} given in Eq 2.103 we have:

$$\begin{aligned} E_{xc} &= T[\rho] - T_S[\rho] - J[\rho] + V_{ee}[\rho] \\ &= F_1[\rho] - F_0[\rho] - J[\rho] \\ &= \int_0^1 d\lambda \frac{\partial F_\lambda}{\partial \lambda} - J[\rho] \end{aligned} \tag{2.140}$$

Using the Hellman-Feynman theorem we can write:

$$E_{xc} = \int_0^1 d\lambda \langle \Psi_\rho^\lambda | \lambda \hat{V}_{ee} | \Psi_\rho^\lambda \rangle - J[\rho] \tag{2.141}$$

If now we evaluate the integral using a two-point quadrature, we just need the value of the integral for $\lambda = 0$ and $\lambda = 1$, the first being the HF-exchange and the latter the full exchange-correlation energy. This leads to the so-called half-and-half formula where 50 % of HF-exchange has been introduced. Successively, Becke[62] proposed a different (empirical) mixing of exact exchange and exchange-correlation energy derived from different exchange-correlation functionals, leading to the family of the three parameters hybrid functional, the most known being B3LYP:

$$B3LYP \equiv AE_x^{Dirac} + (1-A)E_x^{HF} + B\Delta_x^{Becke} + (1-C)E_c^{VWN} + CE_c^{LYP} \tag{2.142}$$

2.2.7.4 *meta*-GGA

With the definition of *meta*-GGA a new family of exchange-correlation functionals was introduced by Perdew.[63] The aim of this new class of functionals is to overcome the shortcomings of LDA and GGA approaches due to their foundation on a strictly local formulation. Therefore, to reach chemical accuracy, non local terms are included in the exchange-correlation functional formulation. In particular we can see, that at a LDA level, E_{XC} is only a function of the density (ρ) and at the GGA level, only a function of the density and its gradient (ρ and $\nabla\rho$). Instead of proposing a fully non local functional, Perdew[63] firstly proposed an exchange and correlation functional which depends on the density and the gradient of the density (ρ and $\nabla\rho$) as a common GGA but also on the Laplacian of the density ($\nabla^2\rho$) or of the kinetic energy density of the occupied orbitals. Different *meta*-GGA functionals have been developed[64–66] but we are not able to use them, up to now, in our LFDFT approach. It comes from the fact that *meta*-GGA functional are implemented in the ADF program as a post-SCF procedure. So we can calculate energies in regards of these kinds of functionals but the density matrix is not optimized according to them. As one can see in the next chapter, we need to extract eigenvectors of the Kohn-Sham molecular orbitals (KS MO) from DFT calculations in our LFDFT approach.

2.2.8 Scaling Relations in DFT

Let us consider a change of the electron coordinates in the system, in order to expand ($\lambda > 1$) or to shrink ($\lambda < 1$) the electron cloud: $r' = \lambda r$. The scaling factor is defined as the operation on the wavefunction or on the density which changes all the coordinates but keeping the normalization condition. Thus we have:

$$\begin{aligned} \Psi_\lambda &= \lambda^{3N/2}\Psi(\lambda r) \\ \rho_\lambda &= \lambda^3\rho(\lambda r) \end{aligned} \tag{2.143}$$

If we express the kinetic energy and the electron-electron interaction as a functional of the wavefunction, they scale homogeneously as λ^2 and λ:

$$\begin{aligned} T[\Psi_\lambda] &= \lambda^2 T[\Psi] \\ V_{ee}[\Psi_\lambda] &= \lambda V_{ee}[\Psi] \end{aligned} \tag{2.144}$$

If, now, we express the T and V_{ee} as a functional of the density, the scaling relations are no more the same. In particular, recalling the Levy constrained search formulation, we

have:

$$\begin{aligned} F[\rho(r)] &= \min_{\Psi\to\rho} \int \Psi^*(r)\big[T(r) + V_{ee}[r]\big]\Psi(r)dr \\ &= \min_{\Psi\to\rho} \lambda^{3N} \int \Psi^*(\lambda r)\big[T(\lambda r) + V_{ee}[\lambda r]\big]\Psi(\lambda r)dr \\ &= \min_{\Psi\to\rho} \lambda^{-2} \int \Psi^*_\lambda(r)\big[T(r) + \lambda V_{ee}[r]\big]\Psi_\lambda(r)dr \\ &= \min_{\Psi\to\rho} \lambda^{-2} \langle \Psi_\lambda | T + \lambda V_{ee} | \Psi_\lambda \rangle \end{aligned} \tag{2.145}$$

$\lambda^{3N/2}\Psi^{min}_\rho(\lambda r)$ gives the density ρ_λ and minimizes the expectation value of $\lambda^{-2}\langle T + \lambda V_{ee}\rangle$, while Ψ^{min}_ρ gives ρ and minimizes $\langle T + \lambda V_{ee}\rangle$. If we define $\Psi^{min}_{\rho\lambda}$ the wavefunction with the corresponding density ρ_λ which minimizes $\langle T + \lambda V_{ee}\rangle$, the following inequality arises:

$$\lambda^{3N/2}\Psi^{min}_\rho(\lambda r) \neq \Psi^{min}_{\rho\lambda} \tag{2.146}$$

As a consequence $T[\rho\lambda]$ and $V_{ee}[\rho\lambda]$ do not scale homogeneously. The following scaling relations have been derived by Perdew and Levy:[67]

$$\begin{aligned} V_{ee}[\rho\lambda] < \lambda V_{ee}[\rho] \quad ; \quad T[\rho\lambda] > \lambda^2 T[\rho] \text{ for } \lambda < 1 \\ V_{ee}[\rho\lambda] > \lambda V_{ee}[\rho] \quad ; \quad T[\rho\lambda] < \lambda^2 T[\rho] \text{ for } \lambda > 1 \end{aligned} \tag{2.147}$$

In case of non-interacting electrons, the KS kinetic energy scales homogeneously:

$$T_S[\rho\lambda] = \lambda^2 T[\rho] \tag{2.148}$$

as well as the exchange-energy functional and the classical Coulomb potential:

$$\begin{aligned} E_x[\rho\lambda] = \lambda E_x[\rho] \\ J[\rho\lambda] = \lambda J[\rho] \end{aligned} \tag{2.149}$$

What does not scale homogeneously is $T_c[\rho]$, the difference between the real kinetic energy and the kinetic energy of a non-interacting electron system:

$$T_c[\rho] = T[\rho] - T_s[\rho] \tag{2.150}$$

The following inequality can be demonstrated:[4,68]

$$T[\rho] \geqslant T_s[\rho] \tag{2.151}$$

Therefore:

$$T_c \geqslant 0 \tag{2.152}$$

Correspondingly the correlation energy reads:

$$E_c[\rho] = V_{ee}[\rho] - J[\rho] - E_x[\rho] + T_c[\rho] \tag{2.153}$$

Therefore $E_c[\rho]$ always contains a positive contribution due to kinetic energy and particular care should be taken in direct comparison of correlation energy derived from correlated

calculations and the correlation energy derived from DFT. As previously seen for E_x, scaling inequalities can be derived also for the correlation energy:[67]

$$\begin{aligned} E_c[\rho_\lambda] &< \lambda E_c[\rho] \text{ for } \lambda < 1 \\ E_c[\rho_\lambda] &> \lambda E_c[\rho] \text{ for } \lambda > 1 \end{aligned} \tag{2.154}$$

The scaling relations in DFT have been reviewed by Levy.[69] As a final remark, it is important to point out that most of the current functionals do not satisfy several of these inequalities or the asymptotic conditions, which in principle, should be taken as a rigourus guide in the design of new functionals.

2.2.9 Janak's Theorem

Looking at the KS Equation 2.108, the choice of expanding the density by using N-orbitals and integer occupation numbers is arbitrary. Janak[70] proposed to define the kinetic energy of the non-interacting electron as:

$$T_J[\rho] = \min n_i \sum_i \int \Psi_i^*(x) - \frac{1}{2}\nabla_i^2 \Psi_i(x) d(x) \tag{2.155}$$

where n_i is $0 \leqslant n_i \leqslant 1$. The number of functions in Janak derivation is arbitrary but subject to the constrain that $\sum_i n_i = N$.
The total density is then defined as:

$$\rho(r) = \sum_i n_i \sum_\sigma |\Psi(x)|^2 \tag{2.156}$$

and the corresponding total energy reads:

$$\begin{aligned} E[\rho] &= T_J[\rho] + V_{ee}[\rho] + \int \rho(r) V_{ext}(r) dr \\ &= -\frac{1}{2}\sum_i n_i \int \Psi_i^*(x)\nabla_i^2\Psi_i(x)d(x) + J[\rho] + E_{xc}[\rho] + \int \rho(r)V_{ext}(r)dr \end{aligned} \tag{2.157}$$

We can minimize $E[\rho]$ with respect to Ψ_i and n_i. For a given set of n_i, we have:

$$\left[-\frac{1}{2}n_i\nabla^2 + n_i V_{eff}(r)\right]\Psi_i = \varepsilon_i'\Psi_i \tag{2.158}$$

The standard KS-like equation can be obtained considering the substitution: $\varepsilon_i = \frac{\varepsilon_i'}{n_i}$. The differentiation of the energy E with respect to n_i gives Eq 2.159 that is usually referred as the *Janak's theorem*:

$$\begin{aligned} \frac{\partial E}{\partial n_i} &= -\frac{1}{2}\int \Psi_i^*(x)\nabla_i^2\Psi_i(x)d(x) + \int \frac{\delta}{\delta\rho(r)}\left[J[\rho] + E_{xc}[\rho] + \int \rho(r)V_{ext}(r)dr\right]\frac{\delta\rho(r)}{\partial n_i} \\ &= -\frac{1}{2}\int \Psi_i^*(x)\nabla_i^2\Psi_i(x)d(x) + \int V_{eff}(r)\Psi_i^*(x)\Psi_i(x)dr \\ &= \varepsilon_i \end{aligned} \tag{2.159}$$

From a practical point of view, the KS implementation is definitely easier because it just fixes the occupation number of the first N orbitals to 1 and the rest to 0, but several and important are the information that can be derived from Janak theorem such as the Electron Affinity or the Ionization Potential in terms of orbitals' eigenvalues.[d]

2.2.10 From Ground to Excited States

As we saw in the previous demonstration, the density provides information about the ground state density but in many works[4–6,38,71–73] the DFT was extended to describe the properties of excited states. These methods are still being developed and we can cite for example the TD-DFT or the CI. In our LFDFT approach, we can consider that we do a "mini"-CI on the MO's with dominant d-character.

[d]In the LFDFT procedure, we use the Janak's theorem when we do the AOC calculation. In fact to satisfy the LFT requirement, we have to occupy all the MO's with dominant d-character with the same amount of electrons.

Chapter 3

LFDFT

The LFDFT method is a LFT based on DFT calculations. The procedure can be divided in three main parts. The first part consists of a set of DFT calculations and the extraction of the necessary data from its outputs. The second part consists in a matlab program, which uses the Slater determinant energies (calculated by DFT) and the eigenvectors of the Kohn-Sham orbitals with dominant *d*-character (extracted from the AOC calculation), to calculate the ligand field matrices and the Racah's parameters. The third and final step corresponds to the utilization of a LF program which can determine, so far, the multiplet structure (discussed in Chapter 4) and the ESR parameters (subject of Chapter 6). The extension of the method to other properties is currently being developed by our group. Figure 3.1 gives an overview of all the procedure. This Chapter is dedicated to the description of the first two parts: the DFT calculations and the LFDFT method while the analysis of the LF program is proposed in Chapter 4. For DFT, the calculations process is described through an example. Afterwards, the theory of LFDFT is presented, then the source code of the LFDFT program, and finally some applications are proposed to test the accuracy of the method. At the end of the chapter, some general conclusions about the LFDFT method are given.

3.1 DFT Calculations

All DFT calculations have been performed using the ADF program package.[74] The DFT part of the LFDFT method is, in its turn, divided in three steps: (i) the first consists either in a single point calculation (if we have the X-ray crystallographic data) or in a geometry optimization, (ii) the second step, called an AOC calculation, is necessary to build the Kohn-Sham orbital diagram in agreement with the LFT requirement, (i.e., the KS MO diagram of an AOC calculation comply with the spherical symmetry inherent to LFT), (iii) the last step, called Slater Determinant (SD) calculations, determine, within the DFT formalism, the energies of all SD's. An overview of these three steps is proposed through an example: the LFDFT method is applied to the $[CoCl_4]^{2-}$ complex (the input files and some extracts of the output files are given). Before a review of the general settings used to perform the DFT calculations is presented.

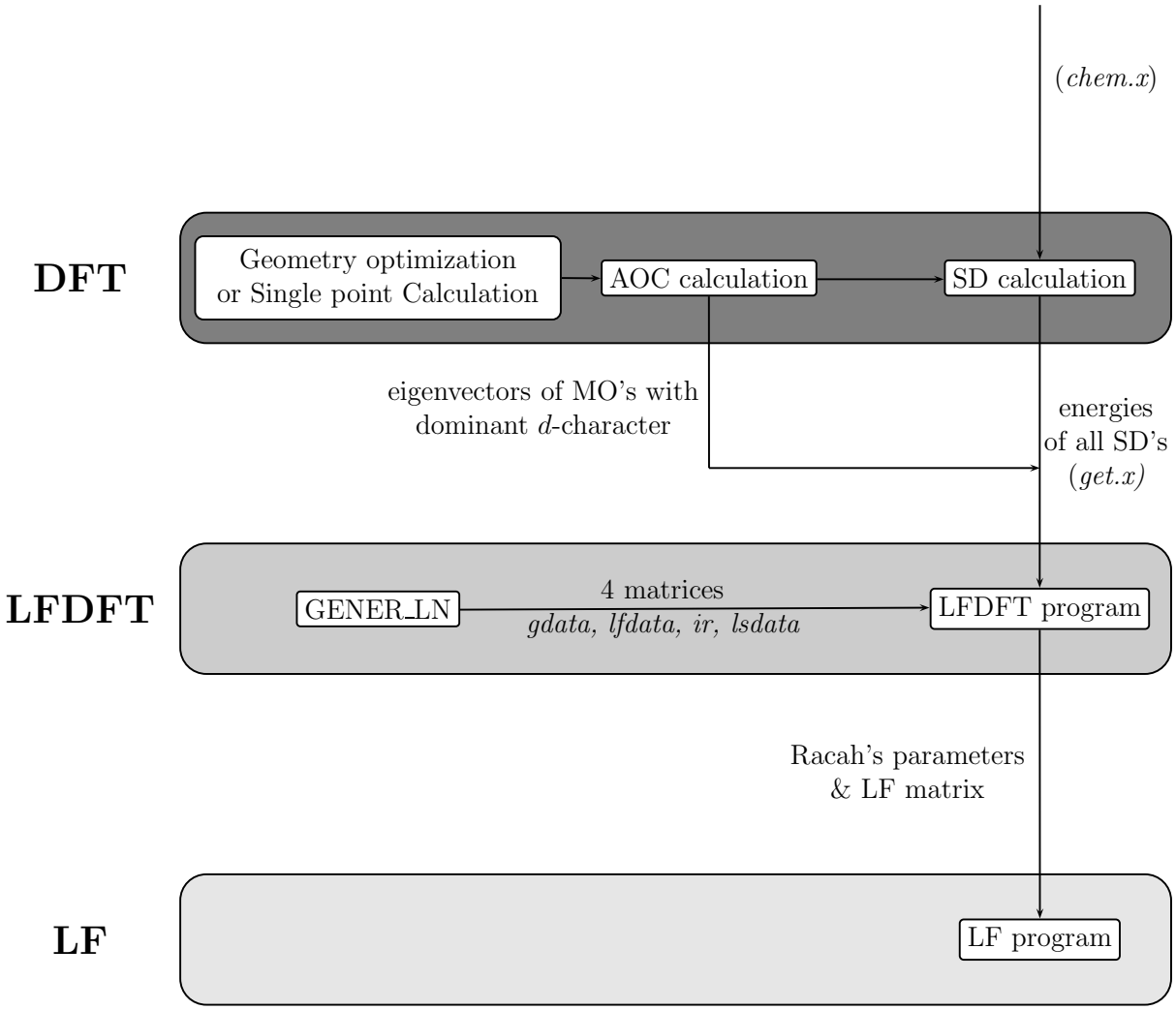

Figure 3.1: *Scheme of the LFDFT calculations procedure. We can see that the DFT part needs three steps, the LFDFT part two and the final step consists in using a LF program.*

ADF version	Acronyms	Exchange	Correlation
2003.01	PW91	PW91x[75]	PW91c[75]
	PBE	PBEx[76]	PBEc[76]
	RPBE	RPBEx[77]	PBEc[76]
	revPBE	revPBEx[78]	PBEc[76]
	Blyp	Becke[58]	LYP[60,79,80]
2000.01	PW91	Becke[58]	Perdew[81]
		PW91x[75]	PW91c[75]

Table 3.1: *Listed in the second column the acronyms of the GGA functional we use depending on the version of ADF. In the third and fourth column, names and references are given on the the exchange and the correlation part used.*

3.1.1 General Settings

For each calculation we have to choose the basis set and the functional but, we can say that we use for almost all the calculations the same settings that are summarized here.[a] In general, the atoms are described through triple-ζ STO basis sets plus one polarization function given in the program database (basis set IV: ADF release 2000, or TZP: ADF release 2003) and the frozen core approximation is used up to $3p$ for the TM and up to $1s$ for second row elements, $2p$ for third row elements and so on.

The choice of the functional for the geometry optimization calculation is discussed in the Section 3.1.2. Within one LFDFT calculation, the functional for the AOC calculations and the SD calculation must be the same. In fact Figure 3.1 shows that data have to be extracted from these two calculations so the two calculations have to refer to the same approximation, i.e. the same functional. We use either the local density approximation (LDA) where exchange-correlation potential and energies have been computed according to the Vosko, Wilk, and Nusair's (VWN)[57] parameterization of the electron gas data or the generalized gradient approximation (GGA) where exchange-correlation and energies have been computed according to the PW91 parametrisation (*cf.* Table 3.1). To test the sensitivity of our method to the functional, we, for some examples, use every functional listed in Table 3.1 (where acronyms are used to define in one stroke the exchange and the correlation part of the functional). We can already underline that if we use the functionals: PW91, PBE, RPBE and revPBE, we get similar results. While the results obtained with the BLYP functional are worst. And for the LB94[82] functional, as it is written in ADF User Guide: *"The energy expression underlying the LB94 functional is very inaccurate"*, so we test and we verify that this functional should not be used in a LFDFT treatment.

3.1.2 Geometry Determination

Two cases can be considered: we know the geometry of the compound from X-ray crystallographic data or not. In the first case, we just have to run a single point calculation on the structure given by the X-ray crystallographic data to know how to specify the occupations for the AOC calculations. Otherwise, we have to do a geometry optimization and then, we choose LDA functional (*cf.* Fig. 3.2) if we have to deal with a small (a tenth of atoms) and negatively charged system because GGA functional overestimate the metal to ligand bond length[83] but GGA functional could be used for cases like porphyrin. In fact, our experience is that for small and negatively charged compounds, geometry optimization with LDA functional gives a very close bond distance compared to experimental data. The Figure 3.2 corresponds to the input for a geometry optimization run.

Whatever the case, the Kohn-Sham orbital diagram is examined to determine which are the molecular orbitals (MO) with a dominant d-character. This KS-MO diagram figures in the output file under the section *List of all MOs, ordered by energy, with the most significant SFO gross populations* and Figure 3.4 shows a part of the KS-MO diagram for the $[CoCl_4]^{2-}$ complex.

[a] However, for each chapter or new calculations, a footnote like this one will summarize the settings: the frozen core approximation, the type of basis sets and the functional used. I will also specify if the geometry comes from either an optimization of geometry or X-ray crystallographic data.

```
TITLE CoCl4

ATOMS cartesian
Co 0.000000 0.000000 0.000000
Cl 1.316090 1.316090 1.316090
Cl -1.316090 -1.316090 1.316090
Cl -1.316090 1.316090 -1.316090
Cl 1.316090 -1.316090 -1.316090
END

BASIS
Co /atomicdata/TZP/Co.3p
Cl /atomicdata/TZP/Cl.2p
END

XC
LDA vwn
END

CHARGE -2

EPRINT
ORBPOPER -1000 1000
END

GEOMETRY
OPTIM cartesian
END

END INPUT
```

Figure 3.2: *Example of the geometry optimization input for the* $[CoCl_4]^{2-}$ *complex.*

```
TITLE CoCl4 AOC

ATOMS cartesian
Co 0.000000 0.000000 0.000000
Cl 1.316090 1.316090 1.316090
Cl -1.316090 -1.316090 1.316090
Cl -1.316090 1.316090 -1.316090
Cl 1.316090 -1.316090 -1.316090
END

BASIS
Co /atomicdata/TZP/Co.3p
Cl /atomicdata/TZP/Cl.2p
END

XC
GGA PW91
END

RESTRICTED
CHARGE -2

OCCUPATIONS
A1 4
T1 6
T2 18 4.2
E 4 2.8
END

END INPUT
```

Figure 3.3: *Example of the AOC calculation input for the* $[CoCl_4]^{2-}$ *complex.*

E(eV)	Occ	MO	%	SFO (first member)	E(eV)	Occ	Fragment
3.748	2.00	2 E:1	84.10%	1 D:z2	-8.771	1.40	1 Co
			15.77%	1 P:x	-8.688	1.67	2 Cl
3.748	2.00	2 E:2	84.10%	1 D:x2-y2	-8.771	1.40	1 Co
			15.77%	1 P:x	-8.688	1.67	2 Cl
4.041	1.00	4 T2:1	73.04%	1 D:yz	-8.771	1.40	1 Co
			22.49%	1 P:x	-8.688	1.67	2 Cl
			2.72%	1 P:y	-8.688	1.67	2 Cl
			1.47%	1 P:x	-0.498	0.00	1 Co
4.041	1.00	4 T2:2	73.04%	1 D:xz	-8.771	1.40	1 Co
			22.49%	1 P:y	-8.688	1.67	2 Cl
			2.72%	1 P:x	-8.688	1.67	2 Cl
			1.47%	1 P:y	-0.498	0.00	1 Co
4.041	1.00	4 T2:3	73.04%	1 D:xy	-8.771	1.40	1 Co
			22.49%	1 P:z	-8.688	1.67	2 Cl
			2.72%	1 P:x	-8.688	1.67	2 Cl
			1.47%	1 P:z	-0.498	0.00	1 Co

Figure 3.4: *Part of the KS molecular orbital diagram (after removing MO's which are not involving the TM d-orbitals) of a geometry optimization output. This occupation corresponds to the ground state configuration.*

In Figure 3.4, the first column corresponds to the eigenvalues of the MO's, the second to the electronic occupation, the third to the number and the label of the MO considered, the fourth and the fifth contain information about the construction of the MO: the MO are build in ADF from SFO, the fourth column gives the square of the coefficient and the fifth the label of the SFO constituting the MO, the sixth gives the eigenvalues of the SFO, the seventh the electronic occupations of the SFO, finally the last column specifies from which atom the SFO comes from (number and label of the atom).

3.1.3 AOC

This step consists in a spin-restricted DFT calculation with an equal electronic occupation on each MO with dominant *d*-character. In our example the cobalt cation has a d^7 configuration so we have to occupy each of the 5 MO with dominant *d*-character by $7/5 = 1.4$ electrons. In a tetrahedral environment, like in our example, the crystal field splitting has to be considered, it means $3 \times 1.4 = 4.2$ electrons on the t_2 MO and $2 \times 1.4 = 2.8$ electrons on the e MO (*cf.* Fig. 3.3). As a result, the Kohn-Sham orbitals obtained are best suited for a ligand field treatment (*cf.* Fig. 3.5) because they comply with the spherical symmetry inherent to ligand field theory. This recipe is consistent with the prerequisites of the LF approach, where orbital relaxation is only taken into account at the level of averaging the electron density to provide proper LF orbitals, while all SD energies for latter LF treatment are calculated without SCF iteration.[84]
Comparing Fig. 3.4 & Fig. 3.5, we can underline the fact that the occupations are different (second column) and the eigenvectors (fourth column represents its square) and eigenvalues (first column) are also different.

E(eV)	Occ	MO	%	SFO (first member)	E(eV)	Occ	Fragment
3.396	1.40	2 E:1	80.92%	1 D:z2	-8.771	1.40	1 Co
			19.04%	1 P:x	-8.688	1.67	2 Cl
3.396	1.40	2 E:2	80.92%	1 D:x2-y2	-8.771	1.40	1 Co
			19.04%	1 P:x	-8.688	1.67	2 Cl
3.913	1.40	4 T2:1	71.73%	1 D:yz	-8.771	1.40	1 Co
			23.69%	1 P:x	-8.688	1.67	2 Cl
			2.89%	1 P:y	-8.688	1.67	2 Cl
			1.50%	1 P:x	-0.498	0.00	1 Co
3.913	1.40	4 T2:2	71.73%	1 D:xz	-8.771	1.40	1 Co
			23.69%	1 P:y	-8.688	1.67	2 Cl
			2.89%	1 P:x	-8.688	1.67	2 Cl
			1.50%	1 P:y	-0.498	0.00	1 Co
3.913	1.40	4 T2:3	71.73%	1 D:xy	-8.771	1.40	1 Co
			23.69%	1 P:z	-8.688	1.67	2 Cl
			2.89%	1 P:x	-8.688	1.67	2 Cl
			1.50%	1 P:z	-0.498	0.00	1 Co

Figure 3.5: *KS orbital diagram of the AOC calculation (after removing parts which are not involving the MO without dominant d-character). We can remark that the occupations are different than in Fig 3.4.*

3.1.4 Slater Determinant Calculation

n	2 or 8	3 or 7	4 or 6	5
number of SD	45	120	210	252

Table 3.2: *Number of SD originating from an open d^n shell.*

The SD calculation consists in a spin-unrestricted calculation of all Slater determinants originating from the d^n configuration (*cf.* Table 3.2). Figure 3.6 shows an input file for our example just for one single determinant: since the cobalt has a d^7 configuration, the normal input has 120 SD. We use as we can see in the input (*cf.* Fig. 3.6), the AOC calculation as a fragment, in doing so, the KS-MO diagram is frozen and during the calculation no SCF procedure occurs. At this step the program changes only the occupations on the *d*-shell according to the *SLATERDETERMINANTS* keyword list in the input. The program *chem.x*, presented in Appendix B.1, is designed to create the input of SD calculation. The output consists then in a list of all the SD energies. It is important to make two remarks concerning this input file. Firstly, the configurations of some Slater determinants are not compatible with the real symmetry of the compound, as a consequence a lower symmetry must be imposed (Nosym in Fig 3.6). Secondly the SD calculation is an unrestricted calculation but the net total spin polarization value doesn't have to be precise for the *CHARGE* keyword because this value changes for each SD.

```
Title Cocl4 SD calculation

Atoms cartesian
Co 0.00000 0.00000 0.00000 f=Av
Cl 1.31609 1.31609 1.31609 f=Av
Cl -1.31609 -1.31609 1.31609 f=Av
Cl -1.31609 1.31609 -1.31609 f=Av
Cl 1.31609 -1.31609 -1.31609 f=Av
End

Charge -2

Unrestricted

Fragments
Av /home/rauzy/cocl4_aoc.TAPE21
End

XC
GGA PW91
End

Symmetry Nosym

SLATERDETERMINANTS
SD 1
A1 2 // 2
E:1 1 0 // 1 0
E:2 1 0 // 1 1
T1:1 1 // 1
T1:2 1 // 1
T1:3 1 // 1
T2:3 3 1 // 3 1
T2:2 3 1 // 3 1
T2:1 3 1 // 3 1
SUBEND
END

End Input
```

Figure 3.6: *Example of a SD calculation input for* $[CoCl_4]^{2-}$.

3.2 Extraction of Data

In LFDFT, we have to extract from the AOC DFT calculations the eigenvectors of the KS molecular orbitals with dominant *d*-character and get the list of SD energies from the SD calculations.

3.2.1 Eigenvectors and Eigenvalues of the Kohn-Sham Orbitals

In this section we explain how to extract eigenvectors and eigenvalues of the KS orbitals for a non relativistic calculation. The extraction of eigenvalues is not necessary for the LFDFT program but it is useful to compare them to the LF matrix after LFDFT treatment.

3.2.1.1 Eigenvectors of KS Orbitals

The determination of the MO eigenvectors is a key point in the LFDFT method. This process can not be easily programmed and we have to do it manually. When the eigenvectors are extracted, they are arranged in a 5×5 matrix format where the columns represent the MO's and the lines represent the d-AO's. The line should be arranged from $m=-l$ to $m=l$ so for a d-shell from $m=-2$ to $m=2$ which corresponds to the following orbital order: d_{xy} , d_{yz} , d_{z^2} , d_{xz} , $d_{x^2-y^2}$ (order fixed by the program "*gener_ln*"). The order of the column is fixed by the program "*chem.x*" and to be consistent with the order of the line, the first column should correspond to the MO which is dominated by d_{xy} , the second to the MO dominated by d_{yz} and so on until $m=2$ for d-shell (in this way we have always the bigger coefficients on the diagonal).
To determine the eigenvectors we have first to note, in the *List of all MOs* section of the AOC calculation output, the numbers and the labels of the MO's with dominant d-character (for our example: 2 E:1, 2 E:2, 4 T2:1, 4 T2:2 and 4 T2:3, *cf.* Fig 3.5). Then in the "*B U I L D*" section of the AOC calculation output, we have to look for the subsections of each MO previously defined: Figure 3.7 corresponds to E:1 MO for our example.

=== E:1 ===

Nr. of SFOs : 8

Cartesian basis functions that participate in this irrep (total number = 81) :

38	36	37	61	59	60	84	82	83	107
105	106	15	10	13	21	16	19	27	22
25	44	42	43	67	65	66	90	88	89
113	111	112	47	45	46	70	68	69	93
91	92	116	114	115	50	48	49	73	71
72	96	94	95	119	117	118	56	51	54
79	74	77	102	97	100	125	120	123	53
55	52	76	78	75	99	101	98	122	124
121									

SFO indx	(index incl.CFs)	Fragment Occup	Orb.Energy	Generating FragmentType	Expansion in Fragment Orbitals Coeff.	Orbital	on Fragment
1	13	1.400	-0.322 au (-8.771 eV)	Co	1.00	1 D:z2	1
2	14	–	0.530 au (14.418 eV)	Co	1.00	2 D:z2	1
3	15	–	5.236 au (142.490 eV)	Co	1.00	3 D:z2	1

Figure 3.7: *Part of the "B U I L D" section of the AOC calculation output for the MO E:1.*

In the column *index incl.CFs*, we have to obtain the number corresponding to the line where the occupation is not null and where the orbital corresponds to a *d*-AO of the Cobalt cation (for our example: 13). Once we know the irrep numbers (2 for the *E* orbitals for our example) and the SFO index (13), under the E:1 part of the "*SFO MO coefficients*" section of the AOC calculation output, which is a matrix where the columns represent the number of the MO's and the lines represent the SFO index (*cf.* Figure 3.8), we take the value corresponding to the line with the label 13 and the column with the label 2.

=== E:1 ===

MOs expanded in CFs+SFOs

MOs :	1	2	3	4	5	6	7	8
13	0.3813	-0.9260	0.0859	0.1467	-0.0288	-0.1414	0.0499	0.0609
14	-0.0343	0.0396	-0.0683	0.4135	-0.0173	1.1269	-0.1916	-0.1877
15	0.0016	-0.0009	-0.0037	0.0041	0.0014	-0.0163	0.0187	-1.0282
16	-0.8563	-0.4882	-0.0913	-0.1476	0.0027	-0.3832	0.0856	0.1910
17	0.0417	0.0537	-0.9665	0.1099	0.1487	0.2568	-0.0701	-0.1372
18	-0.0013	-0.0024	-0.0127	-0.0017	-0.0089	0.0506	1.0138	0.0665
19	0.0146	-0.0341	0.0720	-0.5129	0.7460	0.5180	-0.0405	-0.1238
20	-0.0187	0.0303	0.0800	0.6107	0.6596	-0.5025	0.0921	0.1297

Figure 3.8: *Part of the "SFO MO coefficients" section of the AOC calculation's output.*

We do the same for the five MO's, then we can build the matrix $\boldsymbol{U}$ (in a matlab format) which represents the eigenvectors of the MO with dominant *d*-character respecting the order previously defined (Eq. 3.1).

$$\boldsymbol{U} = \begin{bmatrix} -0.8863 & 0 & 0 & 0 & 0 \\ 0 & -0.8863 & 0 & 0 & 0 \\ 0 & 0 & -0.9260 & 0 & 0 \\ 0 & 0 & 0 & -0.8863 & 0 \\ 0 & 0 & 0 & 0 & -0.9260 \end{bmatrix}; \tag{3.1}$$

We can underline that for highly symmetric compounds the matrix is diagonal but if we go down in symmetry then we generally have a mixing between MO's belonging to the same irrep, in this case the matrix is no more diagonal. With C_1 symmetry, we can have each matrix elements different than zero depending on the mixing.

3.2.1.2 Eigenvalues of KS Orbitals

It is relevant but not necessary to get the eigenvalues of MO's from the AOC calculation output and compare them to the LF matrix. The eigenvalues correspond to the first column of the Figure 3.5.

3.2.2 Energies of Slater Determinants

In the output of Slater determinant calculations figures the list of all the SD energies. It is possible to extract them directly in a vector format with the script based on *awk* language given in Appendix B.2.1. This script acts on the logfile, summary of the output for an ADF calculation, and can be modified to list either the LDA or the GGA SD energies. The execution of this script on the logfile of a SD calculation creates a file *esd* which can be directly loaded by the LFDFT program.

3.3 LFDFT: Theory

As we know how to extract all the data necessary to run the LFDFT program. In this section, we describe the LFDFT method and then give the source code of the LFDFT program.

3.3.1 Introduction

If we consider an octahedral complex, the LF matrix is reduced to one parameter: $10Dq$. We thus have for each SD energy the simple linear expression in terms of B, C and $10Dq$ (Eq. 3.2):

$$\begin{aligned} E(SD^d_\mu) &= E(det|d_{i(\mu,1)}\sigma_{i(\mu,1)}d_{i(\mu,2)}\sigma_{i(\mu,2)}\dots d_{i(\mu,n)}\sigma_{i(\mu,n)}|) \\ &= \sum_i \langle d_i|h_{LF}|d_i\rangle + \sum_{i<j}(J_{ij} - K_{ij}\delta_{\sigma_i\sigma_j}) \\ &= \frac{3m_\mu - 2n_\mu}{5}10D_q + \beta_\mu B + \gamma_\mu C + E_0 \end{aligned} \tag{3.2}$$

The single determinants SD^d_μ are labeled with the subscript $\mu = 1, \dots, \binom{10}{n}$ and with the superscript d to refer to pure d-spinorbitals. The values of m_μ and n_μ specify the electronic configuration $t_{2g}^{n_\mu} e_g^{m_\mu}$ while the β_μ and γ_μ are coefficients obtained after substituting standard expressions for the Coulomb J_{ij} and exchange K_{ij} integrals in terms of d-only orbitals d_i and spin functions σ_i (*cf.* Table 2.1). Having obtained energy expressions of each SD^d_μ, we can determine the ligand field parameters $10Dq$, B and C plus a shift parameter E_0 which is due to the different gauge origin between the DFT and the LF approach. We obtain the Equation 3.3 in which $\vec{X}$ stores the ligand field parameters we should determine plus the shift energy E_0, $\vec{E}$ is an array composed by the SD energies calculated by DFT and $\boldsymbol{A}$ is a matrix which stores the coefficients of the Equation 3.2 (*cf.* Table 3.4):

$$\vec{E} = \boldsymbol{A}\vec{X} \tag{3.3}$$

Eq. 3.3 represents a system of linear equations which is overestimated. We can solve it by least square fit (Eq. 3.4) to obtain the LF parameters:

$$\vec{X} = (\boldsymbol{A}^T\boldsymbol{A})^{-1}\boldsymbol{A}^T\vec{E} \tag{3.4}$$

Then we are able to compare SD energies from DFT with those calculated using the LF parameter values. The determination of the mean square deviation allows us to estimate the accuracy of the fit.

3.3.2 Theory

On one side from the effective Hamiltonian theory,[85,86] we can approximate the h_{ab} LF matrix by using the five KS orbitals with dominant d-character. On the other side, according to the work of Ziegler *et al.*,[10] it is possible to use the single determinant energies obtained by DFT in a LF scheme.
From the first remark, we can extract as it is shown in Section 3.2.1.1, the eigenvectors of the MO's, which correspond to the five MO's orbitals with dominant d-character, and store them in the matrix $\boldsymbol{U}$. Then we introduce the overlap matrix $\boldsymbol{S}$ (Eq. 3.5):

$$\boldsymbol{S} = \boldsymbol{U}\boldsymbol{U}^T \tag{3.5}$$

Since **U** is in general not orthogonal, we use the Löwdin's symmetric orthogonalisation scheme to obtain an equivalent set of orthogonal eigenvectors ($\boldsymbol{C}$):

$$\boldsymbol{C} = \boldsymbol{S}^{-1/2}\boldsymbol{U} \tag{3.6}$$

We identify now these vectors as the eigenfunctions of the effective LF Hamiltonian h_{LF}^{eff} we seek as:

$$\varphi_i = \sum_{i=1}^{5} c_{\mu i} d_\mu \tag{3.7}$$

Thus, the fitting procedure described in the previous section enable us to estimate $h_{ii} = \langle\varphi_i|h_{LF}^{eff}|\varphi_i\rangle$ and hence the full representation matrix of h_{LF}^{eff} as:

$$h_{\mu\nu} = \langle d_\mu|h_{LF}^{eff}|d_\nu\rangle = \sum_{i=1}^{5} c_{\mu i} h_{ii} c_{\nu i} \tag{3.8}$$

The energy of a single determinant becomes thus:

$$\begin{aligned} E(SD_k^{\varphi}) &= E(det|\varphi_{i(k,1)}\sigma_{i(k,1)}\varphi_{i(k,2)}\sigma_{i(k,2)}\cdots\varphi_{i(k,n)}\sigma_{i(k,n)}|) \\ &= \sum_i \langle\varphi_i|h_{LF}|\varphi_i\rangle + \sum_{i<j}(J_{ij} - K_{ij}\delta_{\sigma_i\sigma_j}) \end{aligned} \tag{3.9}$$

where SD_k^{φ} is composed of the spinorbitals.
In order to calculate the electrostatic contribution (2^{nd} term in Eq. 3.9), it is useful to consider basis transformation. So first $\boldsymbol{C}$ is transformed from the orbital basis to the spin-orbital basis:

$$\boldsymbol{C} = \boldsymbol{C} \otimes \sigma \tag{3.10}$$

and then we consider the following transformation from the basis of SD_k^{φ} to the one of SD_ν^d. Using basic linear algebra, we get:

$$|SD_k^{\varphi}\rangle = \sum_\mu T_{k\mu}|SD_\mu^d\rangle \tag{3.11}$$

where $T_{k\mu} = det|c_{i(k,1:n),j(\mu,1:n)}|$ i.e. the determinant of a $n \times n$ sub-matrix of $\boldsymbol{C}$:

$$\begin{vmatrix} c_{i(k,1),j(\mu,1)} & c_{i(k,1),j(\mu,2)} & \cdots & c_{i(k,1),j(\mu,n)} \\ c_{i(k,2),j(\mu,1)} & c_{i(k,2),j(\mu,2)} & \cdots & c_{i(k,2),j(\mu,n)} \\ \cdots & \cdots & \cdots & \cdots \\ c_{i(k,n),j(\mu,1)} & c_{i(k,n),j(\mu,2)} & \cdots & c_{i(k,n),j(\mu,n)} \end{vmatrix} \tag{3.12}$$

with the indices of the spinorbitals $\varphi_{i(k,j)}\sigma_{i(k,j)}$ and $d_{i(\mu,j)}\sigma_{i(\mu,j)}$ respectively. Note that these indices are in fact a two-dimensional array of (*number of SD*) $\times$ (*number of electrons or holes*) integers. Finally the energy of a SD in Eq. 3.9 can be rewritten as:

$$E_k = E(SD_k^{\varphi}) = \sum_i \langle\varphi_i|h_{LF}|\varphi_i\rangle + \sum_{\mu,\nu} T_{k\mu}T_{k\nu}\langle SD_\mu^d|\frac{1}{r_{12}}|SD_\nu^d\rangle \tag{3.13}$$

where G =$1/r_{12}$ i.e. the electrostatic repulsion of all electron pairs in the LF manifold. The matrix elements are obtained using the Slater's rules (*cf.* Section 2.1.3) and the resulting electrostatic two-electron integrals $\langle ab|cd\rangle$ in terms of Racah's parameters. Thus the final equation to estimate the ligand field matrix h_{ab} and the B and C Racah's parameters from the DFT energies, E_k of all the SD within the LF manifold, has the same shape than Eq 3.3 where $\vec{X} = (h_{11}, \ldots, h_{55}, B, C)$ and $\boldsymbol{A}$ are calculated as indicated above (Eq. 3.13). The Matlab script, the LFDFT program, to carry out these calculations for all d^n configurations is proposed in the next section.

3.4 LFDFT: Program

Now, the source code of the LFDFT program is presented in Figure 3.9 with comments referring to previous equations. We have to specify as input $\boldsymbol{U}$, *ne* and *esd* which are, respectively, the eigenvectors of MO with dominant d character (structured as Eq 3.1, the order of d-orbitals being from $m = -2$ to $m = 2$), the number of electron on the d-shell and the list of single determinant energy. One way to do it is to put $\boldsymbol{U}$ and *ne* in a file *matrice.m* and change the name of the file produce by the script *get.x* (*cf.* Appendix B.2.1) from *esd* to *esd.mat* (the energies should be expressed in eV). In the second line of the program, the first one cleaning the memory and the screen, this two files are loaded in the same time than *data.mat* generated by the *Gener_ln* program (presented in section 4.2.3). The *data.mat* file contains 4 matrices *ir, gdata, lfdata* and *lsdata* and we can remark that for the LFDFT program, only the two matrices *ir* and *gdata* are used.
A plot function at the end of the program produces for our example the Figure 3.10 where the x-axis refers to SD and the y-axis corresponds to the energy: for each SD, there are two marks: one referring to the energy calculated by DFT ($*$) and the second to the LFDFT values ((o), SD energies calculated using the B, C and $10Dq$ parameters previously fitted). If for each SD we compare the two marks, we can then appreciate the accuracy of the fit. This kind of picture plus the calculation of the mean square deviation are the two possibilities we haveto appreciate the accuracy of the fit.

```
clc, clear all,
matrice, load data, load esd
if (ne>5), ne=10-ne, end
kphi=ir;[nsd nf]=size(kphi); kkp=0;
for k=1:nsd
  for kp=1:k
    kkp=kkp+1; gb(k,kp)=gdata(kkp,2); gc(k,kp)=gdata(kkp,3);
    if(k =kp)
      gb(kp,k)=gdata(kkp,2); gc(kp,k)=gdata(kkp,3);
    end
  end
end
% Löwdin orthogonalisation: Eqs 3.5 & 3.6
S = U*U'; Shalf=S^(-0.5); S = Shalf*U;
% from orbital basis to spin-orbital basis: Eq 3.10
e=[1 0; 0 1];
c=[S(1,1)*e S(1,2)*e S(1,3)*e S(1,4)*e S(1,5)*e;
S(2,1)*e S(2,2)*e S(2,3)*e S(2,4)*e S(2,5)*e;
S(3,1)*e S(3,2)*e S(3,3)*e S(3,4)*e S(3,5)*e;
S(4,1)*e S(4,2)*e S(4,3)*e S(4,4)*e S(4,5)*e;
S(5,1)*e S(5,2)*e S(5,3)*e S(5,4)*e S(5,5)*e];
c=c';
% get t: |ψ_i⟩ = T_{i,μ} × |φ_μ⟩: Eq 3.12
t=zeros(nsd,nsd);
for i=1:nsd
  for mu=1:nsd
    t(i,mu)=det(c(kphi(i,:),kphi(mu,:)));
  end
end
% Setup LF-model
ivar=[1 1 2 2 3 3 4 4 5 5]; a=zeros(nsd,7);
for i=1:nsd
  for j=1:nf
    k=ivar(ir(i,j));
    a(i,k)=a(i,k)+1;
  end
end
% electrostatic part
a(:,6)=diag(t*gb*t'); a(:,7)=diag(t*gc*t');
% Least square fit: Eq 3.4
lf=inv(a'*a)*a'*esd;
% from eV to cm-1 and calculation of Racah's parameter B and C
lf=lf*8065; B=lf(6); C=lf(7);
fprintf('Racah B= %8.3f cm-1 \n',B), fprintf('Racah C= %8.3f cm-1 \n',C)
% predicted energies of SD
f=a*lf;
% Standard deviation: Eq B.2.4
diff=esd*8065-f; mean=(sqrt(sum(diff.^2))/nsd);
fprintf('Standard deviation: %8.3f cm-1 \n',mean)
% plot function to make figure as the Fig. 3.10
X=1:1:nsd; f=f/8065; plot(X,esd,'*',X,f,'o')
% ligandfield matrix in cm-1
h=S*diag(lf(1:5))*S'
```

Figure 3.9: *Source code of the* **LFDFT** *program.*

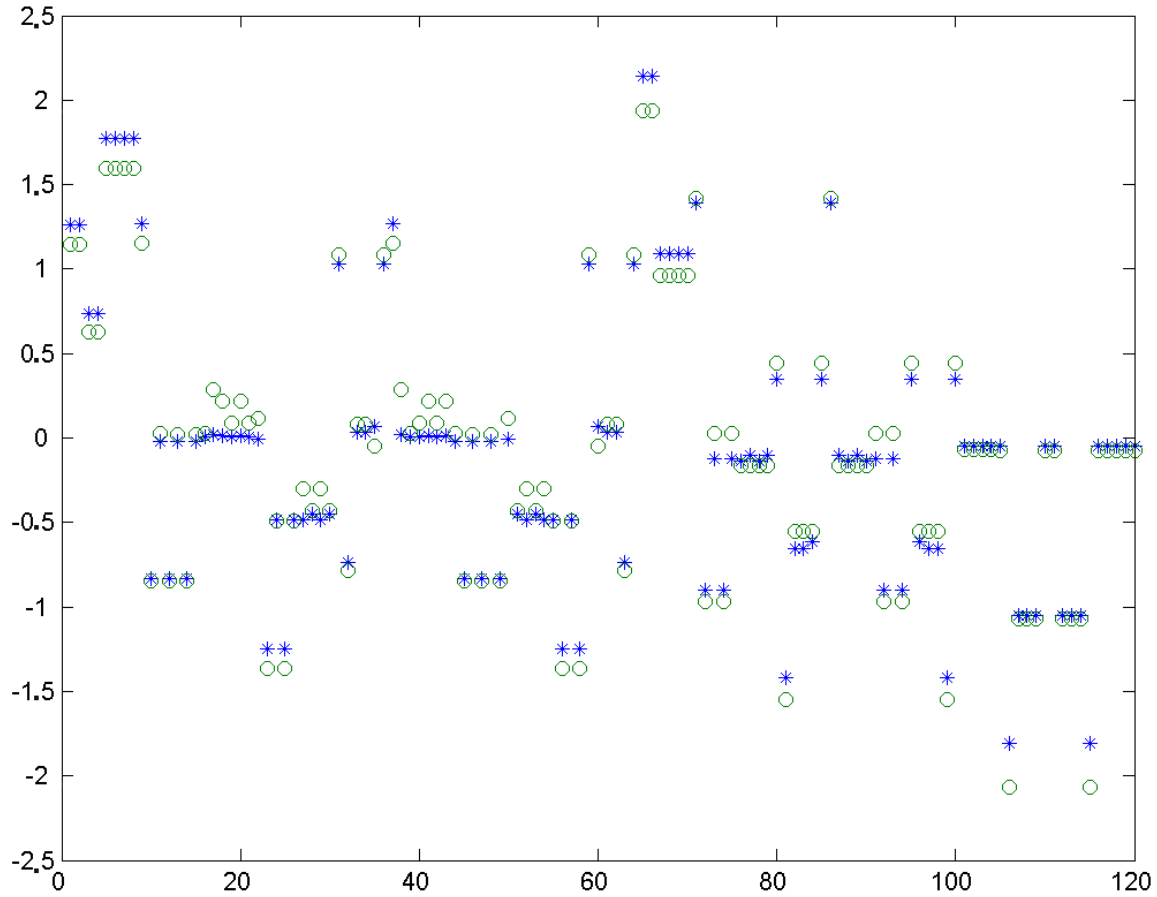

Figure 3.10: *Comparison between SD energies from DFT calculation (∗) and from LFDFT calculation (o). The x-axis refers to SD and the y-axis corresponds to the energy in eV. In fact the 0 eV energy corresponds to the reference which is the energy of the AOC calculation.*

3.5 LFDFT: Applications

In this section, the LFDFT method is applied to some compounds whose UV-Vis spectra can be found in the literature. During the course of this Ph.D., many systems have been studied and the results obtained have been published in two articles.[32,35] Here, only a selection of these results is presented.

3.5.1 Cubic d^2 Systems

The main idea behind our approach is presented using a simple example: CrO_4^{4-}, a d^2 (Cr^{IV}) TM in a tetrahedral coordination environment.[c] We solve the Equation 3.4 where $\vec{E}$ is an array of the 45 SD energies from the DFT calculation (originating from d^2 open shell system) and $\boldsymbol{A}$ stores the coefficients of the 45 linear equations corresponding to Eq 3.2.

[c]The AOC calculation was performed with $e^{4/5}t_2^{6/5}$ using LDA VWN functional (for AOC and SD calculations) and TZP basis sets (IV for ADF v2000.01) with a frozen core approximation up to $3p$ for Co and up to $1s$ for O.

The Racah's parameters B, C and $10Dq$ are then determined by least square fit. We did the manipulation for a geometry optimized using LDA functional and for the experimental geometry.[87] In Table 3.3, we compare the results with those fitted from a UV-Vis spectra. We can see that the results obtained with experimental bond length are really close with the results fitted from the spectra, in spite of the fact that B values are underestimated by the LFDFT procedure. From the list of single determinant energies ($\vec{E}$), we can underline that only 15 SD energies are different at the DFT level (*cf.* Table 3.4), however we take all 45 equations into account. In doing so, we provide a better statistical weight for those SD which have the same energy. In Table 3.4, the 15 non redundant SD energies are given as well as the energy expression in the LF model (the energy of the $|\theta^{+}\varepsilon^{+}|$ ground state is taken to zero and the other energies are expressed relatively to this one).

	R_{opt}	R_{exp}	Exp [b]
$R = d_{Cr-O}$	1.868	1.77[87]	-
B	436	427	555
C	2250	2274	2331
$10Dq$	7315	8847	8950
$(10Dq)_{MO}$	7363	8831	-
$StDev$	290	314	-

Table 3.3: *Comparison between the Racah's parameters obtained from LFDFT calculation for an optimized Cr-O bond length (LDA) and the experimental Cr-O bond length with values fitted from a LF spectra for* CrO_4^{4-} *(values in* cm^{-1}*).*

A comparison between the SD energies calculated by DFT and the SD energies calculated using Equation 3.2 by replacing B, C and $10Dq$ with the values determined by LFDFT shows a nice fit with a rather small standard deviation (0.039 eV). This result illustrates the consistency between the DFT formalism and the LF parameterization.
Moreover, one can make two remarks about the $10Dq$:

- the value of $10Dq$ for the experimental geometry is really close to the one fit from the UV-Vis spectra as we know that $10Dq$ is sensible to the metal to ligand bond length. So if the experimental structure is known, one should use it to run LFDFT calculation,
- the fitted $10Dq$ value is very close to the $10Dq_{\mathrm{MO}}$.

3.5.2 Cubic d^n Systems

The procedure described above has been extended to d^n TM complexes (the number of SD resulting from a d^n configuration is stored in Table 3.2) and the ligand field parameters $10Dq$, B, C have been obtained as for the previous cubic d^2 example. The Table 3.5 is a summary of the results published in the article of the Structure and Bonding volume dedicated to Jørgensen.[32] In the same time, we compared the values obtained by LFDFT to the values fitted directly to experimental LF transition energies (which we call "LFT"). We can underline, that when we use an experimental bond length, the results are very close to the values fitted from the experimental data as we know that $10Dq$ depends strongly on the metal to ligand bond length. The calculations were performed using LDA functional (VWN for AOC and SD calculations) and TZP basis sets with the frozen core approximation; up to $2p$ for TM, $1s$ for C, O, N and F, $2p$ for Cl, and $3d$ for Br.

[b] The abbreviation "Exp" means values fitted from the LF spectra.

Table 3.4: *Energy expressions for the DFT distinguishable Slater determinants of a d^2-configuration in a cubic ligand field and their DFT energies for the tetrahedral CrO_4^{4-} complex. The energy expressions of each determinant within the conventional LFT model (B, C, 10Dq parameterization) are also included.*

SD	DFT Energies CrO_4^{4-}	LF Model (B, C, $10Dq$)
$\|\theta^+\theta^-\|$	1.571	$12B + 3C$
$\|\varepsilon^+\varepsilon^-\|$	1.557	$12B + 3C$
$\|\theta^+\varepsilon^+\|$	0	0
$\|\theta^+\varepsilon^-\|$	0.379	$4B + C$
$\|\theta^+\xi^+\|$	1.564	$9B + 10Dq$
$\|\theta^+\xi^-\|$	1.905	$10B + C + 10Dq$
$\|\theta^+\varsigma^+\|$	1.154	$10Dq$
$\|\theta^+\varsigma^-\|$	1.506	$4B + C + 10Dq$
$\|\varepsilon^+\xi^+\|$	1.288	$3B + 10Dq$
$\|\varepsilon^+\xi^-\|$	1.633	$6B + C + 10Dq$
$\|\varepsilon^+\varsigma^+\|$	1.690	$12B + 10Dq$
$\|\varepsilon^+\varsigma^-\|$	2.031	$12B + C + 10Dq$
$\|\xi^+\xi^-\|$	3.573	$12B + 3C + 20Dq$
$\|\xi^+\eta^+\|$	2.471	$3B + 20Dq$
$\|\xi^+\eta^-\|$	2.811	$6B + C + 20Dq$

Complex		B	C	$10Dq$
CrO_4^{4-}	R_{opt}	436	2250	7315
d^2	R_{exp}	427	2274	8847
	LFT	555	2331	8950
MnO_4^{3-}	R_{opt}	347	1928	9831
d^2	R_{exp}	347	1936	10872
	LFT	430	2600	10515
FeO_4^{2-}	R_{opt}	242	1637	11259
d^2	R_{exp}	242	1645	11952
	LFT	375	1388	12938
$CrCl_4$	R_{opt}	355	1903	7008
d^2	LFT	376	1579	7250
$MnCl_4^-$	R_{opt}	548	2339	3298
d^5	LFT	516	3363	2661

Table 3.5: *Values of B, C and $10Dq$ for various tetrahedral (left) and octahedral (right) complexes, deduced from LFDFT energies (R_{opt} means LFDFT procedure using an LDA optimized structure and R_{exp} means LFDFT procedure using experimental structure) and compared to values obtained from experimental ligand field spectra (LFT).*

Complex		B	C	$10Dq$
CrF_6^{3-}	R_{opt}	605	2694	13598
d^3	LFT	734	3482	15297
$CrCl_6^{3-}$	R_{opt}	484	2403	10911
d^3	LFT	550	3450	12800
$CrBr_6^{3-}$	R_{opt}	427	2395	9816
d^3	LFT	543	3296	12400
$Cr(CN)_6^{3-}$	R_{opt}	452	1919	30760
d^3	LFT	554	2559	26595
$Mn(CN)_6^{3-}$	R_{opt}	444	2361	34085
d^4	LFT	630	2598	36900
$Co(CN)_6^{3-}$	R_{opt}	387	2573	37180
d^6	LFT	456	3184	34944
$Fe(CN)_6^{4-}$	R_{opt}	427	2420	35421
d^6	LFT	411	3566	33678
$CoCl_6^{4-}$	R_{opt}	573	2540	3952
d^7	R_{exp}	548	2436	7436
	LFT	795	3108	7206
$CoBr_6^{4-}$	R_{opt}	492	2444	3782
d^7	R_{exp}	460	2371	6387
	LFT	808	3159	6384

3.5.3 Application to Model the Nephelauxetic Effect

The nephelauxetic effect is modeled using LFDFT on complexes with Cr^{4+}, Mn^{5+} and Fe^{6+} cations which have a d^2 configuration. To evaluate the nephelauxetic effect, we have in a first time to calculate the B_0 and C_0 parameters (Racah's parameters for the free-ion) for each free-ion in a gas phase and the results are stored in the Table 3.6. In this table we compare these values to the ones fitted from atomic spectra (LFT). In a second time, we determine, using the LFDFT method, Racah's parameters for the oxide of these cations, i.e. CrO_4^{4-}, MnO_4^{3-}, FeO_4^{2-} and for the halogen series with the cromium cation, i.e. $[CrF_4]$, $[CrCl_4]$, $[CrBr_4]$ and $[CrI_4]$. The B and C parameters for these complexes are given in Table 3.7.

		LFDFT	LFT
Cr^{4+}	B_0	927	1015
	C_0	4508	4263
Mn^{5+}	B_0	1044	1160
	C_0	5194	4930
Fe^{6+}	B_0	1153	1300
	C_0	5799	5525

Table 3.6: *B and C parameters (in cm^{-1}) for the Cr^{4+}, Mn^{5+} and Fe^{6+} cations derived from LFDFT (using LDA VWN functional and TZP basis sets with frozen core approximation up to 3p) calculations versus values deduced from a fit to atomic spectra (LFT).*

Complex	B	C
CrO_4^{4-}	436[555]	2250[2331]
MnO_4^{3-}	347[430]	1928[2600]
FeO_4^{2-}	242[375]	1637[1388]
CrF_4	476	2452
$CrCl_4$	355	1903
$CrBr_4$	347	1855
CrI_4	323	1758

Table 3.7: *Racah's parameters values (in cm^{-1}) for tetrahedral d^2 (MO_4^z: M(z): Cr^{IV} (-4) ; Mn^{V} (-3); Fe^{VI} (-2); CrX_4, X = F^-, Cl^-, Br^-, I^-) calculated using a LDA functional. Values for the oxo-anions, deduced from a direct fit to LF spectra are included in square brackets.*

The DFT calculations yield values of B which are by 10% smaller and values of C which are by 5 to 12% larger than experiment. In Fig 3.11 we plot the B/B_o and C/C_o ratios for the series of tetrahedral d^2 complexes. We can remark that B is more reduced than C which is in agreement with the study of Ferguson and Wood[88] on Co and Cr complexes. Moreover they claim that the parameters B and C probe influences from different regions in a complex; while B mirrors outer properties and is therefore more affected by covalency, C is a more inner parameter and thus less influenced by the TM-ligand bond. We fully confirm this statement here. The nephelauxetic reduction increases with increasing TM oxidation state from CrO_4^{4-} to MnO_4^{3-} to FeO_4^{2-} and with increasing covalency from F to Cl to Br to I, as it is seen from the series of compounds CrX_4(X = F, Cl, Br, I). It is interesting to note that the F and O in CrO_4^{4-} and CrF_4 are characterized by similar reduction factors, oxygen being slightly more covalent than F. Keeping in mind that the B is more reduced than C in a complex, the ratio B/C, which is usually assumed to be the same as that for the free ion ($C_o/B_o = 4.2 \pm 0.2$), might deviate strongly from it; it is found to increase from CrO_4^{4-} ($C/B = 5.16$) to MnO_4^{3-} (5.55) to FeO_4^{2-} (6.76), i.e. with increasing covalency. We should note, that is this assumption which has led to a definition of variable B values B_{33}, B_{35}, B_{55}.[36]

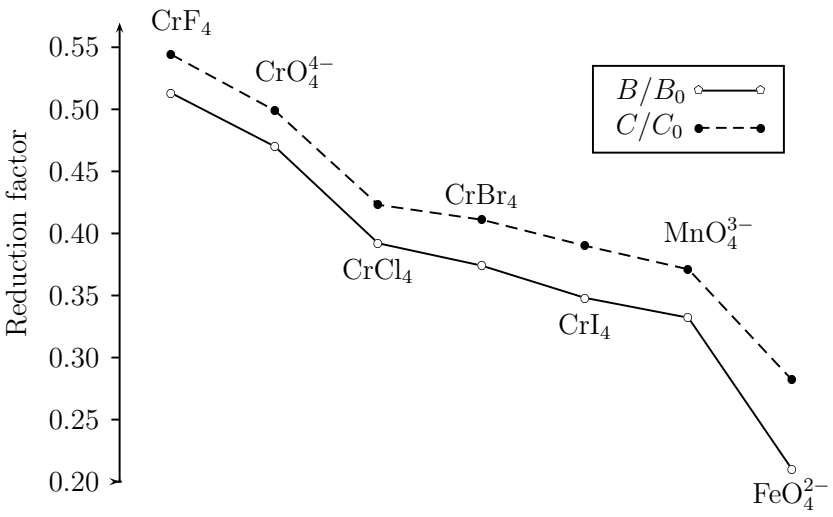

Figure 3.11: *The nephelauxetic reduction factors for B/B_o and C/C_o for the d^2 tetrahedral MO_4^z: M(z) : Cr^{IV}(-4); Mn^V(-3); Fe^{VI}(-2); CrX_4, X = F^-, Cl^-, Br^-, I^-.*

3.5.4 The Effect of Covalency on 10Dq

We have performed a series of calculations of the $(10\mathrm{Dq})_{CFT}$ values resulting to Cr^{3+} surrounded octahedrally by six (-1) point charges. $(10\mathrm{Dq})_{CFT}$ values are plotted against the Cr^{3+}-point charge distance in Fig. 3.12 along with the values of $(10\mathrm{Dq})_{LFDFT}$ that result from LDA geometry optimized CrF_6^{3-}, $CrCl_6^{3-}$ and $CrBr_6^{3-}$ complexes. Comparing the values of $(10\mathrm{Dq})_{CFT}$ corresponding to the Cr-F, Cr-Cl, Cr-Br distances (1.933, 2.419 and 2.588 Å) 0.321, 0.109 and 0.078 eV with the $(10\mathrm{Dq})_{LFDFT}$ 1.727, 1.336 and 1.193 eV respectively. We conclude that crystal field effect do not exceed 18% from the values of $(10\mathrm{Dq})_{LFDFT}$, the latter values being in good agreement with experiment.

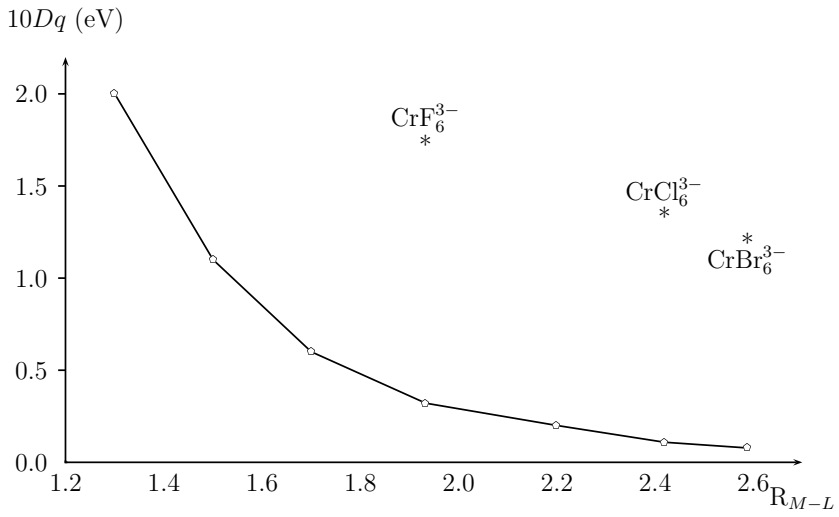

Figure 3.12: *10Dq values (in eV) versus the metal-ligand distance in the ionic (crystal field) approximation for Cr^{3+} cation surrounded octahedrally by six (-1) point charges at different distances (full line). DFT calculations of 10Dq for the LDA optimized geometries of CrX_6^{3-} (X = F, Cl, Br) are also plotted (∗).*

The next step is now to generalize the fitting procedure to treat systems with symmetry lower than cubic or even without any symmetry (C_1).

3.5.5 Applications to a Low Symmetrical Compound

As an application of a complex with low symmetry, we study a $Cr(NH_3)_6^{3+}$ chromophore which has a C_s symmetry. The GGA optimized structure with $R_{Cr-N} = 2.166$ to 2.284 Å yields a value of $10Dq$ resulting from averaging over the C_s split components of t_{2g} (a"+a"+a') and e_g(a'+a') of 19082 cm^{-1}, in reasonable agreement with the experiment (21550 cm^{-1}).[36] An electrostatic calculation taking six (-3) point charges for N and eighteen (+1) for H with coordinates from the $Cr(NH_3)_6^{3+}$ geometry optimization yields a $(10Dq)_{CFT}$ value of 0.435 eV, again reproducing only 18% of the total $(10Dq)_{LFDFT}$ value. We conclude again, that the bulk of the values $10Dq$ is due to covalency, in agreement with Jørgensen's original suggestion.[36]

3.6 General Conclusions

After the discussion of some results obtained by the LFDFT method, we can make some general comments on the method.

The Figure 3.10 confirms that the results obtained by least square fitting are accurate enough to be used because the difference of energies for each single determinant is small. In fact, the standard deviations (*cf.* Appendix B.2.4) between DFT-SD energies and their LFDFT values for the examples considered were calculated between 0.016 and 0.124 eV, i.e. between 130 and 1000 cm^{-1} which are in the order of the DFT calculation precision ($\pm 0.2\ eV$).

From Table 3.3[d], we can remark that $10Dq$ is almost equal to the difference $|\varepsilon_{t_2} - \varepsilon_e|$ referred as $10Dq_{MO}$. From this statement and the effective Hamiltonian theory,[85,86] we justify the construction of h_{ab} LF matrix using the five KS orbitals with dominant d-character. Up to now we also remark, with the exception of CN complexes where $10Dq$ (LFDFT) values are higher than experimental, that LDA and GGA functionals are accurate enough in calculating ligand field matrix elements (h_{ab}) not only for cubic but also for complexes with lower symmetries. This is not the case for B and C. In Table 3.5 we collected LFDFT (LDA) values of B and C of different complexes. For the sake of comparison we also list values of B and C deduced using a fit to LF transitions from experiment. When comparing the two sets of data one should be cautious, because experimental uncertainties prevent an accurate fit of B and C in many cases. In spite of this, we note that the LFDFT B and C values are systematically lower than experimental ones.

[d] This remark is valid for all the compounds treated by LFDFT in this thesis.

Chapter 4

Multiplet Structure

Generally, it is more useful to compare multiplet transition energies with experimental data than to compare ligand field ($10Dq$) and Racah's parameters to those fitted from UV-Vis spectra. Figure 3.1 shows that the last step of the LFDFT method consists in the execution of a LF program to calculate multiplets energies. Two programs are at our disposal: a matlab program (the source code is given in section 4.2.1: a modified version to calculate magnetic properties is presented in Appendix E.2) and the AOMX program.[89] As in the previous chapter we have shown how to calculate Racah's parameters and the $(2l+1)\times(2l+1)$ h_{ab} matrix; these parameters can be given as input for the two programs. After execution, the programs list the energies of all multiplets.[a] In a first time, we will give details about the theory, next the LF matlab program is proposed with the needed *Gener_ln* program and also a brief introduction to AOMX is presented. At the end, applications are proposed to test the theory.

4.1 Theory of Multiplet

There are two ways to calculate the energies of multiplet if we know the energies of SD or the LF and Racah's parameters. One is to express the wavefunction of multiplets arising from a given configuration in a linear combination of SD and, the other one, is to use an Hamiltonian and the ligand field parameters. Thus, a presentation of the two methods is given but all calculations done in this thesis are based on the second one.

4.1.1 Multiplet Energy as a Function of E_{SD}

Following,[8,9] the energy of a multiplet can be expanded in first order as a weighted sum of single determinant energies. And according to the work of Ziegler *et al.*,[10] the energy of a single determinant can be replaced by the corresponding energy obtained by the DFT. In order to illustrate the method, as a first example, we consider the singlet and triplet energies arising from an a^1b^1 configuration. While spin-unrestricted calculations with two up (+) spins, $|a^+b^+|$, yields directly the energy of the $S=1$, $M_s=1$ state, a calculation with one spin-up (+) and one spin-down (−), $|a^+b^-|$ (or equivalently $|a^-b^+|$) gives the

[a] The output of AOMX is more complete than the matlab program one because it specifies the label of the multiplets.

average energy between the $S = 0$ and $S = 1$ with $M_s = 0$ for both states:

$$E(|a^+b^+|) = E(ab\,^3B, M_s = 1) \tag{4.1}$$

$$E(|a^+b^-|) = \frac{1}{2}\left[E(ab\,^3B, M_s = 0) + E(ab\,^1B)\right] \tag{4.2}$$

From these equations the energy of $E_{S=0}(M_s = 0)$ can be extracted as the weighted sum:

$$E(ab\,^1B) = 2E(|a^+b^-|) - E(|a^+b^+|) \tag{4.3}$$

The situation becomes more involved when going to TM complex with highly degenerate orbitals. However we fully exploit the symmetry in order to simplify the relation between the multiplet splitting and SD energies. In general, we can write the multiplet wavefunction as:

$$\Psi_i = |\alpha\Gamma m_\Gamma S m_s > \tag{4.4}$$

where Γ is the label of the irreducible representation of the space part of the wavefunction, m_Γ refers to its component in case of degeneracy, S is the spin part of the wavefunction with component m_s in case of spin multiplicity larger than 1. The relation between multiplet 1^{st} order energies, $E(\psi_k)$ and the energies of some symmetry independent (non-redundant) SD $E(\phi_\mu)$ is given by Eq. 4.5, where the coefficient $F_{k\mu}$ are the symmetry dependent weights:

$$E(\psi_k) = \sum_k F_{k\mu} E(\varphi_\mu) \tag{4.5}$$

In two articles published by Daul *et al.*,[11,90] the full description of the method is given.

4.1.2 Multiplet Energy as Solution of $\mathscr{H}$

Another way to determine the multiplet structure is to consider that the multiplet wavefunctions, Ψ_i, are solution of an Hamiltonian $\mathscr{H}$:

$$\mathscr{H} = \sum_i f_i + \sum_i \sum_{j>i} \frac{1}{r_{ij}} + \sum_i \zeta_i \cdot l_i \cdot s_i \tag{4.6}$$

where f_i, $1/r_{ij}$ are respectively the one-electron and the two-electrons operators. This method is the one implemented in the LF matlab program and the AOMX program: the only difference between them is that the one-electron operator is not defined in the same manner. When we introduce LFT (*cf.* section 2.1.3), we show how to determine the matrices equivalent operator by using the Slater's rules and next, how to parameterize the two-electrons operator in function of Racah's parameters. The last term to consider is the spin orbit coupling contribution and since our study is limited to d-electrons ($l = 2$ and $s = 1/2$), the spin orbit coupling matrix element can be easily obtained. So from the LFDFT program, we know the B and C Racah's parameters and the LF matrix and, if in a first time, we consider ζ (the spin-orbit constant) equal to zero, we can determine the eigenvalues of the Hamiltonian.

4.2 LF Programs

4.2.1 Matlab Program

The output of the LF matlab program is less elaborated than the AOMX one because it does not give information about the label of the multiplet term but the big advantage is that it is very short and easily modifiable. We have just to enter the B and C Racah's parameters in r, the ligand field matrix elements in $lfpar$ where the columns and the lines are ordered from $m = -2$ to $m = 2$ and ζ different than zero if we want to consider spin-orbit coupling. This program like the LFDFT program loads the file *data.mat*, generated by the program *Gener_ln* which is given in the Section 4.2.3, which contains the *gdata* matrix (2 electrons electrostatic matrix elements in the basis of microstates), the *lfdata* matrix (1 electron ligand field matrix elements in the basis of microstates) and the *lsdata* matrix (spin and angular momentum 1-electron matrix elements in the basis of microstates). The Figure 4.1 consists in the source code of the program. We can see that the multiplet energies are determined by calculating the eigenvalues of the Hamiltonian (Eq 4.6), subtracting the lower one and ordering them. The number of time the energy appears is equal to $(2S + 1) \times m_\Gamma$ where $(2S + 1)$ is the spin multiplicity and m_Γ the number of time the level is degenerate. At the end, the multiplet energies are printed. All the inputs: $lfpar$ (ligand field matrix in a vector form), r (B and C Racah parameters) and ζ (the spin-orbit constant) has to be entered in kK. To determine ζ, two options can be considered: we use the value given for free ion in the Griffith's book or we determine the value by DFT using a Relativstic ZORA calculation on the free ion. Then we reduce the obtained value by the orbital reduction factor, k, which is defined by:

$$k = \frac{1}{2l+1} \sum_{i=1}^{2l+1} \sum_{\mu=1}^{2l+1} (\boldsymbol{U}(i,\mu))^2 \tag{4.7}$$

where $\boldsymbol{U}(i,\mu)$ are the matrix elements of Eq 3.1 and $l = 2$ for open d-shell TM. The matlab program does not present any difficulties and the more interesting part is contained in the *Gener_ln* program.

4.2.2 AOMX

The last version of the AOMX program[89] reads the ligand field matrix so the inputs are the same than the ones used in the previous matlab program. If we use an older version, we need to derive AOM parameters from the ligand field matrix obtained by the LFDFT program. A set of 1, 3 or 5 AOM parameters e_λ can be precised: e_σ, e_{π_s}, e_{π_c}, e_{δ_s} and e_{δ_c} and one has to refer to the AOMX manual to know how to determine them. For the interelectronic repulsion, the Racah's parameters can be enter directly.

```
load data
% Input of Racah's parameter: r=[A B C]
r=[0; B; C];
% Input of LF mat. el. <di|LF|dj>
lfpar=[ h(1,1) ; h(2,1) ; h(2,2) ; h(3,1) ; h(3,2) ; h(3,3) ; h(4,1) ;
h(4,2) ; h(4,3) ; h(4,4) ; h(5,1) ; h(5,2) ; h(5,3) ; h(5,4) ; h(5,5)];
% Spin-orbit coupling constant
zeta=0
%
ge=2.0023;
[nsd ne]=size(ir);
ij=0;
% h = er + lf + so: Eq 4.6
for i=1:nsd
  for j=1:i
    ij=ij+1;
    h(i,j)=gdata(ij,:)*r+lfdata(ij,:)*lfpar+lsdata(ij,7)*zeta;
    h(j,i)=conj(h(i,j));
  end
end
% get Eigenvalues(e) and Eigenvectors(c) of h
[c,e]=eig(h);
% sort eigenvectors and create an array of number: ie
[e,ie]=sort(real(diag(e))); e(:)=e(:)-e(1); c=c(:,ie);
% find the multiplicity of one energy
i0=1;
i1=0;
for i=2:nsd
  if abs(e(i)-e(i-1))>0.001
    i1=i1+1;
    w(i1)=e(i-1);
    mul(i1)=i-i0;
    i0=i;
  end
end
fprintf('---------------------------- \n')
fprintf('(2S+1)*M(gamma) E \n')
fprintf('---------------------------- \n')
for i=1:i1
  fprintf(' %3i %12.3f \n',mul(i),w(i))
end
fprintf('---------------------------- \n')
```

Figure 4.1: *Source code of the LF matlab program.*

4.2.3 Program Gener_ln

In the two matlab programs presented, the LFDFT and the LF one, a file "data.mat" is loaded, it contains four matrices which are generated by the *Gener_ln* matlab program. For this program, we just must specify the type of shell: *lq* should be equal to 2 for *d*-electrons, and the number of electrons on this shell: *ne*. It produces the *ir, gdata, lfdata* and *lsdata* matrices for the given configuration. The script is short, the source code figures in Figure 4.2, and the essential parts are contained in the called functions. From the Figure 4.3, two parts can be distinguished in the program: firstly, the two functions "*GET2EI4A*" and "*GETLS*" are calculating matrix elements in the basis of spin orbitals, and in a second part, the three functions "*ZAB*", "*GAB*" and "*LFAB*" correspond to the implementation of the Slater's rule to determine the matrix elements of the one- and two-electron operator in the basis of μ-states. All the functions used by this program are given in Appendix C.

```
clear all
clc
global iabcd vabcd lq lx ly lz sx sy sz ls
% Type of shell lq: s(0), p(1), d(2) , f(3) and number of electrons:
ne
lq=[2];
ne=3;
% Generate single determinants or microstates for lq^ne
ir=GENERSD(ne,1,2*sum(lq+lq+1));
% Get <ab|cd>
[vabcd,iabcd]=GET2EI4A(lq);
% Get l, s and l*s 1-e matrices (s=1/2)
[lx,ly,lz,sx,sy,sz,ls]=GETLS(lq,1/2);
%
nsd=length(ir);
ij=0;
for i=1:nsd
  for j=1:i
    ij=ij+1;
    lfdata(ij,:)=LFAB(ir(i,:),ir(j,:));
    lsdata(ij,:)=ZAB(ir(i,:),ir(j,:));
    gdata(ij,:)=GAB(ne,ir(i,:),ir(j,:));
  end
end
gdata_racah(:,1)= gdata(:,1);
gdata_racah(:,2)= (49.0/5.0)*gdata(:,2);
gdata_racah(:,3)= (7.0/5.0) *(gdata(:,1)+gdata(:,2)+gdata(:,3));
gdata(:,:)=gdata_racah(:,:);
save data ir lfdata lsdata gdata
```

Figure 4.2: *Source code of the Gener_ln program.*

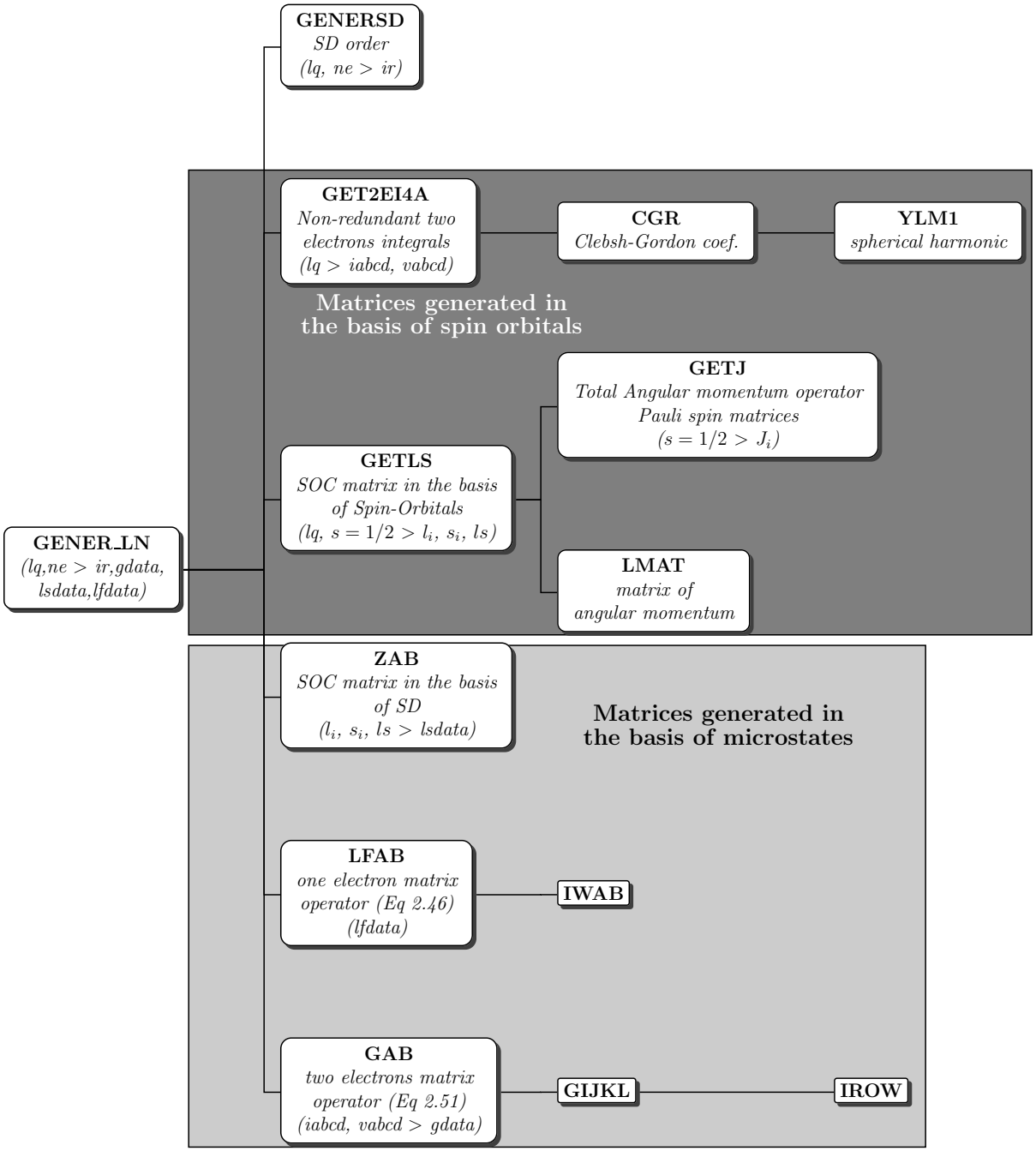

Figure 4.3: *The structure of the "Gener_ln" matlab program, the lines represent the subroutines called in the program. In each frame, there is the name of the function, a short explanation of the function's role and between parenthesis the input variables needed then the sign ">" and the outputs variables ($i \in \{x, y, z\}$).*

4.3 Applications

4.3.1 Octahedral Cr^{III} d^3 and Co^{II} d^7 Complexes

In Tables 4.1 and 4.2 we list, respectively, multiplet energies for the d^7 CoX_6^{4-} (X = Cl^-, Br^-) and the CrX_6^{3-} (X = F^-, Cl^-, Br^-, CN^-) complexes. We use a LDA functional and the optimized Co^{II}-X and Cr^{III}-X bond lengths for the DFT calculations. The multiplet energies obtained are compared to the ones from a LF calculation utilizing the values of B, C and $10Dq$ fitted to the UV-Vis spectra. In lines with section 3.1.2, in Table 4.1 one can remark that the LDA bond lengths are too long and so, the values of $10Dq$ are too small compared to experiment. Hence, the energies obtained are shifted compared to the experimental ones. The situation improves if instead of optimized bond lengths, experimental ones are taken into account for the calculation (*cf.* Table 4.1). Even in this case, spin-forbidden transitions come out by 3000-4000 cm^{-1} too low in energy compared to experiment.
For the CrX_6^{3-} (X = F^-, Cl^-, Br^-, CN^-) complexes (*cf.* Table 4.2), the results are less accurate even if for CrF_6^{3-} and $Cr(CN)_6^{3-}$ the optimized bond lengths are close to experiment. Moreover for the $Cr(CN)_6^{3-}$ we note a LDA value of $10Dq$ which is by 4000 cm^{-1} higher than the experimental one. This is unusual and not expected. For these complexes with a $^4A_2$ ground state, spin-forbidden transitions deviate from reported experimental energies by about 6000 cm^{-1}; a result due to a drastic lowering of the B and C energies. We can conclude that for the latter systems, existing DFT functionals do not perform properly. In addition standard deviations comparing DFT and LFDFT numerical values are too high.

Term	$CoCl_6^{4-}$				$CoBr_6^{4-}$			
	R_{opt}	R_{exp}	LFT-fit	Exp.	R_{opt}	R_{exp}	LFT-fit	Exp.
$^4T_1$	0	0	0	-	0	0	0	-
$^4T_2$	3384	6613	6261	6600[91]	3258	5687	5506	5700[92]
^2E	7772	3980	7794	-	7171	4307	8817	-
$^4A_2$	7335	14050	13467	13300[91]	7041	12074	11890	11800[92]
$^2T_1$	10688	10134	13542	-	9960	9481	13789	-
$^2T_2$	10804	10479	13783	-	10124	9836	13969	-
$^4T_1$	11412	14008	17241	17250[91]	10113	11886	16748	16750[92]
$R(M-X)$	2.684	2.414	2.414	-	2.821	2.589	-	-
B	573	548	795	-	492	460	808	-
C	2540	2436	3108	-	2444	2371	3159	-
10Dq	3952	7436	7206	-	3782	6387	6384	-
StDev	0.108	0.110	-	-	0.122	0.124	-	-

Table 4.1: *Theoretical and experimental electronic transition energies of high-spin CoX_6^{4-}, $X = \{Cl^-, Br^-\}$ octahedral d^7 complexes for LDA optimized and experimental geometries. Theoretical values are obtained using LFDFT taken as reference an AOC corresponding to $2t_{2g}^{4.2}4e_g^{2.8}$ configuration. Fitted B, C and 10Dq parameters from experimental transition energies are also included.*

Term	CrF_6^{3-}			$CrCl_6^{3-}$			$CrBr_6^{3-}$			$Cr(CN)_6^{3-}$		
	LDA	LFT-fit	Exp.	LDA	LFT-fit	Exp.	LDA	LFT-fit	Exp.	LDA	LFT-fit	Exp.
$^4A_{2g}(t_{2g}^3)$	0	0	0	0	0	0	0	0	0	0	0	0
$^2E_g(t_{2g}^3)$	12497	15802	16300[93]	10756	14426	14430[94]	10333	13900	13900[94]	9413	12034	12460[95]
$^2T_{1g}(t_{2g}^3)$	13044	16461	16300[93]	11180	14873	-	10694	14348	-	9682	12425	13070[95]
$^2T_{2g}(t_{2g}^3)$	18628	23260	23000[93]	15918	21037	-	15185	20281	-	15234	19084	18370[95]
$^4T_{2g}(t_{2g}^1e_g^1)$	13569	15298	15200[93]	10911	12800	12800[94]	9816	12400	12400[94]	30760	26595	26700[95]
$^4T_{1g}(t_{2g}^1e_g^1)$	19443	22262	21800[93]	15618	18198	18200[94]	13992	17700	17700[94]	35910	32743	32680[95]
$^2A_{1g}(t_{2g}^1e_g^1)$	24071	28709	-	20056	25351	-	18709	24459	-	38324	36488	-
$^2T_{1g}(t_{2g}^1e_g^1)$	26348	31473	-	21878	27421	-	20316	26503	-	40022	38569	-
$^2T_{2g}(t_{2g}^1e_g^1)$	25959	30970	-	21568	27079	-	20047	26159	-	39983	38438	-
$^2E_g(t_{2g}^1e_g^1)$	27819	33341	-	23147	29098	-	21530	28126	-	41084	39952	-
$^4T_{1g}(t_{2g}^1e_g^1)$	30339	34636	35000[93]	24375	28455	-	21861	27643	-	63147	55352	-
R(M-X)	1.957	-	1.933[96]	2.419	-	2.335[12]	2.588	-	2.47[12]	2.071	-	2.077[97]
B	605	734	-	484	550	-	427	543	-	452	554	-
C	2694	3492	-	2403	3450	-	2395	3296	-	1919	2559	-
10Dq	13598	15297	-	10911	12800	-	9816	12400	-	30760	26595	-
StDev	0.113	-	-	0.105	-	-	0.113	-	-	0.105	-	-
$(10Dq)_{orb}$	13928	-	-	10775	-	-	9622	-	-	30953	-	-

Table 4.2: *Electronic transition energies of CrX_6^{3-}, X = F^-,Cl^-,Br^- and CN^- complexes with geometries optimized using LDA functionals calculated using values of B,C and 10Dq from least square fit to DFT energies (LDA) of the Slater determinants and to experiment (LFT fit to exp.). The values of $(10Dq)_{orb}$ as deduced from the $e_g - t_{2g}$ Kohn-Sham orbital energy difference taken from the $t_{2g}^{1.8}e_g^{1.2}$ SCF Kohn-Sham energies are also listed. Experimental transition energies are also listed.*

Table 4.3: *Theoretical and experimental electronic transition energies of the low-spin $Mn(CN)_6^{3-}$ octahedral d^4 complex. Theoretical values are obtained using geometries from a LDA geometry optimization utilizing values of B, C and 10Dq resulting from least square fit to the energies of Slater determinants constructed from $2t_{2g}^{2.4}4e_g^{1.6}$ SCF Kohn-Sham orbitals. Best fitted B, C and $10Dq$ parameters from experimental transition energies are also included.*

Electronic state	LDA	LF-fit	Exp.
$^3T_{1g}$	0	0	
$^1T_{2g}$	6796	7948	7984[99]
^1E_g	7242	8710	8710[99]
$^1A_{1g}$	16028	18519	18470[99]
^5E_g	20013	20699	20700[99]
^3E_g	31746	34326	
$^3T_{1g}$	32354	34966	
$^3T_{2g}$	32935	35713	
$^3A_{1g}$	33453	36761	
$^3A_{2g}$	34591	38130	
^3E_g	35499	39630	
B	444	630	
C	2361	2598	
10Dq	34085	36900	
StDev	0.082		

4.3.2 Octahedral Cyano Mn^{III} (d^4), Co^{III} and Fe^{II} (d^6) Complexes

In this section we are interested in the three following octahedral cyano complexes: $Mn(CN)_6^{3-}$ (d^4), $Fe(CN)_6^{4-}$ (d^6) and $Co(CN)_6^{3-}$ (d^6).

$Mn(CN)_6^{3-}$ is a low-spin complex with a $^3T_{1g}$ ground state. The LDA optimized bond distance (1.99 Å) matches perfectly the experimental one (1.98 Å)[98] and calculated multiplet energies agree reasonably with the experimental spectrum (Table 4.3) - the highest deviation (2400 cm^{-1}) being met for the $^3T_{1g} \rightarrow^1 A_{1g}$ transition.

$Fe(CN)_6^{4-}$ and $Co(CN)_6^{3-}$ possess a $^1A_{1g}$ ground state. The multiplet enegies determined by LFDFT using LDA optimized bond lengths ($d_{Fe-C} = 1.930$ Å and $d_{Co-C} = 1.899$ Å) are listed in Table 4.4. Owing to the over estimatation of the $10Dq$ value by 1740 and 2230 cm^{-1} for the Fe and Co complex respectively, DFT energies of $^1A_{1g} \rightarrow^1 T_{1g}$, $^1T_{2g}$ transition are higher in energy than the experimental values, values of B from LFDFT and experiment being very close in these complexes. Differences in the C parameter are just the opposite (this is due to the least square fit procedure), they would lead to lowering of energies of spin-forbidden transitions. However this is overcompensated by the larger DFT value of the parameter $10Dq$.

Electronic State	$Fe(CN)_6^{4-}$			$Co(CN)_6^{3-}$		
	LDA	LF-fit	Exp.	LDA	LF-fit	Exp.
$^1A_{1g}$	0	0		0	0	
$^3T_{1g}$	28516	23698	23700[100]	29845	25969	25969[100]
$^3T_{2g}$	31669	26664	-	32721	29276	-
$^1T_{1g}$	33499	30969	30970[100]	35107	32500	32500[100]
$^1T_{2g}$	39842	37001	37000[100]	40900	39194	39200[100]
$^5T_{2g}$	50080	38067		52577	43240	
$^3T_{1g}$	62079	54723		65030	58538	
$^3T_{2g}$	62543	55010		65391	58948	
^3E_g	63939	56352		66667	60430	
B	427	411		387	456	
C	2420	3566		2573	3184	
10Dq	35421	33678		37180	34944	
StDev	0.082			0.112	-	

Table 4.4: *Theoretical and experimental electronic transition energies of low-spin $Fe(CN)_6^{4-}$ and $Co(CN)_6^{3-}$ octahedral d^6 complexes. Theoretical values are obtained using geometries from a LDA geometry optimization utilizing values of B, C and 10Dq resulting from least square fit to the energies of Slater determinants constructed from $2t_{2g}^{3.6}4e_g^{2.4}$ SCF Kohn-Sham orbitals. Best fitted B, C and $10Dq$ parameters from experimental transition energies are also included.*

4.3.3 Applications to Tetrahedral d^5 $MnCl_4^{2-}$ and $FeCl_4^{1-}$ Complexes

In the discussions so far, we noted, that because B and C deduced using DFT data are smaller than parameters from a direct fit to experiment, electronic transitions with change of the spin multiplicity are calculated at lower energies than experiment. In this respect high-spin d^5complexes with tetrahedral geometry and a $^6A_1$ ground state, such as $MnCl_4^{2-}$ and $FeCl_4^{-}$ provide a stringent test of the ability of the up-to-date functionals to calculate multiplet structures for such cases. In Table 4.5 we list such energies and compare them with experiment and with energies using a direct fit of B, C and $10Dq$ to experiment. We base our treatment on LDA optimized Mn-Cl (2.385 Å) and Fe-Cl (2.207 Å) bond distances. For both systems we obtain the remarkable result that all transitions match with the observed transition energies with a shift of about 6000 cm^{-1}. The origin of this correction is possibly due to the fact that DFT leads to lower values in particular of the parameter C.

Electronic state	$MnCl_4^{2-}$			$FeCl_4^{1-}$		
	LDA	LFT-fit	Exp.[101]	LDA	LFT-fit	Exp.[101]
$^6A_1$	0	0		0	0	
$^4T_1$	15253	20954	21250	8875	14835	15600
$^4T_2$	16720	21720	22235	11060	16836	16300
$^4A_1$, ^4E	17175	21975	23020	12940	18230	18800
$^4T_2$	20359	25198	26080	14554	20271	20100
^4E	21011	25587	26710	15705	21366	22400
$^4T_1$	21922	28051	27770	18436	25114	
$^4A_2$	28429	34883	33300	21276	29106	
$^4T_1$	28638	34998	34500	22255	29774	
$^4T_2$	29536	35514	36650	24307	32917	
B	548	516		395	448	
C	2339	3363		1798	[b]	
10Dq	3298	2661		5395	5320	
StDev	0.061	-		0.051		

Table 4.5: *Theoretical and experimental electronic transition energies of high-spin tetrahedral ($MnCl_4^{2-}$ and $FeCl_4^{1-}$) d^5 complexes. Theoretical values are obtained using geometries from a LDA geometry optimization utilizing values of B, C and 10Dq resulting from least square fit to the energies of Slater determinants constructed from $2t_2^3 4e^2$ SCF Kohn-Sham orbitals. Best fit B, C and 10Dq parameters from experimental transition energies are also included.*

4.3.4 Tetrahedral d^2 Complexes

Tetrahedral d^2 complexes possess a $^3A_2(e^2)$ ground state and $^3A_2 \rightarrow ^3T_2$ and $^3A_2 \rightarrow ^3T_1$, $e \rightarrow t_2$ singly excited states. They give rise to broad $d-d$ transitions in the optical spectra. In addition, spin-flip transitions within the e^2 configuration lead to sharp line excitations.

In this section we consider the three oxoanions of Cr^{IV}, Mn^{V}, Fe^{VI} complexes and the CrX_4 (X = F^-, Cl^-, Br^-, I^-) complexes. For the three oxanions, multiplet energies from LDA LFDFT agree within 2000 cm^{-1} with experimental data (*cf.* Table 4.6) supposed that we use experimental rather than of LDA optimized M-O bond lengths. In particular the $^3A_2 \rightarrow ^3T_2$ transition energy and thus $10Dq$ nicely agrees with experiment. LDA optimized M-O bond lengths are larger than the experimental values. This becomes more pronounced with increasing anionic charge from FeO_4^{2-} (0.02 Å) MnO_4^{3-} (0.05 Å) and CrO_4^{4-} (0.1 Å). This is reflected in the values of $10Dq$ which are distinctly smaller than $10Dq$ from experiment (by 1680, 680 and 1600 cm^{-1}, respectively). B and C parameters from DFT (LDA) are by 20-35% smaller than those deduced from a fit to observed LF transitions. Thus the $^3A_2 \rightarrow ^3T_1$ and the spin-forbidden $^3A_2 \rightarrow ^1E$, $^1A_1$ transitions, being sensitive to B and C, respectively, are underestimated by DFT (LDA) by 15-20 %.

In order to study the effect of the adopted functional we calculated multiplet energies of CrX_4 (X = F^-, Cl^-, Br^-, I^-) (Table 4.7). Going from the LDA functional to the gradient corrected GGA functional we get a lengthening of the geometry optimized Cr-X bond distances accompanied with a decrease of the value of 10Dq. On the other hand the value of B increases by 15-20 % going from the LDA to the GGA functional.

[b] calculated using a C/B ratio equal to 6.14

Term	CrO_4^{4-}				MnO_4^{3-}				FeO_4^{2-}			
	R_{opt}	R_{exp}	AOM fit	Exp.	R_{opt}	R_{exp}	AOM fit	Exp.	R_{opt}	R_{exp}	AOM fit	Exp.
$^3A_2(e^2)$	0	0	0	-	0	0	0		0	0	0	-
$^1E(e^2)$	7838	7844	8904	-	6560	6583	8537	8432[102]	5179	5197	5712	6215[103]
$^1A_1(e^2)$	13136	13412	15276	14730[104]	11546	11698	14633	-	9369	9446	10605	9118[103]
$^3T_2(e^1t_2^1)$	7315	8847	8949	9087[104]	9837	10872	10515	10380[102]	11259	11952	12939	12940[103]
$^3T_1(e^1t_2^1)$	11125	12892	13714	13887[104]	13408	14512	14790	14266[102]	13936	14645	16936	17700[103]
$^1T_2(e^1t_2^1)$	15019	16580	17677	-	16329	17393	18956	-	16408	17121	18589	-
$^1T_1(e^1t_2^1)$	17047	18519	20271	-	17857	18908	20875	-	17437	18146	20215	-
$^1A_1(t_2^2)$	36567	39265	42471	-	37278	39268	44416	-	36109	37491	40514	-
$^1E(t_2^2)$	23203	26204	27754	-	26726	28804	30202	-	28000	29401	32092	-
$^3T_1(t_2^2)$	17359	20053	21459	-	21309	23309	23203	23430[102]	23470	24841	27505	-
$^1T_2(t_2^2)$	23337	26314	27930	-	26794	28866	30298	-	28030	29429	32154	-
R(M-O)	1.868	1.77[87]	-	-	1.746	1.700[102]	-	-	1.674	1.65[c]	-	-
B	436	427	555	-	347	347	430	-	242	242	375	-
C	2250	2274	2331	-	1928	1936	2600	-	1637	1645	1388	-
10Dq	7315	8847	8950	-	9831	10872	10515	-	11259	11952	12938	-
StDev	0.036	0.039	-	-	0.025	0.027	-	-	0.016	0.016	-	-
$(10Dq)_{orb}$	7363	8831	-	-	9984	11025	-	-	11436	12130	-	-

Table 4.6: *Electronic transition energies in CrO_4^{4-}, MnO_4^{3-} and FeO_4^{2-} oxo-anions calculated using values of B, C and 10Dq as obtained from a fit to DFT energies for LDA geometrically optimized clusters (R_{opt}), for T_d geometries with metal-ligand distances from experiment(R_{exp}), from an AOM fit to experimental transition energies(AOM fit) and experiment (Exp.). Values of B, C and 10Dq and mean square deviations (StDev) between DFT and fitted energies (for R_{opt} and R_{exp}) are listed for each entity. The values of $(10Dq)_{orb}$ as deduced from the $4t_2$-2e Kohn-Sham orbital energy difference taken from the $2e^{0.8}4t_2^{1.2}$ SCF Kohn-Sham energies are also listed.*

[c]The distance is estimated as a sum of i = 1 ionic radii of Fe^{VI} (0.25 Å) and O^{-II} (1.40 Å),[105]

Term	CrF_4		$CrCl_4$				$CrBr_4$			CrI_4	
	LDA	GGA	LDA	GGA	LF-fit	Exp.[106]	LDA	GGA	Exp.[106]	LDA	GGA
$^3A_2(e^2)$	0	0	0	0	0	0	0	0	0	0	0
$^1E(e^2)$	8583	9092	6542	7101	6089	-	6373	6832	6666	5986	6514
$^1A_1(e^2)$	14804	15630	11114	11971	10586	-	10698	11364	10869	9921	10705
$^3T_2(e^1t_2^1)$	10259	9677	7008	6524	7010	7250	6163	5605	-	5267	4781
$^3T_1(e^1t_2^1)$	14825	14571	10316	10062	10440	10000	9269	8820	-	8054	7663
$^1T_2(e^1t_2^1)$	18723	18608	13454	13489	12991	12000	12434	12295	-	8054	7663
$^1T_1(e^1t_2^1)$	20875	21141	15074	15456	14718	-	14037	14215	-	12659	13021
$^1A_1(t_2^2)$	43965	44352	32099	32891	30599	-	30120	30531	-	27416	28198
$^1E(t_2^2)$	29834	29354	21121	20878	20716	-	19271	18777	-	17070	16819
$^3T_1(t_2^2)$	23091	22681	16033	15795	16229	16666	14424	14043	13258	12591	12486
$^1T_2(t_2^2)$	29953	29516	21217	21014	20822	-	19373	18920	-	17172	16969
R(M-X)	1.710	1.735	2.104	2.144	-	-	2.264	2.318	-	2.489	2.547
B	476	548	355	419	376	-	347	403	-	323	387
C	2452	2444	1903	1952	1579	-	1855	1887	-	1758	1798
10Dq	10259	9678	7008	6524	7250	-	6162	5605	-	5266	4782
StDev	0.034	0.043	0.030	0.039	-	-	0.030	0.038	-	0.032	0.033
$(10Dq)_{orb}$	10549	9928	7258	6686	-	-	6371	5726	-	5605	4984

Table 4.7: *Electronic transition energies of CrX_4, $X = F^-$, Cl^-, Br^- and I^- ions with geometries optimized using LDA and GGA functionals calculated using values of B, C and 10Dq from least square fit to DFT energies of the Slater determinants. The values of $(10Dq)_{orb}$ as deduced from the $4t_2$-2e Kohn-Sham orbital energy difference taken from the $2e^{0.8}4t_2^{1.2}$ SCF Kohn-Sham energies are also listed. Experimental transition energies for $CrCl_4$ and $CrBr_4$ as well as values of B, C and 10Dq deduced from a fit to experiment for $CrCl_4$ are also included.*

4.4 General Conclusions

In conclusion, our LFDFT allows to calculate multiplet energies in TM complexes, similar to the empirical CI-DFT procedure described by Grimme *et al.*[107,108] In this approach, KS potentials and energies have been used to approximate the exact CI Hamiltonian by introducing scaling factors, thus avoiding double counting of electron correlation in the off-diagonal CI matrix elements. Though, principally able to treat open-shell TM complexes as well, the method has been applied thus far only to closed shell ground state systems.
Considering the LFDFT, we can make the same remark than in the previous chapter: if we have the experimental structure, it is better to use this one than the optimized, as the $10Dq$ value depend strongly on the bond length. In the set of compounds we study in this chapter, we saw that sometimes we were in perfect agreement with the expimental data which means that the theory is valid, but sometimes we had a constant shift in energy between experiment and LFDFT results or a less accurate description of the multiplet structure and this can be due to the fact that the functional used does not describe well the compounds considered.

Chapter 5

Relativistic Effect within LFDFT

In this chapter we extend the LFDFT with the inclusion of spin-orbit coupling. A good opportunity to achieve this consist in using for the DFT calculations the Zero-Order Regular Approximation[109] (ZORA) which permits to include spin-orbit coupling effects variationally. ZORA has been implemented into the Amsterdam Density Functional (ADF) program[74] and has been proven to work well.
This chapter is organized as follows: in Section 5.1 spin-orbit coupling in T_d symmetry and in its subgroup D_{2d} is described, in Section 5.2 the implementation of the formalism along the lines of LFDFT is presented. It is, thus, possible to get symmetry consistent spin-orbit coupling parameters without recourse to implicit use of orbital reduction factors. We intend to show that orbital dependence of that kind can be larger than one might expect. We will show that it is possible to apply the formalism using data from DFT-ZORA calculations. Finally, we apply the theory to the NiX_4^{2-} (X = F^-, Cl^-, Br^-, I^-) series of compounds and compare the results with experimental data from literature. An outlook towards an extension of the theory to systems with little or no symmetry will also be given.

5.1 Spin-Orbit Coupling

5.1.1 Theoretical Description

The spin-orbit operator in Eq 2.58 enables the expression of matrix elements of spin-orbit coupling in and between sub-shells in terms of molecular orbitals. Thus, any arbitrary one-electron spin-orbit coupling matrix element can be written as:

$$\begin{aligned}\langle s\, m_s, a\, \alpha|\, \hat{\mathrm{H}}_{SO}\, |s\, m_s', b\, \beta\rangle &= \langle s\, m_s, a\, \alpha|\, \vec{u}\cdot\vec{s}\, |s\, m_s', b\, \beta\rangle \\ &= \sum_{k=x,y,z} \langle s\, m_s|\, s_k\, |s\, m_s'\rangle\, \langle a\, \alpha|\, u_k\, |b\, \beta\rangle\end{aligned} \tag{5.1}$$

where s is the spin of a single electron with component m_s, a and b are the irreducible representations (irreps.) of the molecular orbitals and α and β the corresponding components in case of degeneracy. The 1^{st} term on the right hand side of Eq 5.1 is nothing but the Pauli matrices and the 2^{nd} term can be further reduced using Wigner-Eckhardt's theorem:

$$\langle a\, \alpha|\, u_k\, |b\, \beta\rangle = \langle a\, \alpha|b\, \beta, t_1 k\rangle\, \langle a\|\, u\, \|b\rangle \tag{5.2}$$

where $\langle a\,\alpha|b\,\beta,t_1k\rangle$ are coupling coefficients for the tetrahedral group and $\langle a\|\,u\,\|b\rangle$ are reduced matrix elements. Combining Eqs 5.1 & 5.2 enables us to express any arbitrary spin-orbit matrix element as a product of symmetry coefficients and reduced matrix elements:

$$\langle s\,m_s,a\,\alpha|\hat{H}_{SO}|s\,m'_s,b\,\beta\rangle=\langle a||u||b\rangle\sum_{k=x,y,z}\langle s,m_s|\hat{s}_k|s\,m'_s\rangle\langle a\,\alpha|b\,\beta,t_1k\rangle \tag{5.3}$$

In order to estimate the yet unknown reduced spin-orbit coupling matrix elements $\langle a\|\,u\,\|b\rangle$ we shall map Eq 5.3 onto a ZORA-DFT calculation and adjust the reduced matrix elements in order to reproduce the calculated ligand field levels as done previously in LF-DFT. This task requires a symmetry adaptation of the Kohn-Sham molecular orbitals to the double-group T_d^* i.e.:

$$\begin{aligned}
&e\otimes\Gamma_6\,(\alpha,\beta)=\Gamma_8:\\
&\qquad|\Gamma_8\,(e):\ \kappa\rangle=-\,|e\,\varepsilon,\ \beta\rangle\,;\\
&\qquad|\Gamma_8\,(e):\ \lambda\rangle=\ \ |e\,\theta,\ \alpha\rangle\,;\\
&\qquad|\Gamma_8\,(e):\ \mu\rangle=-\,|e\,\theta,\ \beta\rangle\,;\\
&\qquad|\Gamma_8\,(e):\ \nu\rangle=\ \ |e\,\varepsilon,\ \alpha\rangle\,;\\
&t_2\otimes\Gamma_6\,(\alpha,\beta)=\Gamma_8:\\
&\qquad|\Gamma_8\,(t_2):\ \kappa\rangle=\frac{1}{\sqrt{6}}\,|t_2\,\xi,\ \alpha\rangle-\frac{i}{\sqrt{6}}\,|t_2\,\eta,\ \alpha\rangle+\frac{2}{\sqrt{6}}\,|t_2\,\zeta,\ \beta\rangle\,;\\
&\qquad|\Gamma_8\,(t_2):\ \lambda\rangle=-\frac{1}{\sqrt{2}}\,|t_2\,\xi,\ \beta\rangle+\frac{i}{\sqrt{2}}\,|t_2\,\eta,\ \beta\rangle\,;\\
&\qquad|\Gamma_8\,(t_2):\ \mu\rangle=\ \ \frac{1}{\sqrt{2}}\,|t_2\,\xi,\ \alpha\rangle+\frac{i}{\sqrt{2}}\,|t_2\,\eta,\ \alpha\rangle\,;\\
&\qquad|\Gamma_8\,(t_2):\ \nu\rangle=-\frac{1}{\sqrt{6}}\,|t_2\,\xi,\ \beta\rangle-\frac{i}{\sqrt{6}}\,|t_2\,\eta,\ \beta\rangle+\frac{2}{\sqrt{6}}\,|t_2\,\zeta,\ \alpha\rangle\\
&t_2\otimes\Gamma_6\,(\alpha,\beta)=\Gamma_7:\\
&\qquad|\Gamma_7\,(t_2):\ \alpha"\rangle=\frac{1}{\sqrt{3}}\,|t_2\,\xi,\ \beta\rangle+\frac{i}{\sqrt{3}}\,|t_2\,\eta,\ \beta\rangle+\frac{1}{\sqrt{3}}\,|t_2\,\zeta,\ \alpha\rangle\,;\\
&\qquad|\Gamma_7\,(t_2):\ \beta"\rangle=\frac{1}{\sqrt{3}}\,|t_2\,\xi,\ \alpha\rangle-\frac{i}{\sqrt{3}}\,|t_2\,\eta,\ \alpha\rangle-\frac{1}{\sqrt{3}}\,|t_2\,\zeta,\ \beta\rangle\,;
\end{aligned} \tag{5.4}$$

where the notation of the double-group representation is according to Bethe and their components are Griffith's.[31] Using this basis transformation along with spin-orbit coupling elements (*cf.* Appendix D.1), the one-electron spin-orbit coupling and LF matrix reduces to:

	$\Gamma_8(e)$	$\Gamma_8(t_2)$	$\Gamma_7(t_2)$
$\Gamma_8(e)$	h_{ee}	$-\sqrt{\frac{3}{2}}i\zeta^{t_1}_{et_2}$	0
$\Gamma_8(t_2)$	$\sqrt{\frac{3}{2}}i\zeta^{t_1}_{et_2}$	$h_{t_2t_2}-\frac{1}{2}\zeta^{t_1}_{t_2t_2}$	0
$\Gamma_7(t_2)$	0	0	$h_{t_2t_2}+\zeta^{t_1}_{t_2t_2}$

(5.5)

where h_{ee} and $h_{t_2t_2}$ are the one-electron ligand field matrix elements, the $h_{t_2t_2}$ - h_{ee} difference being the cubic field splitting Δ and $\zeta^{t_1}_{et_2}$ and $\zeta^{t_1}_{t_2t_2}$ the reduced matrix elements:

$$\begin{aligned}\zeta^{t_1}_{et_2} &= \langle e||\vec{s}\vec{u}(t_1)||t_2\rangle \\ \zeta^{t_1}_{t_2t_2} &= \langle t_2||\vec{s}\vec{u}(t_1)||t_2\rangle\end{aligned} \tag{5.6}$$

which we derive in a form to be directly compared to the free Ni^{2+} spin-orbit coupling constant ($630cm^{-1}$). In section 5.3.3, we describe a procedure of getting these parameters from ZORA-DFT calculations.
The $^3T_1$ ground state of Ni^{2+} (d^8) in a tetrahedral (T_d) ligand field is Jahn-Teller unstable and distorts towards tetragonal D_{2d} symmetry with elongation along the S_4 axis of the tetrahedron. For this point group, the symmetry species $t_2(\xi,\eta,\zeta)$ and e (θ,ε) split into e (ξ,η) + b_2 (ζ) and a_1 (θ) + b_1 (ε) respectively. Symmetry adaptation of the Kohn-Sham molecular orbitals to the D^*_{2d} double group yields:

$$\begin{aligned}
a_1 \otimes \Gamma_6(\alpha,\beta) = \Gamma_6 :& \\
|\Gamma_6(a_1),\alpha'\rangle &= |a_1\theta,\alpha\rangle \\
|\Gamma_6(a_1),\beta'\rangle &= |a_1\theta,\beta\rangle \\
e \otimes \Gamma_6(\alpha,\beta) = \Gamma_6 :& \\
|\Gamma_6(e),\alpha'\rangle &= \frac{1}{\sqrt{2}}|e\xi,\beta\rangle - \frac{i}{\sqrt{2}}|e\eta,\beta\rangle \\
|\Gamma_6(e),\beta'\rangle &= \frac{1}{\sqrt{2}}|e\xi,\alpha\rangle + \frac{i}{\sqrt{2}}|e\eta,\alpha\rangle \\
b_1 \otimes \Gamma_6(\alpha,\beta) = \Gamma_7 :& \\
|\Gamma_7(b_1),\alpha''\rangle &= -|b_1\varepsilon,\beta\rangle \\
|\Gamma_7(b_1),\beta''\rangle &= |b_1\varepsilon,\alpha\rangle \\
b_2 \otimes \Gamma_6(\alpha,\beta) = \Gamma_7 :& \\
|\Gamma_7(b_2),\alpha''\rangle &= |b_2\zeta,\beta\rangle \\
|\Gamma_7(b_2),\beta''\rangle &= |b_2\zeta,\alpha\rangle \\
e \otimes \Gamma_6(\alpha,\beta) = \Gamma_7 :& \\
|\Gamma_7(e),\alpha''\rangle &= \frac{1}{\sqrt{2}}|e\xi,\alpha\rangle - \frac{i}{\sqrt{2}}|e\eta,\alpha\rangle \\
|\Gamma_7(e),\beta''\rangle &= -\frac{1}{\sqrt{2}}|e\xi,\beta\rangle + \frac{i}{\sqrt{2}}|e\eta,\beta\rangle
\end{aligned} \tag{5.7}$$

where again double-group representation are according to Bethe. Using this basis transformation along with the spin-orbit coupling matrix elements (*cf.* Appendix D.1) we obtain the spin-orbit coupling and LF matrix for this symmetry:

	$\Gamma_6(a_1)$	$\Gamma_6(e)$	$\Gamma_7(b_1)$	$\Gamma_7(b_2)$	$\Gamma_7(e)$
$\Gamma_6(a_1)$	$h_{a_1a_1}$	$\sqrt{\frac{3}{2}}i\zeta^e_{a_1e}$	0	0	0
$\Gamma_6(e)$	$-\sqrt{\frac{3}{2}}i\zeta^e_{a_1e}$	$h_{ee}-\frac{1}{2}\zeta^{a_2}_{ee}$	0	0	0
$\Gamma_7(b_1)$	0	0	$h_{b_1b_1}$	$-i\zeta^{a_2}_{b_1b_2}$	$\frac{-i}{\sqrt{2}}\zeta^e_{b_1e}$
$\Gamma_7(b_2)$	0	0	$i\zeta^{a_2}_{b_1b_2}$	$h_{b_2b_2}$	$\frac{-1}{\sqrt{2}}\zeta^e_{b_2e}$
$\Gamma_7(e)$	0	0	$\frac{i}{\sqrt{2}}\zeta^e_{b_1e}$	$\frac{-1}{\sqrt{2}}\zeta^e_{b_2e}$	$h_{ee}+\frac{1}{2}\zeta^{a_2}_{ee}$

(5.8)

where $h_{a_1a_1}$, h_{ee}, $h_{b_1b_1}$, $h_{b_2b_2}$ are the (diagonal in this case as well) one-electron ligand field matrix elements and ζ_{ij}^{k} are the reduced matrix elements:

$$\begin{aligned}
\zeta_{a_1e}^{e} &= \langle a_1||\vec{s}\vec{u}(e)||e\rangle \\
\zeta_{b_1b_2}^{a_2} &= \langle b_1||\vec{s}\vec{u}(a_2)||b_2\rangle \\
\zeta_{b_1e}^{e} &= \langle b_1||\vec{s}\vec{u}(e)||e\rangle \\
\zeta_{ee}^{a_2} &= \langle e||\vec{s}\vec{u}(a_2)||e\rangle \\
\zeta_{b_2e}^{e} &= \langle b_2||\vec{s}\vec{u}(e)||e\rangle
\end{aligned} \tag{5.9}$$

We note that in D_{2d}^{*} symmetry the cubic quantities $\zeta_{et_2}^{t_1}$ and $\zeta_{t_2t_2}^{t_1}$ split into three and two different reduced matrix elements thus yielding a total of five independent parameters. In ligand field studies, thus far the variation of spin-orbit coupling between the various symmetries of the involved ligand field orbitals have been approximated in terms of orbital reduction factors. In the next section, we derive a rigorous procedure allowing us to deduce these quantities from DFT-ZORA calculations.

5.2 Computational Procedure

The DFT calculations have been performed with the aid of the ADF program code (release 2003.01).[74]

For the exchange-correlation functionals, both, the local density approximation (LDA, for geometry optimizations) and the generalized gradient approximation (GGA , for energies of electronic states) have been used. For LDA we adopt an Xα functional for exchange ($\alpha = 0.7$)[110] and Vosko, Wilk and Nusair functional for correlation.[57] The GGA has been introduced in the form given by Perdew-Wang.[111] The frozen core approximation was used for inner core electrons. The orbitals up to $3p$ for Ni, $1s$ for fluorine, $2p$ for chlorine, $3d$ for bromine and up to $4d$ for iodine were kept frozen. The valence shells were described by triple zeta plus one polarization function (TZP basis set). Spin-restricted relativistic ZORA calculations have been done adopting the ZORA basis set (TZP). Using basis functions of increasing quality from TZP to TZ2P to TZ2P+ does not change results significantly.

5.2.1 Geometry Optimizations

Geometry optimizations of the NiX_4^{2-} species have been done in non-relativistic spin-unrestricted (M_s=1) formalism, using the LDA-only functional, which we know from experience[35] to yield TM-ligand bond distances in good agreement with experiment. In order to study the Jahn-Teller activity within the $^3T_1$ ground state, separate optimizations imposing a D_{2d} geometry have been done following the guidelines of accounting for the Jahn-Teller effect within DFT.[112] It should be noted that, being a single determinant method, DFT is not able to yield optimized geometries in the case where two or more configurations mix with each other. This is the case in our study, where two $^3A_2$ states (originating from $^3T_1$ in tetrahedral symmetry) - corresponding to the ground configuration ($e^4t_2^4$) and to the excited configuration ($e^3t_2^5$) - mix and reduce the extent of the structural distortion and of the Jahn-Teller stabilization (E_{JT}).[113] A procedure to solve

this problem is briefly outlined in Appendix D.2 and is used here to get ground state D_{2d} geometries for all NiX_4^{2-} species.

The geometries optimized, the LFDFT method is used to determine the B and C Racah's parameters and the 5×5 LF matrix for the two symmetries, which in our cases take a diagonal form with two different energies (e and t_2) for T_d and 4 different energies ($h_{a_1a_1}$, $h_{b_1b_1}$, $h_{b_2b_2}$ and h_{ee}) for D_{2d}.

5.2.2 Calculation of Reduced Matrix Elements of Spin-Orbit Coupling from ZORA-DFT

Let us consider the Kohn-Sham eigenvalues in the basis of the double group symmetry adapted fragment orbitals (SFO) and the symmetry adapted fragment spin-orbitals (see Eq 5.4 & Eq 5.7). To be more specific let us take as an example $NiCl_4^{2-}$. Focusing on the T_d complex, the $5t_1$, $16t_2$ and $8e$ spin-orbitals give rise to a total of $29\Gamma_8$ and $16\Gamma_7$ KS-orbitals, from which we identify the $6\Gamma_8$, $7\Gamma_8$ and $4\Gamma_7$ ones with dominant $3d$ character. We correspondingly occupy these evenly in the ZORA input with occupation numbers and ZORA eigenvalues taken from the output listed in Table 5.1.

Double group KS-orbital	Occupancy	ε_{KS}(eV)	Symmetry and number of SFO		
			8E $3d$ Nr.1	$5T_1$ no $3d$-species	$16T_2$ $3d$ Nr.2
$6\Gamma_8$	3.2	2.940	c(1,6)=-0.842i	X	c(15,6)=-0.104
$7\Gamma_8$	3.2	3.458	c(1,7)=-0.135i	X	c(15,7)= 0.789
4 Γ_7	1.6	3.509	0	0	c2(2,4)=-0.816

Table 5.1: *The selecting scheme for ZORA spin-orbit coupling eigenvalues, 3d-eigen-functions and their occupations for tetrahedral $NiCl_4^{2-}$ as a model example.*

We further find from the table of the SFO 8, 5 and 16 species of E, T_1 and T_2 symmetry, to yield a total of 29 basis functions for Γ_8 and 16 T_2 species to give rise to the same number of Γ_7 species. It is further important that the $3d$ orbitals, whose identity is sought, are the first and the second in the list for the E and T_2, representation, respectively. These yield the coefficients of the $6\Gamma_8$, $7\Gamma_8$ and $4\Gamma_7$ KS-ZORA eigenvectors (Table 5.1, to be extracted from the TAPE15 output after saving and converting into ASCII). We thus get truncated ZORA-KS eigenvectors and (diagonal) eigenvalues matrices $\mathbf{U}$ and Λ (Eq 5.10) which after

$$U = \begin{array}{c} \\ e \\ t_2 \\ t_2 \end{array} \begin{array}{c} \begin{array}{ccc} 6\Gamma_8 & 7\Gamma_8 & 4\Gamma_7 \end{array} \\ \begin{bmatrix} -0.842 & -0.135 & 0.0 \\ -0.104 & 0.789 & 0.0 \\ 0.0 & 0.0 & -0.816 \end{bmatrix} \end{array} \qquad \Lambda = \begin{array}{c} \\ 6\Gamma_8 \\ 7\Gamma_8 \\ 4\Gamma_7 \end{array} \begin{array}{c} \begin{array}{ccc} & & \end{array} \\ \begin{bmatrix} 2.940 & 0.0 & 0.0 \\ 0.0 & 3.458 & 0.0 \\ 0.0 & 0.0 & 3.509 \end{bmatrix} \end{array} \tag{5.10}$$

$$S = U.U^T \tag{5.11}$$

$$h = \{h_{\mu\nu}\} = S^{-(1/2)} U \Lambda U^T S^{(-1/2)} \tag{5.12}$$

$$h = \begin{array}{c} \\ e(\Gamma_8) \\ t_2(\Gamma_8) \\ t_2(\Gamma_7) \end{array} \begin{array}{c} \begin{array}{ccc} e(\Gamma_8) & t_2(\Gamma_8) & t_2(\Gamma_7) \end{array} \\ \begin{bmatrix} 2.951 & -0.074i & 0.0 \\ 0.074i & 3.447 & 0.0 \\ 0.0 & 0.0 & 3.509 \end{bmatrix} \end{array} \tag{5.13}$$

manipulations as described by Eq 5.11 and Eq 5.12 yields the one-electron Hamiltonian matrix (Eq 5.13). The comparison with Eq 5.5 yields directly the reduced matrix elements $\zeta^{t_1}_{t_2t_2}$ and $\zeta^{t_1}_{et_2}$ as well as the cubic ligand splitting Δ (333, 487 and 4166 cm^{-1}, respectively). In a similar way, the matrices of the spin-orbit coupling plus the ligand field for $NiCl_4^{2-}$ in D_{2d} symmetry are derived from matrix 5.14 to give using definition Eq 5.9 the ligand field and

$$\begin{array}{c} \\ \Gamma_6(a_1) \\ \Gamma_6(e) \\ \Gamma_7(b_1) \\ \Gamma_7(b_2) \\ \Gamma_7(e) \end{array} \begin{array}{c} \begin{array}{ccccc} & & & & \end{array} \\ \begin{bmatrix} 2.991 & 0.072i & 0.0 & 0.0 & 0.0 \\ -0.072i & 3.582 & 0.0 & 0.0 & 0.0 \\ 0.0 & 0.0 & 2.950 & -0.063i & -0.040i \\ 0.0 & 0.0 & 0.063i & 3.301 & -0.029 \\ 0.0 & 0.0 & 0.040i & -0.029 & 3.623 \end{bmatrix} \end{array} \tag{5.14}$$

spin-orbit coupling matrix elements listed in Table 5.2. Thus, from a single ZORA calculation both the ligand field and spin-orbit coupling matrices are obtained. In order to facilitate the analysis of the ADF output a series of MATLAB scripts are used as interfaces.

		$[NiF_4]^{2-}$		$[NiCl_4]^{2-}$		$[NiBr_4]^{2-}$		$[NiI_4]^{2-}$	
T_d	D_{2d}	T_d	D_{2d}	T_d	D_{2d}	T_d	D_{2d}	T_d	D_{2d}
h_{ee}	$h_{a_1a_1}(d_{z^2})$ $h_{b_1b_1}(d_{x^2-y^2})$	-2622	-1904 -3600	-2500	-2410 -2736	-2277	-2310 -2386	-2037	-2150 -2151
$h_{t_2t_2}$	$h_{b_2b_2}(d_{xy})$ $h_{ee}(d_{xz}, d_{yz})$	1748	-990 3247	1667	95 2526	1518	178 2259	1358	310 1945
$\zeta^{t_1}_{et_2}$	$\zeta^{e}_{a_1e}$ $\zeta^{e}_{b_1e}$ $\zeta^{a_2}_{b_1b_2}$	588	576 566 598	488	474 461 510	373	337 300 452	375	222 198 410
$\zeta^{t_1}_{t_2t_2}$	$\zeta^{a_2}_{ee}$ $\zeta^{e}_{b_2e}$	518	516 516	332	326 329	-242	-242 -253	-832	-824 -837

Table 5.2: *Ligand field (diagonal) matrix elements and reduced spin-orbit coupling matrix elements for T_d and elongated T_d →D_{2d} DFT optimized (spin-unrestricted, LDA-functional) $[NiX_4]^{2-}$ ($X = F^-$, Cl^-, Br^-, I^-) geometries from ZORA (spin-restricted, LDA+PW91 functional) calculations.*

5.3 Results and Discussion

5.3.1 The Jahn-Teller Effect and the Geometries of NiX_4^{2-} (X = F^-, Cl^-, Br^-, I^-).

NiX_4^{2-} (X = Cl^-, Br^- and I^-) are well studied structurally[114,115] and/or spectroscopically[116–119] and found to exist as slightly distorted ($NiCl_4$) or almost regular tetrahedra ($NiBr_4$ and NiI_4). NiF_4^{2-} is not known yet, Ni^{2+}-F^- complexes tending invariably to adopt a regular octahedral geometry. In line with these observations, our geometry optimizations (Table 5.3) show, that the extent of the Jahn-Teller elongation (Fig. 5.1) and the stabilization energy is strongly reduced due to mixing between the $e^4t_2^4$ and $e^3t_2^5$ configurations (*cf.* Appendix D.2), the latter configuration being Jahn-Teller stabilized by a D_{2d} compression.

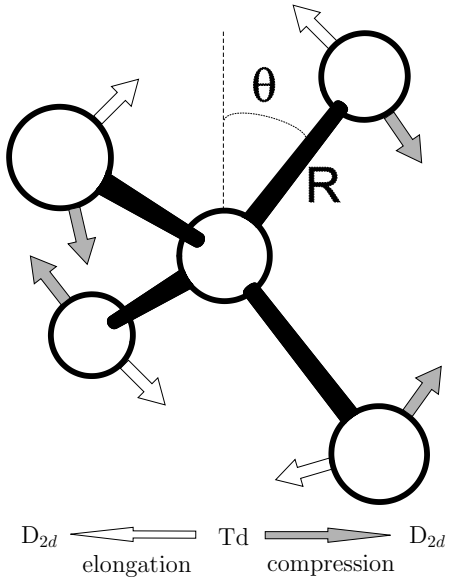

Figure 5.1: *The angle θ describing the tetrahedral distortion due to Jahn-Teller activity in NiX_4^{2-}.*

In this respect, the $e^3t_2^5$ configuration resembles very much the Jahn-Teller activity in Cu^{2+} with a single hole in the t_2-shell, which readily explains the different stereochemistries of these two ions.[113] In Table 5.3, we also list geometries and E_{JT} values of NiX_4^{2-} neglecting the $^3T_1(e^4t_2^4)$-$^3T_1(e^3t_2^5)$ mixing. It is this geometry with more pronounced distortions, which we use in order to explore the effect of symmetry lowering on the anisotropy of spin-orbit coupling. However in the discussion of electronic transitions and comparison with experiment we make use of the correct geometry.

X	R	$\delta\theta_{min}$	E_{JT}
F	1.94	-5.2 [-8.3]	-335 [-825]
Cl	2.29	-3.1 [-5.5]	-83 [-260]
Br	2.44	-2.9 [-5.3]	-62 [-198]
I	2.64	0.0 [-4.6]	0 [-49]

Table 5.3: *Bond lengths (in Å), the extent of Jahn-Teller elongation of the tetrahedral into the D_{2d} ground state energy minima ($\delta\theta_{min}$ in ^{o}) and the Jahn-Teller stabilization energy E_{JT} (in cm^{-1}) for NiX_4^{2-}(X=F^-,Cl^-,Br^- and I^-). Spin unrestricted DFT geometry optimizations (VWN-LDA functional) with and without (in square brackets) taking mixing between $^3T_1(e^4t_2^4)$ and $^3T_1$ $(e^3t_2^5)$ into account (still described by single determinants) have been performed, using a strategy described in Appendix D.2.*

5.3.2 Spin-Orbit Coupling in T_d Symmetry

The (α,β) - e, t_2 ($3d$) spin-orbit coupling in T_d symmetry gives rise to Γ_8 (e) and $\Gamma_8 + \Gamma_7$ (t_2) spinor levels, whose ZORA energies we plot in Fig. 5.2.

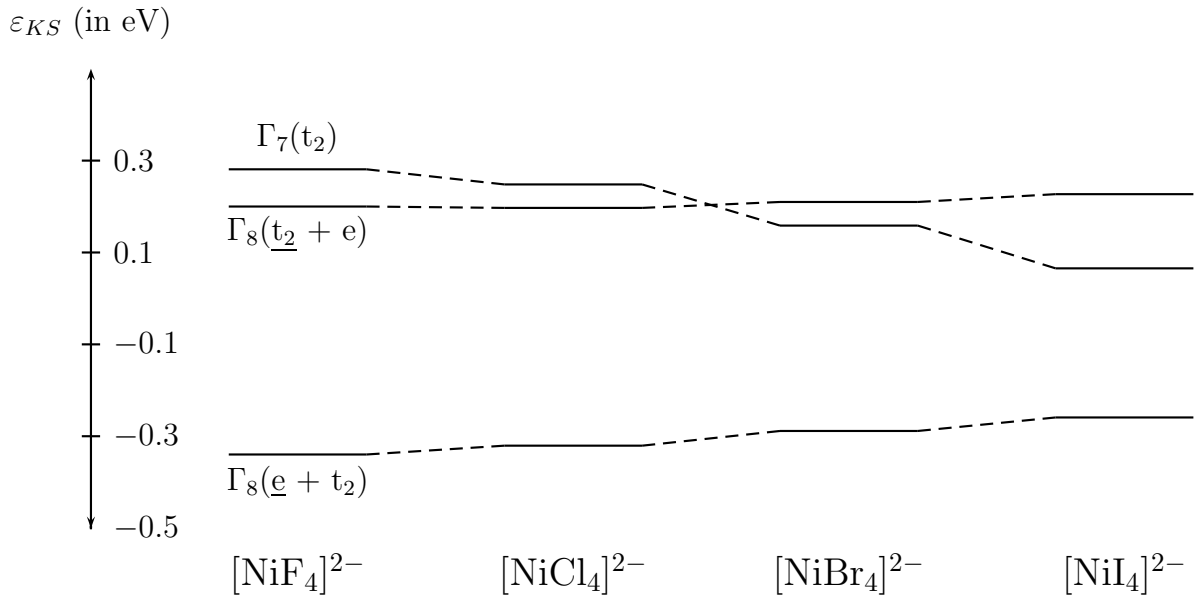

Figure 5.2: *Relative energies of Kohn-Sham orbitals with dominant 3 d character from a ZORA spin-orbit calculation of $[NiX_4]^{2-}$ (X=F^-, Cl^-, Br^-, I^-).*

While spin-orbit coupling leads to splitting of $t_2(\alpha,\beta)$ in first order. It causes a mixing of Γ_8 (t_2) and Γ_8 (e) to second order. Ligand field splitting $\Delta(T_d)$ is calculated in the range of 4370 (NiF_4^{2-}) to 3395 (NiI_4^{2-}) and dominates over the spin-orbit coupling: ζ(Ni^{2+})= 630 cm^{-1}; this is accounted for in Fig. 5.2, where dominant contributions from e and t_2 are underlined. We notice that when moving from NiF_4^{2-} to $NiCl_4^{2-}$ the Γ_8 ($\underline{t_2}$+e)-$\Gamma_7(t_2)$ energy separation (which equals (3/2) $\zeta^{t_1}_{t_2t_2}$, see Eq 5.5) gets smaller and it is lowered further going to $NiBr_4^{2-}$ and NiI_4^{2-}. It is important to observe that the sign of the splitting changes in the latter two complexes. The analysis of the energy levels (Fig. 5.2) in terms of the parameters $h_{t_2t_2}$-h_{ee}, $\zeta^{t_1}_{et_2}$ and $\zeta^{t_1}_{t_2t_2}$ (*cf.* Eq 5.5, calculated values are listed Table 5.2) shows indeed that $\zeta^{t_1}_{t_2t_2}$ becomes negative in the case of $NiBr_4^{2-}$ and NiI_4^{2-}. As has been pointed out previously,[119] ligand spin-orbit coupling (as large as 5000 cm^{-1} for I^-!) in combination with the metal($3d$)-ligand(np) mixing can strongly modify the effective spin-orbit coupling constant; this contribution can be of different sign and can even outweigh the spin-orbit coupling due to the $3d$ electrons; this turns the sign of the $\Gamma_8(\underline{t_2}$+e)-$\Gamma_7(t_2)$ splitting. Our ZORA calculations lend full support of this proposition, initially observed by MCD data on NiI_4^{2-}.[119] Contrary to earlier interpretations[120,121] our results indicate that spin-orbit coupling undergoes a stronger decrease with increasing metal-ligand covalency than Stevens' orbital reduction factors in the magnetic moment operator (amenable from a fit to magnetic susceptibilities). Indeed, with increasing covalency from F^- to Cl^- to Br^- to I^-, $\zeta^{t_1}_{et_2}$ and $\zeta^{t_1}_{t_2t_2}$ show a much stronger reduction than deduced from orbital reduction factors as the squared MO coefficients c^2_{3d} for $3d$ in the e and t_2 MOs and their combinations [0.82, 0.72, 0.68, 0.66 (e) and 0.75, 0.63, 0.60, 0.56 (t_2) for F^-, Cl^-, Br^-, I^- complexes, respectively]. The order of values for the reduced matrix elements in a

given complex $\zeta^{t_1}_{et_2} > \zeta^{t_1}_{t_2t_2}$ (obeyed for all cases in Table 5.3) reflects also subtle changes in the metal-ligand overlap (differential covalency) being larger for the more strongly ($\sigma + \pi$)-antibonding t_2, compared to the only weakly (π) - antibonding e orbital.

5.3.3 Spin-orbit Coupling in D_{2d} Symmetry

Going to a D_{2d} distorted T_d complex, the e(d_{z^2},$d_{x^2-y^2}$) and t_2(d_{xy}, d_{xz}, d_{yz}) orbitals split into a_1(d_{z^2})+b_1($d_{x^2-y^2}$) and b_2(d_{xy})+e(d_{xz},d_{yz}) species and the ligand field matrix becomes fully defined in terms of 10Dq plus the t_2 and e splitting parameters $3\delta_2$ and $2\delta_1$, respectively. This is illustrated on Figure 5.3 with parameter values pertaining to $NiCl_4^{2-}$.

Figure 5.3: *Orbital level splittings and notations for a symmetry based on description of the D_{2d} distorted (elongated) $NiCl_4^{2-}$ complex for a geometry obtained without correction for $^3T_1(e^4t_2^4)$-$^3T_1(e^3t_2^5)$ missing.*

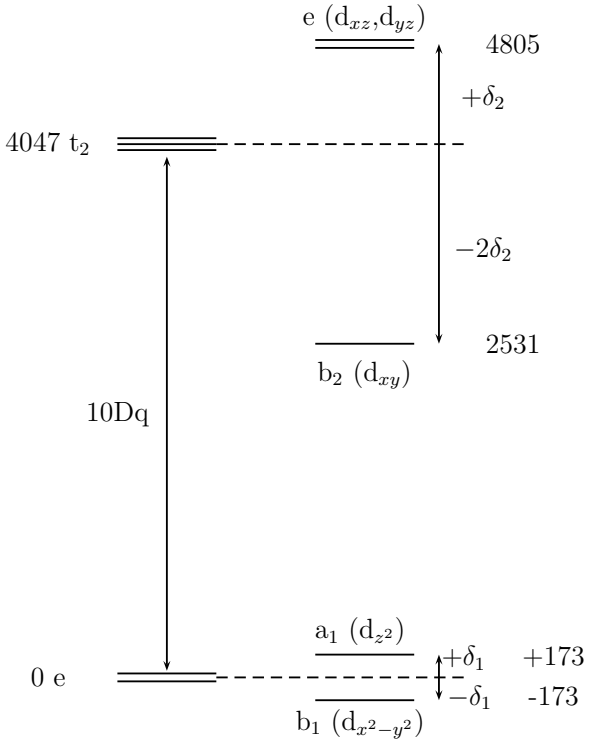

In parallel with this increase of the level of parameterization, the matrix of spin-orbit coupling becomes dependent on five reduced matrix elements (eq 5.8). In Figure 5.4 we show their variation with the angular geometry for $NiCl_4^{2-}$, changing the θ-angle in wide range from elongated to compressed D_{2d} structures. It is striking that the variations of the spin-orbit coupling parameters ζ^k_{ij} follow the same trends as the energies of the correspondingly involved orbitals i and j (Fig. 5.5 & 5.4); the stronger the extend of anti-bonding is (increasing the energy of the involved orbitals i, j) the stronger the ζ^k_{ij} reduction is.
Thus, the ζ^k_{ij} parameters reflect, in attenuated way, the angular dependence of the ligand field matrix. In classical LF theory, the parameter ζ has been deemed to be of atomic nature, being scaled by some reduction factor, occasionally accounting for axial anisotropy as well. In view of our results we suggest that such treatments are incomplete. The strong interrelation between the ligand field and molecular spin-orbit forces can even invalidate the common opinion of the two physical effects being opposite to each other.[122] In cases of very low-symmetry (causing non-zero off-diagonal elements in the matrix $h_{\mu\nu}$) it can

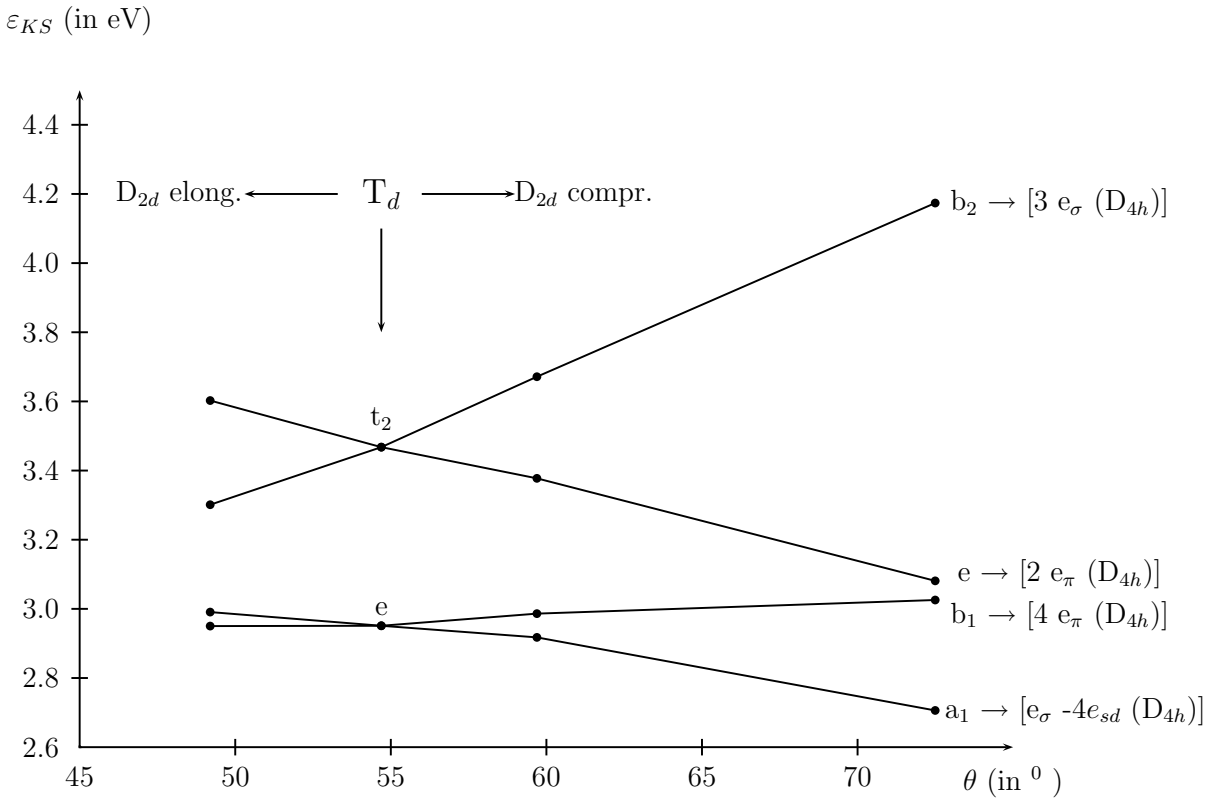

Figure 5.4: *The dependence of the Kohn-Sham orbital energies from non-relativistic calculation with average-of-configuration occupancies (T_d: $e^{3.2}t_2^{4.8}$; D_{2d}: $a_1^{1.6}b_1^{1.6}b_2^{1.6}e^{3.2}$) on the geometrical angle θ for $NiCl_4^{2-}$ (R = 2.29 Å, PW91-functional, TZP basis). Orbital energy expressions on the right hand side refer to the limiting case of a compression - square planar geometry and angular overlap model expressions (see Section 5.3.4).*

		$[NiF_4]^{2-}$		$[NiCl_4]^{2-}$		$[NiBr_4]^{2-}$		$[NiI_4]^{2-}$	
T_d	D_{2d}	T_d	D_{2d}	T_d	D_{2d}	T_d	D_{2d}	T_d	D_{2d}
h_{ee}	$h_{a_1a_1}(d_{z^2})$ $h_{b_1b_1}(d_{x^2-y^2})$	-2494	-1696 -3528	-2428	-2320 -2666	-2274	-2321 -2363	-2034	-2226 -2032
$h_{t_2t_2}$	$h_{b_2b_2}(d_{xy})$ $h_{ee}(d_{xz}, d_{yz})$	1662	-999 3111	1619	146 2420	1516	247 2218	1356	445 1906
B	B	715	713	521	521	462	458	401	399
C	C	2732	2685	2136	2126	1944	1948	1804	1844

Table 5.4: *Ligand field (diagonal) matrix elements and interelectronic repulsion B and C energies (in cm^{-1}) for Td and elongated Td-D_{2d} DFT-optimized (spin-unrestricted, LDA-functional) $[NiX_4]^{2-}$ ($X = F^-$, Cl^-, Br^-, I^-) geometries from LFDFT (LDA+PW91 functional) calculations.*

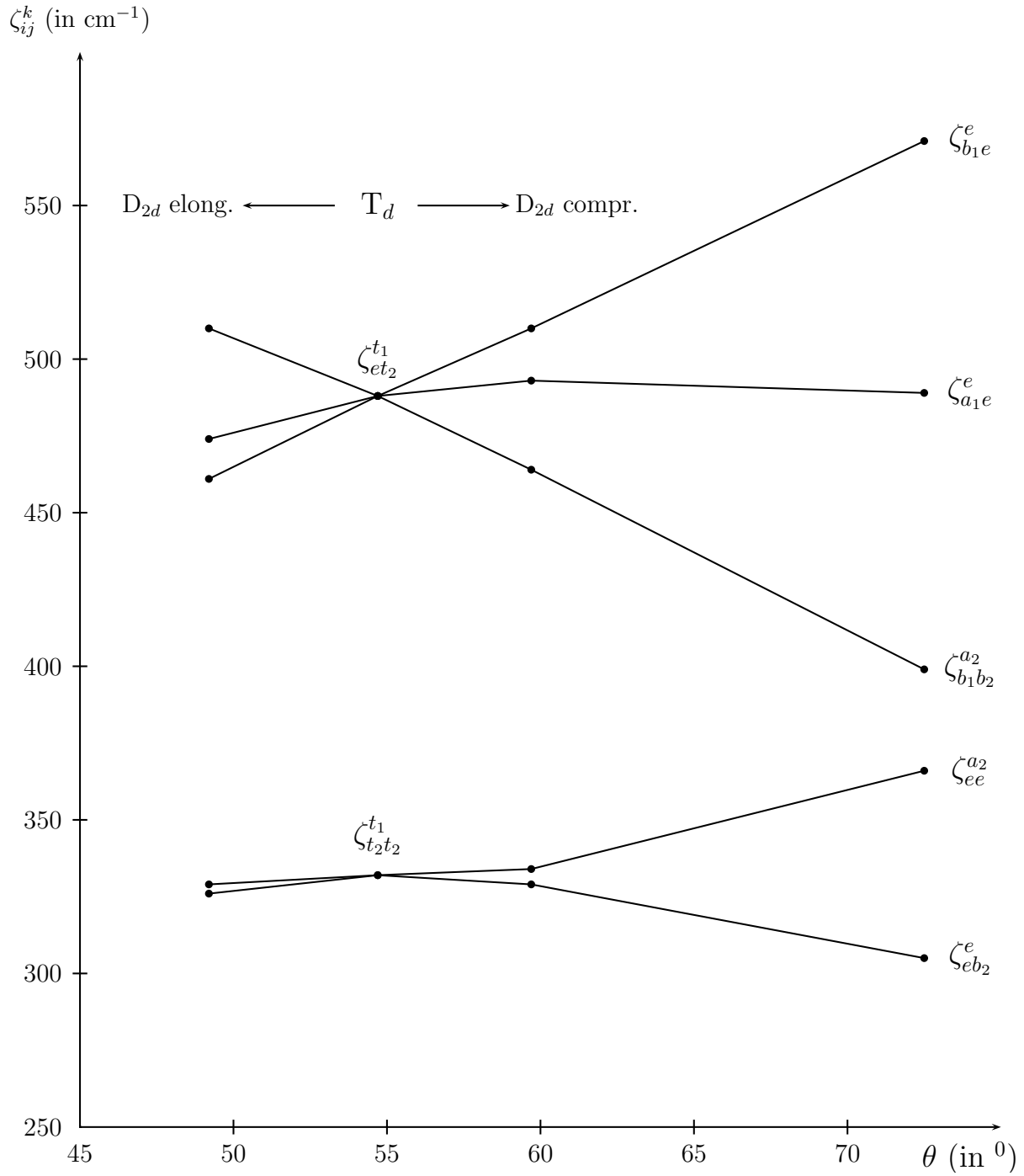

Figure 5.5: *Reduced matrix elements of the spin-orbit coupling operator from ZORA-ADF calculations in the T_d and D_{2d} geometries of the $NiCl_4^{2-}$ and their dependence in the geometrical anlge θ (see fig. 5.1).*

		B	C	Δ
Experiment[116]		810 cm^{-1}	3150 cm^{-1}	3500 cm^{-1}
GGA	PW91	521 cm^{-1}	2136 cm^{-1}	4155 cm^{-1}
	PBE	518 cm^{-1}	2196 cm^{-1}	4147 cm^{-1}
	RPBE	535 cm^{-1}	2218 cm^{-1}	4106 cm^{-1}
	revPBE	530 cm^{-1}	2212 cm^{-1}	4115 cm^{-1}
	BLYP	521 cm^{-1}	1576 cm^{-1}	4220 cm^{-1}
	LB94	359 cm^{-1}	1596 cm^{-1}	3041 cm^{-1}

Table 5.5: *The Racah's parameters determined with LFDFT method for $[NiCl_4]^{2-}$ using the exchange and correlation functionals available in ADF2003.01*

even prevent the separation of the one-electron Hamiltonian, in parts due to ligand field and spin-orbit coupling. This is fortunately not the case here ($h_{\mu\nu}$ is fully diagonal) to enable a neat analysis of the two effects separately.

5.3.4 Ligand Field-Parameters, Ground and Excited States Energies of NiX_4^{2-} (X=Cl^-, Br^-, I^-) and Comparison with Experimental Data

A list of ligand field parameters - the (diagonal) ligand field matrix and the B and C values for NiX_4^{2-} halide complexes in T_d and D_{2d} symmetry are listed in Table 5.4. There is a good agreement between the LFDFT values of 10Dq for $NiCl_4^{2-}$(4150 cm^{-1}) and the one deduced from a direct fit to the spectrum (3500 cm^{-1},[116] referred to hereafter as "experimental"). However, values of B and C are correspondingly 64% and 68% off from the experimental ones (810 and 3150 cm^{-1}, respectively[116]). This can be traced back to the functionals in use which overestimate 3*d*-electron delocalization. A list of LF parameters in dependence of the functionals offered by the ADF code (Table 5.5) shows a weak sensitivity with respect to this choice.

Likewise, use of more sophisticate basis functions, such as a quadruple 3*d* basis for Ni^{2+} (TZ2P+) does not alter the values of ζ (causing an increase of ζ's (Table 5.2) by $3-4\%$).

Excited state energies (Table 5.7) for geometries, corresponding to the T_d and D_{2d} energy minima (in this case taking $^3T_1(e^4t_2^4) \rightarrow {}^3T_1(e^3t_2^5)$ mixing into account) shows a good agreement between LFDFT and experimental values for the energies of the transitions $^3T_1 \rightarrow {}^3T_2$ and $^3T_1 \rightarrow {}^3A_2$, while the energies to the spin-forbidden transitions to $^1T_2$, ^1E and $^1T_2$,$^1T_1$,$^1A_1$, as well as the spin-allowed one to $^3T_1$ are found to be by about 4000 cm^{-1} and 5500 cm^{-1} smaller than the experimental ones. This is in accordance with the smaller B and C values and the stronger dependence of the energies of the mentioned states on B and C.

It is interesting that LF matrices from a non-relativistic LFDFT calculation and from ZORA differ from each other. These are compared in Table 5.6 taking the $b_1 \rightarrow a_1$, $b_1 \rightarrow b_2$ and $b_1 \rightarrow e$ energy differences. One can easily show when taking the angular geometry into account that these differences can be translated into an angular overlap parameterization to yield values of the parameters for σ and π-bonding and for the mixing

	$[NiF_4]^{2-}$		$[NiCl_4]^{2-}$		$[NiBr_4]^{2-}$		$[NiI_4]^{2-}$	
	LFDFT	ZORA	LFDFT	ZORA	LFDFT	ZORA	LFDFT	ZORA
$E(b_1 \rightarrow a_1)$	1832	1696	346	326	42	76	-194	10
$E(b_1 \rightarrow b_2)$	2529	2610	2812	2831	2610	2564	2477	2461
$E(b_1 \rightarrow e)$	6639	6847	5086	5262	4581	4645	3938	4096
e_σ	6488	6688	4980	5350	4457	4735	3734	4231
e_π	2612	2690	1594	1857	1379	1622	1012	1397
e_{sd}	2277	2629	3402	4094	3910	4382	4359	4562
10 Dq	4353	4597	4155	4289	3903	3913	3548	3550
$3\delta_2$	4110	4237	2274	2431	1971	2081	1461	1635

Table 5.6: *Orbital interpretations of ligand field energies from LFDFT and ZORA calculations in terms of the AOM parameterization scheme (e_σ, e_π, e_{sd}) along with values of 10Dq and the t_2-splitting $3\delta_2$ for tetragonally (D_{2d}) elongated $[NiX_4]^{2-}$ ($X = F^-$, Cl^-, Br^-, I^-).*

of d_{z^2} and 4s (which, being of the same symmetry, i.e. a_1, in D_{2d} can mix with each other)- yielding e_σ, e_π and e_{sd}, respectively. Remarkably, ZORA results reflect a distinctly larger extent of σ- and π-antibonding and e_{sd}-mixing compared to the non-relativistic LFDFT result. The effect of sd-mixing has a crucial influence via the Fermi contact terms κ on the hyperfine structure: A-tensor (treated in Section 6.1.1.2). We also notice that the value of the parameter ζ^{t1}_{t2t2} for $NiCl_4^{2-}$ we deduce from the ZORA results (332 cm^{-1}, Table 5.2) is found in excellent agreement with the one deduced from a fit to magnetic susceptibility data (380 cm^{-1}).[120,121] It is this parameter (in combination with the $^3T_1 \times$ e ground state Jahn-Teller activity, see Appendix D.2) which affects the $^3T_1$ ground state splitting. These are shown in Figure 5.6 for NiX_4^{2-} (X = Cl^-, Br^- and I^-). In accordance with large negative ζ^{t1}_{t2t2} value for NiI_4^{2-} a inverted zero-field splitting pattern for the ground state is calculated with a T_2 ground state and an E excited state 33 cm^{-1} higher in energy. In $NiBr_4^{2-}$ an intermediate coupling scheme is realized with an E ground state and T_2 next in energy. A D_{2d} distortion leads to an A_1 ground state, as it is the case as in $NiCl_4^{2-}$, however originating from the tetrahedral E, rather than from the tetrahedral A_1 state as in $NiCl_4^{2-}$. Therefore it follows that the sign and magnitude of the parameter $\zeta^{t_1}_{t_2t_2}$ is crucial importance for the ground state splitting. This, as well of Jahn-Teller activity in the $^3T_1$ ground state is a further experimental challenge for these systems. For more conclusive results, these compounds should be studied with more modern tools, such as resonance Raman and high-field - high-frequency EPR. We hope this study will motivate further experimental work in this direction.

5.4 Conclusions

In this chapter, we extended our LFDFT proposed with spin-orbit coupling, developing a procedure allowing one to extract spin-orbit coupling matrix elements from spin-restricted ZORA calculations. We show, using a symmetry analysis, that a set spin-orbit coupling parameters, rather than a single value or values scaled for anisotropy using (Stevens) orbital reduction factors are needed in order to properly describe a realistic situation. In particular, highly covalent ligands such as Br^- and I^- and their own spin orbit coupling

contributions can lead to unexpected, unprecedented splitting patterns of the ground state (zero-field splitting) which deserve further theoretical justification and testing and motivates further experimental work. In following contributions we will extend the formalism to systems with lower or no symmetry, calculating zero-field splitting for systems well characterized by EPR, thus extending the applicability of our LFDFT approach to fine structure tensor and hyperfine coupling effects.

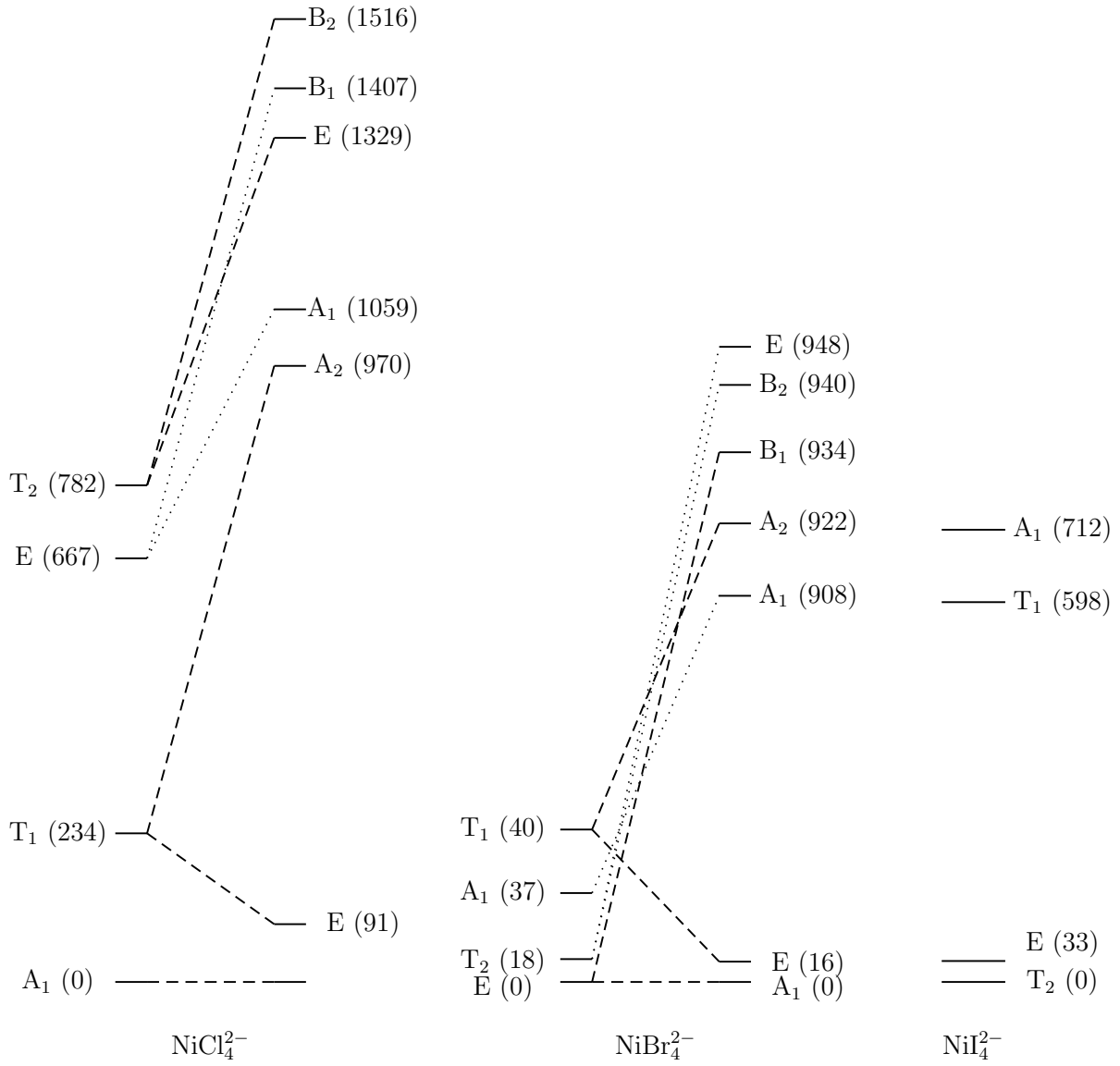

Figure 5.6: *The splitting of the* $^3T_1$ *ground state in the* T_d *geometry due to the spin-orbit coupling and in the lower* D_{2d} *symmetry minimum [for* $NiCl_4^{2-}$ *and* $NiBr_4^{2-}$, $^3T_1$ $(e^4t_2^4)$-$^3T_1$ $(e^3t_2^5)$ *mixing is taken into account]. Data for* $NiBr_4^{2-}$ *are plotted schematically, not following the energy scale used for* $NiCl_4^{2-}$ *and* NiI_4^{2-}.

Electronic State	$NiCl_4^{2-}$		$NiBr_4^{2-}$		NiI_4^{2-}	
T_d (D_{2d})	LFDFT	Exp.[118]	LFDFT	Exp.[117]	LFDFT	Exp.[119]
$^3T_1(^3A_2, {}^3E)$	0.0 (0.0, 1.87)		0.0 (0.0, 1.65)		0.0 (0.0, 1.24)	
$^3T_2(^3E, {}^3B_2)$	3.48 (4.20, 6.21)	3.84 - 4.76	3.28 (3.86, 5.80)		2.93 (3.39, 4.99)	
$^3A_2(^3B_1)$	7.53 (9.03)	6.90	7.06 (8.41)	6.40	6.32 (7.47)	
$^1T_2(^1B_2, {}^1E)$	7.64 (7.67, 9.40)	11.69	6.89 (6.92, 8.44)		6.22 (6.34, 7.46)	
$^1E\ (^1B_1, {}^1A_1)$	7.99 (7.80, 10.08)	12.22	7.19 (7.03, 9.02)		6.47 (6.44, 7.98)	
$^3T_1(^3E, {}^3A_2)$	10.74 (11.44, 13.57)	$\sim$ 14.70	9.69 (10.32, 12.01)		8.49 (9.09, 10.19)	
$^1T_2(^1E, {}^1B_2)$	12.69 (13.61, 15.10)	18.18	11.50 (12.26, 13.75)	(16.50, 17.44)	10.30 (10.94, 12.22)	
$^1T_1(^1E, {}^1A_2)$	14.01 (14.55, 17.06)	19.48	12.71 (13.23, 15.24)	18.13	11.35(11.97, 13.28)	(13.60, 14.64)
$^1A_1(^1A_1)$	13.79 (15.49)	-	12.47 (14.03)		11.15 (12.45)	14.08
$^1E\ (^1B_1, {}^1A_1)$	16.38 (17.78, 18.09)	22.08	14.99 (16.25, 16.42)	19.00	13.43 (14.59, 14.66)	(15.75, 15.62)
$^1A_1(^1A_1)$	30.12 (31.55)	-	27.29 (28.56)		24.58 (25.89)	

Table 5.7: *Multiplet energies (in kK=10^3 cm^{-1}) for NiX_4^{2-} (X=Cl^-,Br^-,I^-) complexes from LFDFT calculations (zero spin-orbit coupling) in their T_d and D_{2d}-elongated geometries (from DFT geometry optimizations taking mixing between $^3T_1(e^4t_2^4)$ and $^3T_1$ $(e^3t_2^5)$ into account) in comparison to experimental data from literature.*

Chapter 6

ESR Parameters within LFDFT

A wealth of information is encoded in the electron paramagnetic resonance (EPR) spectra of a given molecule. The EPR spectroscopy provides unique insights into the structural and electronic features of both organic and inorganic paramagnetic compounds. In organic chemistry, the technique is mostly used to get access to information about free radicals, since it provides a direct experimental measure for the distribution of the unpaired spin density. In the field of inorganic, or bio-inorganic, chemistry, the method is applied to examine the splitting of orbital and spin levels and the molecular symmetry and environment.
Consequently, it is of great interest to compute and analyze the relevant quantities (g- and A-tensors) of an EPR spectrum from first principle calculations. The area of theoretical and computational chemistry has in the last couple of years shown an increasing interest in the calculation of magnetic coupling parameters.
The application of Density Functional Theory (DFT) to EPR spectroscopy is relatively recent excepting the pioneering work of Daul and Weber[123] based on multiple-scattering Xα. Schreckenbach and Ziegler[124] have presented energy derivative calculations for the g-tensor with the usage of gauge including atomic orbitals (GIAO). Baerends and al. as well as Bruyndonckx[125] have published results of DFT calculations for the g- and A-tensors of TiF_3 by means of second order perturbation theory.[126] Furthermore, with the recent developments to include relativistic effects in modern DFT calculations, spin-orbit coupling (SOC) can be taken into account variationally using the zeroth-order regular approximation (ZORA) to the Dirac equation.[109,127–129] To obtain then the g-tensor, the effect of the external homogeneous magnetic field has only to be treated with first order perturbation theory.[130,131]
In this chapter, we present the result of calculations of the g- and A-tensors components for a transition metal complex: [Co(acacen)] or N,N'-ethylenebis(acetylacetoneiminato)cobalt (II) , as obtained from two methods: by the LFDFT and by calculating the Zeeman splitting of the ground Kramers doublet obtained by using ZORA calculation and second-order perturbation theory implemented in ADF for the hyperfine interaction.[130,132]

The choice of this complex was motivated by two reasons: firstly, the [Co(acacen)] complex belongs to a series of complexes with tetradentate Schiff bases which received much attention during the last decades,[133,134] largely because of their ability to reversibly absorb molecular oxygen under certain conditions. Secondly, it is a planar molecule (ligands are present only on a square planar environment) so it can be expected to show a

large anisotropy of the ESR parameters.
In the next sections, a description of the methodological and computational details is given. We show then, that with two methods, LFDFT and ZORA, this anisotropy is nicely reproduced. However, an analysis of the various contributions to the g- and A-tensors is only possible using the LFDFT method.

6.1 Methods

6.1.1 LFDFT: a New Way to Calculate ESR Parameters

As we know well the LFDFT method now, we will just give the details of the calculation of the g- and A-tensor components. The program which contains the implementation of these calculations is a modified version of the LF matlab program and is proposed in Appendix E.2.

6.1.1.1 Calculation of g-tensor

For TM complexes with light atoms such as carbon, nitrogen and oxygen, the spin-orbit coupling on the ligand can be completely neglected.

The methodology we consider in the preceding section is based on LF theory, it is therefore justified to express the spin-orbit interaction of the whole d- or f-manifold by a single parameter ζ_{nl}, i.e.:

$$\langle s\, m_s, a\, \alpha|\, \hat{\mathrm{H}}_{SO}\, |s\, m'_s, b\, \beta\rangle \approx \zeta_{nl}\, \langle s\, m_s, \ell\, m_\ell\, (a,\alpha)|\, \vec{l}\cdot\vec{s}\, |s\, m'_s, \ell\, m'_\ell\, (b,\beta)\rangle \tag{6.1}$$

where: $\zeta_{n\ell} = \langle R_{n\ell}|\, \frac{1}{r}\frac{dV}{dr}\, |R_{n\ell}\rangle$ and $|\mathrm{lm}_l>$ are real spherical harmonics. In practice $\zeta_{n\ell}$ is evaluated from the SO splitting obtained by a DFT spin-orbit ZORA caculation on the free ion ($\zeta = -598cm^{-1}$) and reduce further it by the orbital reduction factor ($k = 0.77$, *cf.* Eq 4.7). The ground state Kramers doublet $|0\pm\rangle$ is obtained by diagonalization of the full configuration interaction matrix: $\left\langle SD^d_\mu\right|\, \hat{h}_{LF} + \hat{g}_{ER} + \hat{h}_{SO}\, \left|SD^d_\nu\right\rangle$, where h_{LF} and h_{SO} have been defined previously[32] and where $\hat{g}_{ER}$ represents the electrostatic inter-electronic repulsion.[32] The g-tensor can be calculated from the equation for the Zeeman matrix elements $\langle 0\pm|\, k\hat{L}_\alpha + g_e\hat{S}_\alpha\, |0\pm\rangle$ equating them with those of the spin-hamiltonian $\langle\pm|\, g\cdot\vec{S}^{eff}|\pm\rangle$, i.e.:

$$\begin{array}{cc} |+\rangle & |-\rangle \\ \left(\begin{array}{cc} \frac{1}{2}g_{\alpha z} & \frac{1}{2}(g_{\alpha x}+ig_{\alpha y}) \\ \frac{1}{2}(g_{\alpha x}-ig_{\alpha y}) & -\frac{1}{2}(g_{\alpha z}) \end{array}\right) \end{array} = \begin{array}{cc} |0+\rangle & |0-\rangle \\ \left(\begin{array}{cc} \langle 0+|\, k\hat{L}_\alpha + g_e\hat{S}_\alpha\, |0+\rangle & \langle 0+|\, k\hat{L}_\alpha + g_e\hat{S}_\alpha\, |0-\rangle \\ \langle 0-|\, k\hat{L}_\alpha + g_e\hat{S}_\alpha\, |0+\rangle & \langle 0-|\, k\hat{L}_\alpha + g_e\hat{S}_\alpha\, |0-\rangle \end{array}\right) \end{array} \tag{6.2}$$

or

$$\begin{aligned} g_{\alpha z} &= \langle 0+|k\hat{L}_\alpha + g_e\hat{S}_\alpha|0+\rangle - \langle 0-|k\hat{L}_\alpha + g_e\hat{S}_\alpha|0-\rangle \\ g_{\alpha x} &= \langle 0+|k\hat{L}_\alpha + g_e\hat{S}_\alpha|0-\rangle + \langle 0-|k\hat{L}_\alpha + g_e\hat{S}_\alpha|0+\rangle \\ g_{\alpha y} &= i\,(\langle 0-|\, k\hat{L}_\alpha + g_e\hat{S}_\alpha\, |0+\rangle - \langle 0+|\, k\hat{L}_\alpha + g_e\hat{S}_\alpha\, |0-\rangle) \end{aligned} \tag{6.3}$$

where: k is the orbital reduction factor used to scale the spin-orbit coupling constant of the free ion, $\alpha = x, y, z$ and $\vec{L_\alpha}$ and $\vec{S_\alpha}$ are the orbital and spin-angular momentum operators. For n-electrons, we have:

$$\hat{L}_\alpha = \sum_{i=1}^{n} l_{i\alpha} \tag{6.4}$$

$$\hat{S}_\alpha = \sum_{i=1}^{n} s_{i\alpha} \tag{6.5}$$

6.1.1.2 Calculation of A-tensor

The ligand field description of the hyperfine interaction is already well described in literature,[31,135] but we summarize it briefly here. The interaction between the nuclear and electrons angular momenta of a many-electron system is described by the hyperfine coupling Hamiltonian:

$$H_{HF} = \hat{\Delta}_{HF} \cdot \vec{I} \tag{6.6}$$

where $\hat{\Delta}_{HF}$, the hyperfine coupling operator is given by equations 6.7 and 6.8, summation being carried out over all electrons (see Ref[31] for more details):

$$\vec{H_{HF}} = P \sum_{i=1}^{n} \left(\vec{l_i} + \frac{1}{7}\vec{a_i} - \kappa \vec{s_i} \right) \cdot \vec{I} \tag{6.7}$$

and

$$\vec{a_i} = 4\vec{s_i} - (\vec{l_i} \cdot \vec{s_i})\vec{l_i} - \vec{l_i}(\vec{l_i} \cdot \vec{s_i}) \tag{6.8}$$

The first term corresponds to the interaction of the nuclear spin with the orbital angular momentum of the electron, the second term to the interaction of the nuclear spin with the electronic spin and the last term is the Fermi contact term. P in equation 6.7 is the electron-nuclear dipolar coupling constant defined as:

$$P = g_e \beta \gamma_N \hbar \langle r^{-3} \rangle_{3d} \tag{6.9}$$

where γ_N is the giromagnetic ratio of the nucleus N (for Co: $\gamma_N = 0.63171 \cdot 10^4 G^{-1}$),[136] β the bohr magneton and $\langle r^{-3} \rangle_{3d}$ the expectation value of the $1/r^3$ operator over the $3d$ wavefunction. The Parameter κ is related with the Fermi hyperfine coupling constant a_F ($g_e = 2.0023$):

$$a_F = \frac{8\pi}{3} g_e \beta \gamma_N \hbar \sum_i \left[\rho_{i\uparrow}(0) - \rho_{i\downarrow}(0) \right] \tag{6.10}$$

as

$$\kappa = -\frac{a_F}{P} \tag{6.11}$$

Direct substitution yields:

$$\kappa = -\frac{8\pi}{3} \sum_i \left[\rho_{i\uparrow}(0) - \rho_{i\downarrow}(0) \right] \frac{1}{\langle r^{-3} \rangle_{3d}} \tag{6.12}$$

with γ_N in G^{-1}, P in cm^{-1} and $\langle r^{-3}\rangle_{3d}$ in atomic units, we have explicitly:

$$P = g_e \gamma_N \times 332.5258 \times 10^{-9} \times \langle r^{-3}\rangle_{3d} \tag{6.13}$$

Finally, the A-tensor can be calculated, similarly to the g-tensor, from the aforementioned ground Kramers doublet $|0\pm\rangle$ evaluating the hyperfine matrix elements $\langle 0\pm|\,\Delta_\alpha^{hf}\,|0\pm\rangle$ as:

$$\begin{aligned} A_{\alpha z} &= \langle 0+|\Delta_\alpha^{hf}|0+\rangle - \langle 0-|\Delta_\alpha^{hf}|0-\rangle \\ A_{\alpha x} &= \langle 0+|\Delta_\alpha^{hf}|0-\rangle + \langle 0-|\Delta_\alpha^{hf}|0+\rangle \\ A_{\alpha y} &= i\left(\langle 0-|\Delta_\alpha^{hf}|0+\rangle - \langle 0+|\Delta_\alpha^{hf}|0-\rangle\right) \end{aligned} \tag{6.14}$$

where $\alpha = x, y, z$ and k is the orbital reduction factor used to scale the spin-orbit coupling constant of the free ion and is determined according to Eq 4.7.

We now consider the numerical evaluations of P and κ which are used in the calculation of the A-tensor components.
The value of P has been calculated using TZP exponents given by the ADF data base and a numerical integration resulting to $\langle r^{-3}\rangle_{3d} = 5.83\ \mathrm{cm}^{-3}$ for the free ion: Co^{2+}. The corresponding value: $P = 245 \cdot 10^{-4}\ \mathrm{cm}^{-1}$ has been further reduced according to Eq 4.7 to $P = 188 \cdot 10^{-4}\ \mathrm{cm}^{-1}$.
The value of a_F needed to obtain κ (Eq 6.11) is more subtle to evaluate and deserves a bit of explanation. In fact there is no Fermi interaction within d^n configuration. However, the analysis of the hyperfine structure of supposedly d-electrons clearly requires an isotropic contribution denoted here as a_F. This term has two well-known contributions: (i) the spin polarization of the closed $|ns\rangle$ shells through the unpaired electron occupying the ground Kramers-doublet and (ii) the direct admixture of $|4s\rangle$ into the ground Kramers doublet through spin-orbit coupling with the low-lying $|d^1_{z^2}, A_1\rangle$ excited state that is contaminated by orbital interaction with $|4s\rangle$ of Co because of the low symmetry of [Co(acacen)]. Indeed, this mixing amounts to 4%. The first contribution to a_F is easily obtained using the DENSF utility program of ADF to compute $\rho_{i\uparrow}(0) - \rho_{i\downarrow}(0)$ (Eq 6.10) from an all-electron spin-polarized KS-calculation of [Co(acacen)]. The second contribution to a_F is obtained from the weight of all SD that contain d_{z^2} present in the ground Kramers doublet. The resulting parameters $a_F = -28 \cdot 10^{-4}$ and $P = 188 \cdot 10^{-4}\ \mathrm{cm}^{-1}$ lead to $\kappa = 0.147$ which was used in the calculation of the A-tensor. Table 6.1 summarizes all non-empirically determined parameters used in the calculation of the ESR and multiplet fine structure.

6.1.2 Spin-Orbit ZORA Approach

We use the ZORA implementation available in the ADF code to calculate g- and A-tensors in order to compare the results with those from LFDFT and with experiment. This method, developed by van Lenthe et al.,[130,132] uses GIAO, where the g- and A-tensors are calculated in a spin-orbit relativistic calculation using ZORA Hamiltonian with a spin restricted wavefunction.

6.2 Computational Details

The DFT calculations were performed with the Amsterdam Density Functional (ADF) program package (release 2003.01).[74] Both the local density approximation (LDA) and

Table 6.1: *All non-empirically determined parameters used in the calculation of the g- and A-tensors and in the calculation of multiplet fine structure*

Racah's parameters	B C	512 cm^{-1} 3118 cm^{-1}
Ligand Field matrix elements	$\langle x'y'\|h_{LF}\|x'y'\rangle$ $\langle y'z'\|h_{LF}\|y'z'\rangle$ $\langle z'^2\|h_{LF}\|z'^2\rangle$ $\langle x'^2-y'^2\|h_{LF}\|x'^2-y'^2\rangle$ $\langle z'^2\|h_{LF}\|x'^2-y'^2\rangle$ $\langle x'z'\|h_{LF}\|x'z'\rangle$	-1071 cm^{-1} 6308 cm^{-1} 5052 cm^{-1} 3731 cm^{-1} 2771 cm^{-1} -24003 cm^{-1}
spin-orbit coupling constant	ζ	460 cm^{-1}
orbital reduction factor	k	0.77
electron-nuclear dipolar coupling constant	P	$188 \cdot 10^{-4}$ cm^{-1}
	κ	0.147

the generalized gradient approximation (GGA) for exchange-correlation functionals were used. The LDA was applied with the Vosko, Wilk, and Nusair functional[57] and the GGA by using the exchange-correlation Perdew-Wang 91 functional.[111] The atoms were described by a triple-ζ Slater Type Orbital (STO) basis sets plus one polarization function and the frozen core (FC) approximation was used up to $3p$ for cobalt and up to $1s$ for carbon, nitrogen and oxygen for the g-Tensor calculation and the LFDFT calculations. For the calculation of A-tensor, we used all electrons basis sets.

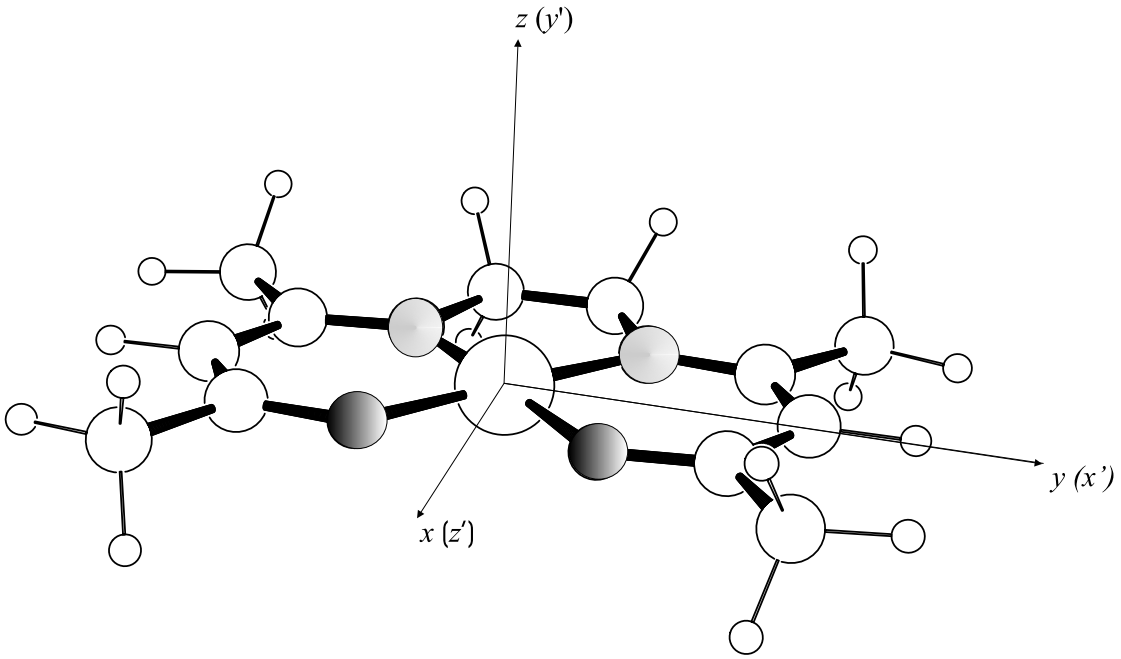

Figure 6.1: *The axial coordinates of the system in the discussion (x, y, z) and in the ADF calculations (x′, y′, z′) are represented along with the [Co(acacen)].*

Table 6.2: *Multiplet splitting energies determine by LFDFT method using GGA functional and frozen core approximation and compare to experiment (in cm^{-1}).*

	LFDFT	Exp.
$^2A_2$	0.0	-
$^2A_1$	4665	-
$^2B_1$	7036	4000
$^2A_1$	10885	8000
$^4B_1$	13021	-
$^4A_1$	12835	-
$^4B_1$	14694	-

The geometry of the complex has been adopted from X-ray crystallographic data determined by Cariati et al.[137] Since the deviation from C_{2v} symmetry is not significant we have chosen to impose this symmetry in our calculations. The coordinate system of Co(acacen) which by convention, has always been used to discuss this type of complexes is shown in Figure 6.1. In this way the molecule belongs actually to the point group C_{2v}(x), with x as the principal symmetry axis instead of the more conventional z-axis. The d-orbitals have hereby the following symmetry labels: d_{z^2} and $d_{x^2-y^2}$, a_1; d_{xy}, b_2; d_{xz}, b_1 ; d_{yz}, a_2. In the ADF calculations another orientation has been adopted (x', y', z': Fig 6.1) with two-fold axis along z. However, results have been always converted back to the traditional one (x, y, z).

6.3 Results and Discussion

The Co(acacen) with a d^7-configuration for Co^{II} has low-spin S=1/2 ground state. It shows a large anisotropy of both the g- and A-tensors (Tables 6.3 & 6.4) related to the low (C_{2v}) symmetry of the Co^{2+} coordination centers. A MO-diagram comprising MO's dominated by the 3d-atomic orbitals (Fig. 6.2) shows the typical splitting for square planar coordination with the σ-antibonding $d_{xy}(b_2)$-orbital, separated by about 27.4 kK from the weaker σ - d_{z^2}, the in-plane π - $d_{x^2-y^2}$ (both of a_1 symmetry) and the π out-of-plane yz (a_2) and xz (b_1) orbitals. The latter ones are much less separated in energy, covering a narrow range of energies (7.4 kK), as shown in Fig. 6.2. The d_{xz} and d_{yz} π-orbitals which are degenerate in a square planar complex (e_g, D_{4h} symmetry) are found in [Co(acacen)] to be considerably split (7.0 kK), this being responsible for large in-plane anisotropy of the main values of the g- and A-tensors. The underlying cause of this large splitting can be understood in the context of the molecular orbital model. Restricting to the highest occupied $\pi(a_2)$ (HOMO) and lowest unoccupied $\pi^*(b_1)$ (LUMO) ligand orbitals, we notice that the corresponding 3d-orbitals with the same symmetry, d_{yz} (d_{xz}) become destabilized (stabilized) by the interplay of π-donation (π-back donation). The consequences of this anisotropic π-bonding effects have been accounted for in refined LF models, such as the phase coupling concept of Ceulemans et al.,[138–140] quantifying an early idea of Orgel.[141] However, quantitatively, a large number of ill defined model parameters had to be introduced in order to account for this effect. Our LFDFT results lend full support of the π-anisotropy, as reflected by the calculated LF transitions (Table 6.2) and the calculated g- and A-tensors (Tables 6.3 & 6.4).

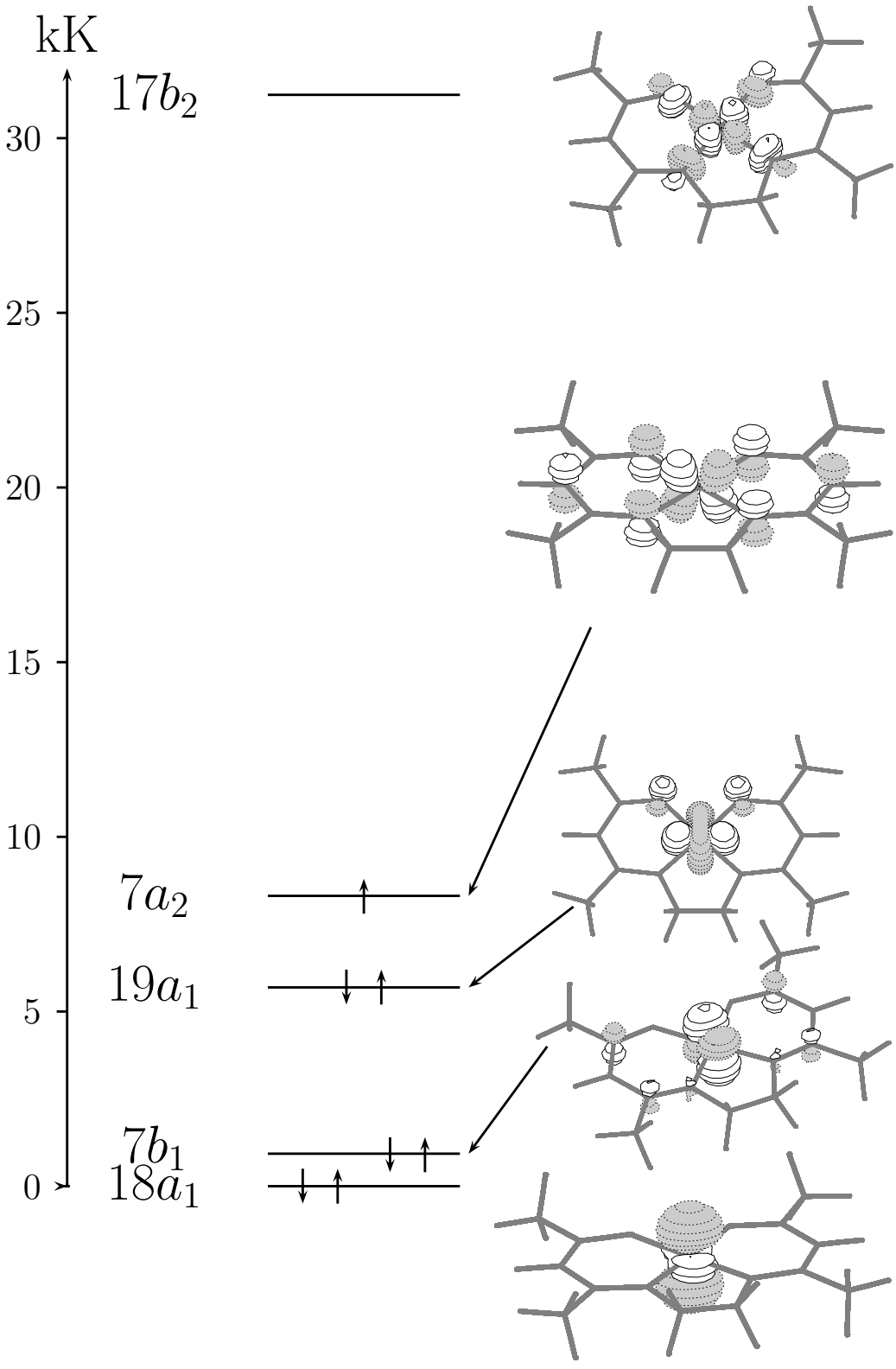

Figure 6.2: *KS MO diagram for the ground state configuration.*

	ZORA		LFDFT GGA		EXP[134]
	LDA	GGA	A	B	
g_{xx}	2.85	2.76	3.21	2.80	2.92/3.26
g_{yy}	1.89	1.93	1.87	1.94	1.90($\pm$0.03)
g_{zz}	1.91	1.92	1.87	2.11	2.00($\pm$0.02)
g_{iso}	2.22	2.20	2.28	2.32	

Table 6.3: *g-tensor values of [Co(acacen)] determined by spin-orbit restricted spin-orbit ZORA calculation and the LFDFT approaches and compared to a set of experimental data. LFDFT column A corresponds to the two states model: 97% $|d^1_{yz}d^2_{xy},\ ^2A_2\rangle$ + 3% $|d^1_{z^2}d^2_{xy},^2A_1\rangle$, and column B to the full calculation. For the expermimental data, we give a range of values because of a strong dependency upon the host lattice.*

	ZORA		LFDFT GGA		EXP[134]
	LDA	GGA	A	B	
A_{xx}	151	108	95	55	100/128
A_{yy}	25	28	12	14	32/40
A_{zz}	66	71	39	19	29/34

Table 6.4: *A-tensor values of [Co(acacen)] determined by spin-orbit restricted spin-orbit ZORA calculation and the LFDFT approaches and compared to a set of experimental data. LFDFT column A corresponds to the two states model: 97% $|d^1_{yz}d^2_{xy},\ ^2A_2\rangle$ + 3% $|d^1_{z^2}d^2_{xy},^2A_1\rangle$, and column B to the full calculation. For the expermimental data, we give a range of values because of a strong dependency upon the host lattice.*

With 7 electrons on the closely spaced a_2, a_1, b_1 and a_1-orbitals we have a $|d^1_{yz},^2A_2\rangle$ ground state. Mixing with excited states via spin-orbit coupling then leads to the observed anisotropic g- and A-tensors. These are given in Tables 6.3 & 6.4, where we also include results of ZORA spin-orbit calculations. Both the ZORA and the LFDFT show largest values for g_{xx} and A_{xx}. However, finer details in the g-tensor anisotropy, in particular the $g_{zz} > g_{xx}$ relationship are better reproduced the LFDFT method. As far as the overall agreement between theoretical and experimental A-tensor components goes, both the ZORA and the LFDFT calculations are of comparable moderate quality. However, we must keep in mind that experimental values of A_{xx}, A_{yy} and A_{zz} are less accurately determined. Thus, coordination to more distant atoms in the solid seems to make important contributions.[134] However, this is beyond the scope of the present study. Finally, we should mention that models of g and A-tensors, confined to one or two excited states (resulting in two-state model $|d^1_{yz},\ ^2A_2\rangle$-$|d^1_{z^2},\ ^2A_1\rangle$,[134] or three state model $|d^1_{yz},\ ^2A_2\rangle$-$|d^1_{z^2},\ ^2A_1\rangle$-$|d^1_{xz},\ ^2B_1\rangle$,[139,140] respectively) reflect essential features of the physical origin of the anisotropy. In Tables 6.3 & 6.4 we list the results from a consideration using a two-state model. The overall features are reasonably reproduced using this simplified approach. However, our present calculation enables a more detailled description of the experimental findings, particularly the difference between g_{yy} and g_{zz} for the g-tensor, and important contributions to A_{xx} from other excited states, ignored by the two or three states models are taken into account.

6.4 Conclusions

In this chapter we have extended our LFDFT approach with ESR fine structures, demonstrating that the model works, even in such complicated situations as the Co(acacen) complex. No doubt, the method can be refined including anisotropic covalent reduction factors and anisotropic spin-orbit coupling and inter-electronic repulsion. However we have found that calculating all these quantities using an average-of-configuration concept, thus introducing non-empirical atomic like B, C and ζ parameters and further, a single overall parameter k-in order to account for covalent reduction is a reasonable approximation, capable of describing electronic transitions and multiplet fine structures.

Chapter 7

Conclusions and Outlook

7.1 Conclusions

We have developed a DFT based LF model which utilizes SD energies in order to determine ligand field parameters from first principles. The formalism has been implemented using the following recipe:

1. make a geometry choice; for neutral complexes we recommend a GGA geometry optimization. For complexes with negative charges use of experimental bond lengths or LDA geometry optimization is preferable,
2. construct KS-LF orbitals with the average of configuration (AOC) providing n/5 occupancy of each d-MO for a TM with a d^n configuration,
3. calculate the set of *all* SD energies using these orbitals without allowing for orbital relaxation (no SCF iteration)
4. determine B,C and the 5x5 LF matrix h_{ab} from these data,
5. introduce these parameters into a favourite LF -program to get all multiplet energies.

The rather consistent fit for cubic symmetry reproducing the total manifold of symmetry independent SD shows, that DFT and LF theory are compatible. A theoretical justification (analysis) of this result is still lacking (but see the discussion in Ref.[84]). Comparing LF parameters deduced from DFT calculations with those resulting from fit to experimental spectra in high resolution, we can conclude that existing functionals are able to describe properly not only cubic but also low-symmetric ligand fields. In contrast parameters of interelectronic repulsion are calculated systematically smaller than values from spectral data. Similar observations have been reported by Solomon *et al.*.[142] Moreover, in Chapter 3, comparing results for both $10Dq$ and the parameters of interelectronic repulsion we can conclude, based on DFT considerations, that both the effect of the ligands in regards of spectrochemical series and the nephelauxetic effect are well reproduced by LFDFT. On the basis of these results we can conclude that DFT provides a rigorous interpretation of the LF parameters and leads to a justification of the parametric structure of the classical LF theory.

Thus fine structure tensors in EPR became a good candidate for application using this approach. In Chapter 6, we proove the ability of the method to determine the value of g and A-tensors.

Modern functionals which are all based on quantum Monte-Carlo treatment of a homogeneous electron gas contain most of the dynamical correlation. The non-dynamical or near degeneracy correlation however is missing. The key feature of our approach is the explicit treatment of near degeneracy correlation using adhoc Configuration Interaction (CI) within the active space of Kohn-Sham (KS) orbitals with dominant d-character. The calculation of the CI-matrices is based on a ligandfield analysis of the energies of all single determinants (micro-states) calculated according to Density Functional Theory (DFT) for frozen KS-orbitals corresponding to the averaged configurationof the d-orbitals. This procedure yields multiplet energies with an accuracy within 2000 cm^{-1}. The accuracy of this approximation can be judged from the agreement between calculated and observed transition energy.[32,35]

7.2 Outlook

We can use these results in order to motivate further work aimed at developing functionals and/or basis sets for spectroscopic purposes. But another aim is to extend the domain of applications of this method and we can cite for examples:

1. treat complexes with Lanthanides or Actinides (f-shell): progress in this direction are already done since first results are published or are in press.[26–28] But further work should be done because up to now, real description of the LF for these complexes can be obtained essentially by using the Kohn-Sham Equations with Constrained Electron Density (KSCED) method.[143]

2. model magnetic susceptibility: magnetic susceptibility has been described by Griffith and to model it should be a good extension to the LFDFT method.

3. use *meta*-GGA functional: up to now, the *meta*-GGA functional can only be used as a post-SCF procedure in ADF, as we need to run SCF procedure on the AOC, we can not use this functional for the LFDFT but it will be interesting to see, if in the future we are able to use it in an SCF procedure, the results we will obtain for our LFDFT treatment.

4. treat TM complexes including more than one TM: up to now, we focus on complexes with one TM but more often, we have to model properties for crystals and extend the LFDFT to, in the first time, dinuclear complex can be a good way to extend step by step the field of application of this method.

5. model MCD spectra of biological metal complexes: the program "Gener_ln" accept in the version which is presented in this thesis for the l value an integer like we used it along this thesis but can also accept an array, so up to now, we can generate the matrices we need in our method to model MCD spectra. So one has to extend the LFDFT matlab program to fit values of LF parameters for system which have more than one value of l.

These are only some suggestions and the list is not exhausive.

Bibliography

[1] Solomon E.I. and Hodgson K.O. *Spectroscopic Methods in Bioinorganic Chemistry.* Oxford University Press, **1998**.

[2] Bertini I., Gray H.B., Lippard S.J., and Valentine J.S. *Bioinorganic chemistry.* University Science, **1994**.

[3] Kohn W. and Sham L.J. Self-consistent equations including exchange and correlation effects. *Phys. Rev.*, 140, p:A1133, **1965**.

[4] Theophilou A. The energy density functional formalism for excited states. *J. Phys. C.*, 12, p:5419, **1979**.

[5] Gross E.K.U., Oliveira L.N., and Kohn W. Rayleigh-ritz variational principle for ensembles of fractionally occupied states. *Phys. Rev.* **A**, 37, p:2805, **1988**.

[6] Gross E.K.U., Oliveira L.N., and Kohn W. Density-functional theory for ensembles of fractionally occupied states. i. basic formalism. *Phys. Rev.* **A**, 37, p:2809, **1988**.

[7] Gross E.K.U., Oliveira L.N., and Kohn W. Density-functional theory for ensembles of fractionally occupied states. ii. application to the he atom. *Phys. Rev.* **A**, 37, p:2821, **1988**.

[8] Slater J.C. *Adv. Quantum Chem.*, 6, p:1, **1972**.

[9] Messmer R.P. and Salahub D.R. *J. Chem. Phys.*, 65, p:779, **1976**.

[10] Ziegler T., Rauk A., and Baerends E.J. *Theor. Chim. Acta*, 43, p:261, **1977**.

[11] Daul C.A. *Int. J. Quantum Chem.*, 52, p:867, **1994**.

[12] Gilardoni F., Weber J., Bellafrouh K., Daul C.A., and Guedel H.U. *J. Chem. Phys.*, 104, p:7624, **1996**.

[13] Aramburu J.A., Moreno M., Doclo K., Daul C.A., and Barriuso M.T. *J. Chem. Phys.*, 110, p:1497, **1999**.

[14] Deghoul F., Chermette H., Rogemond F., Moncorge R., Stueckl C., and Daul C.A. *Phys. Rev.* **B**, 60, p:2404, **1999**.

[15] Dunlap B.I. *Adv. Chem. Phys.*, 69, p:287, **1987**.

[16] Löwdin P.-O. *Adv. Chem. Phys.*, 14, p:283, **1969**.

[17] Goerling A. Symmetry in density-functional theory. *Phys. Rev.* **A**, 47, p:2783, **1993**.

[18] Sala F.D. and Goerling A. Open-shell localized hartree-fock approach for an efficient effective exact-exchange kohn-sham treatment of open-shell atoms and molecules. *J. Chem. Phys.*, 118, p:10439, **2003**.

[19] Mineva T., Goursot A., and Daul C.A. Atomic multiplet energies from density functional calculations. *Chem. Phys. Lett.*, 350, p:147–154, **2001**.

[20] Bethe H. *Ann. Phys.*, 3, p:133, **1929**.

[21] Ilse F.E. and Hartmann H. *Z. Phys.*, 197, p:239, **1951**.

[22] Hartmann H. and Schlaefer H.L. *Z. Naturforsch.*, 6a, p:751, **1951**.

[23] Hartmann H. and Schlaefer H.L. *Z. Phys.*, 197, p:239, **1951**.

[24] Jørgensen C.K., Pappalardo R., and Schmidtke H. *J. Chem. Phys.*, 39, p:1422, **1963**.

[25] Schaeffer C.E. and Jørgensen C.K. *Mol. Phys.*, 9, p:401, **1965**.

[26] Borel A., Helm L.E., and Daul C.A. Hybrid ligand-field theory/quantum chemical calculation of the fine structure and zfs in lanthanide(iii) complexes. *Chem. Phys. Lett.*, 383, p:584–591, **2004**.

[27] Zbiri M., Atanasov M., Daul C.A., Garcia-Lastra J., and Wesolowski T.A. *Chem. Phys. Lett.* in press.

[28] Atanasov M., Daul C.A., Guedel H.U., Wesolowski T.A., and Zbiri M. *Inorg. Chem.* in press.

[29] van Vleck J.H. Valence strength and the magnetism of complex salts. *J. Chem. Phys.*, 3, p:807, **1935**.

[30] Mulliken R.S. *Phys. Rev.*, 40, p:55, **1932**.

[31] Griffith J.S. *The Theory of Transition-Metal Ions.* Cambridge University Press, **1971**.

[32] Atanasov M., Daul C.A., and Rauzy C. *Struct. Bond.*, 106, p:97–125, **2004**.

[33] Slater J.C. *Quantum Theory of Atomic Structure, Vol. 2.* McGraw-Hill, London, **1960**.

[34] Misetich A.A. and Buch T. *J. Chem. Phys.*, 41, p:2524, **1964**.

[35] Atanasov M., Daul C.A., and Rauzy C. *Chem. Phys. Lett.*, 367, p:737–746, **2003**.

[36] Jørgensen C.K. *Struct. Bond.*, 1, p:3–31, **1966**.

[37] Schaeffer C.E. and Jørgensen C.K. *J. Inorg. Nucl. Chem.*, 8, p:143, **1958**.

[38] Parr R.G. and Yang W. *Density Functional Theory of Atoms and Molecules*. New York, Oxford University Press, **1998**.

[39] Koch W. and Holthausen M. *A chemist's Guide to Density Functional Theory*. New York, Wiley-VCH, **2000**.

[40] Dreizler R.M. and Gross E.K.U. *Density Functional Theory, an approach to Quantum Many-Body Problem*. New York, Springer-Verlag, **1990**.

[41] Labanowsky J.K. and Andzelm J.W. *Density Functional Methods in Chemistry*. Springer-Verlag, **1991**.

[42] Fermi E. *Rend. Accad. Lincei*, 6, p:602, **1927**.

[43] Thomas H. *Z. Phys.*, 48, p:73, **1928**.

[44] Thomas H. *Proc. Camb. Phil. Soc.*, 23, p:542, **1927**.

[45] Hohenberg P. and Kohn W. *Phys. Rev.* **B**, 136, p:864, **1964**.

[46] Teller E. *Rev. Mod. Phys.*, 34, p:627, **1962**.

[47] Dirac P.A.M. *Proc. Camb. Phil. Soc.*, 26, p:376, **1930**.

[48] von Weizsacker C.F. *Z. Phys.*, 96, p:431, **1935**.

[49] Yonei K. and Tomishima Y. *J. Phys. Soc. Japan*, 20, p:1051, **1965**.

[50] Lieb E.H. *Rev. Mod. Phys.*, 53, p:603, **1981**.

[51] Yang W. *Phys. Rev.* **A**, 34, p:4575, **1986**.

[52] Brack M. *Density Functional Methods in Physics*, page 331. Kluwer Academic/Plenum Publishers, **1985**.

[53] Levy M. *Proc. Natl. Acad. Sci*, 76, p:6062, **1879**.

[54] Levy M. *Phys. Rev.* **A**, 26, p:1200, **1982**.

[55] Perdew J. *Phys. Rev.* **B**, 31, p:6264, **1985**.

[56] Ceperley D.M. and Alder B.J. *Phys. Rev. Lett.*, 45, p:566, **1980**.

[57] Vosko S.H., Wilk L., and Nusair M. *Can. J. Chem.*, 58, p:1200, **1980**.

[58] Becke A.D. *Phys. Rev.* **A**, 38, p:3098, **1988**.

[59] Colle R. and Salvetti O. *Theor. Chim. Acta*, 37, p:329, **1975**.

[60] Lee C., Yang W., and Parr R.G. *Phys. Rev.* **B**, 37(2), p:785, **1988**.

[61] Miehlich B., Savin A., Stoll H., and Preuss H. *Chem. Phys. Lett.*, 157, p:200, **1989**.

[62] Becke A.D. *J. Chem. Phys.*, 98, p:5648, **1993**.

[63] Perdew J.P. and Kurth S. *Phys. Rev. Lett.*, 82, p:2544, **1999**.

[64] Proynov E., Chermette H., and Salahub D.R. *J. Chem. Phys.*, 113, p:10013, **2000**.

[65] Ernzerhof M. and Scuseria G.E. *J. Chem. Phys.*, 111, p:911, **1999**.

[66] van Voorhis T. and Scuseria G.E. *J. Chem. Phys.*, 109, p:400, **1998**.

[67] Levy M. and Perdew J. *Phys. Rev.* **A**, 32, p:2010, **1985**.

[68] Levy M. and Perdew J. *Density Functional Methods in Physics*, page 11. Kluwer Academic/Plenum Publishers, **1985**.

[69] Levy M. *Single-Particle Density in Physics and in Chemistry*, page 45. London, Academic Press, **1987**.

[70] Janak J.F. *Phys. Rev.* **B**, 18, p:7165, **1978**.

[71] Goerling A. Density functional theory for excited states. *Phys. Rev.* **A**, 54, p:3912, **1996**.

[72] Nagy A. Excited states in density functional theory. *Int. J. Quantum Chem.*, 70, p:681, **1998**.

[73] Nagy A. Kohn-sham equations for multiplets. *Phys. Rev.* **A**, 57, p:1672, **1998**.

[74] te Velde G., Bickelhaupt F.M., Baerends E.J., Fonseca Guerra C., van Gisbergen S.J.A, Snijders J.G., and Ziegler T. *J. Comput. Chem.*, 22, p:931–967, **2001**.

[75] Perdew J.P., Chevary J.A., Vosko S.H., Jackson K.A., Pederson M.R., Singh D.J., and Fiolhais C. Atoms, molecules, solids, and surfaces: Applications of the generalized gradient approximation for exchange and correlation. *Phys. Rev.* **B**, 46, p:6671, **1992**.

[76] Perdew J.P., Burke K., and Ernzerhof M. *Phys. Rev. Lett.*, 77, p:3865, **1996**.

[77] Hammer B., Hansen L.B., and Norskov J.K. *Phys. Rev.* **B**, 59, p:7413, **1999**.

[78] Zhang Y. and Yang W. *Phys. Rev. Lett.*, 80, p:890, **1998**.

[79] Johnson B.G., Gill P.M.W., and Pople J.A. *J. Chem. Phys.*, 98(7), p:5612, **1993**.

[80] Russo T.V., Martin R.L., and Hay P.J. *J. Chem. Phys.*, 101(9), p:7729, **1994**.

[81] Perdew J.P. Density-functional approximation for the correlation energy of the inhomogeneous elctron gas. *Phys. Rev.* **B**, 33, p:8822, **1986**.

[82] van Leeuwen R. and Baerends E.J. Exchange-correlation potential with correct asymptotic behaviour. *Phys. Rev.* **A**, 49(4), p:2421–2431, **1994**.

[83] Ziegler T. *Chem. Rev.*, 91, p:651, **1991**.

[84] Bridgeman A.J. and Gerloch M. *Chem. Phys. Lett.*, 45, p:179, **1997**.

[85] Durand P.H. and Malrieu J.P. *Adv. Chem. Phys.*, 67, p:321, **1987**.

[86] Des Cloizeaux J. Extension d'une formule de Lagrange à des problèmes de valeurs propres. *Nucl. Phys.*, 20, p:321, **1960**.

[87] Shigekazu U., Kazuyori U., and Keiichi K. *Semento Gijetsu Nenpo*, 29, p:32, **1975**.

[88] Ferguson J. and Wood D.L. Crystal field spectra of $d^{3,7}$ ions. vi the weak field formalism and covalency. *Austr. J. Chem.*, 23, p:861, **1970**.

[89] Adamsky H. PhD thesis, University of Düsseldorf, **1995**. AOMX is available in the Internet at the address *http://www.aomx.de* This site provides selected examples and an AOM parameter database, and will be further developed to a forum for scientific exchange about Angular Overlap Model applications to TM complexes.

[90] Daul C.A., Doclo K.G., and Stueckl C. *Recent Advances in Density Functional Methods (Part II)*, page 61. World Scientific, **1997**.

[91] Ferguson J., Wood D.L., and Knox K. *J. Chem. Phys.*, 39, p:881, **1963**.

[92] Ludi A. and Feitknecht W. *Helv. Chim. Acta*, 46, p:2226, **1963**.

[93] Allen G.C., El-Sharkawy A.M., and Warren K.D. *Inorg. Chem.*, 10, p:2538, **1971**.

[94] Schwartz R.W. *Inorg. Chem.*, 15, p:2817, **1976**.

[95] Witzke H. *Theor. Chim. Acta*, 20, p:171, **1971**.

[96] Knox K. and Mitchell D.W. *J. Inorg. Nucl. Chem.*, 21, p:253, **1961**.

[97] Jagner S., Ljungstroem E., and Vannerberg N.G. *Acta Chem. Scand.*, A28, p:623, **1974**.

[98] Gupta M.P., Milledge H.J., and McCarthy A.E. *Acta Cryst. B.*, 30, p:656, **1974**.

[99] Mukherjee R.K. and Chowdhury M. *Chem. Phys. Lett.*, 34, p:178, **1975**.

[100] Alexander J.J. and Gray H.B. *J. Am. Chem. Soc.*, 90, p:4260, **1968**.

[101] Lever A.B.P. *Inorganic Electronic Spectroscopy*, page 450. Elsevier, 2 edition, **1984**.

[102] Cohen S., Mayer I., and Reinen D. *J. Solid State Chem.*, 107, p:218, **1993**.

[103] Brunold T.C., Hauser A., and Guedel H.U. *J. Luminescence*, 59, p:321, **1994**.

[104] Hazenkamp M.F., Guedel H.U., Atanasov M., Kesper U., and Reinen D. *Phys. Rev.* **B**, 53, p:2357, **1996**.

[105] Shannon R.D. *Acta Cryst*, A32, p:751, **1976**.

[106] Studer P. PhD thesis, University of Fribourg, **1975**.

[107] Grimme S. *Chem. Phys. Lett.*, 259, p:128, **1996**.

[108] Grimme S. and Waletzke M. *J. Chem. Phys.*, 111, p:5645, **1999**.

[109] van Lenthe E., Baerends E.J., and Snijders J.G. *J. Chem. Phys.*, 99, p:4597, **1993**.

[110] Slater J.C. A simplification of the hartree-fock method. *Phys. Rev.*, 81, p:385, **1951**.

[111] Perdew J.P., Chevary J.A., Vosko S.H., Jackson K.A., Pederson M.R., Singh D.J., and Fiolhais C. *Phys. Rev.* **B**, 46, p:6671–6687, **1992**.

[112] Bruyndonckx R., Daul C.A., Manoharan P.T., and Deiss E. *Inorg. Chem.*, 36, p:4251–4256, **1997**.

[113] Reinen D., Atanasov M., Nikolov G.S., and Steffens F. *Inorg. Chem.*, 27, p:1678–1686, **1988**.

[114] Pauling P. *Inorg. Chem.*, 5, p:1498–1505, **1966**.

[115] Stucky C.D., Folkers J.B., and Kistenmacher T.J. *Acta Cryst*, 23, p:1064, **1967**.

[116] Liehr A.D. and Ballhausen C.J. *Ann. Phys.*, 6, p:134, **1959**.

[117] Mooney A., Nuttal R.H., and Smith W.E. *J. Chem. Soc., Dalton Trans.*, page 1920, **1973**.

[118] Koester V.J. and Dunn T.M. *Inorg. Chem.*, 14, p:1811, **1975**.

[119] Collingwood J.C., Day P., and Dennning R.G. *J. Chem. Soc. Faraday Trans. II*, 69(4), p:591–607, **1973**.

[120] Gerloch M. and Slade R.C. Paramagnetic susceptibilities and anisotropies of nickel$^{(II)}$ ions in "tetrahedral" environments. I. general behavior of a spin-triplet model. *J. Chem. Soc. (A)*, 6, p:1012–1022, **1969**.

[121] Gerloch M. and Slade R.C. Paramagnetic susceptibilities and anisotropies of nickel$^{(II)}$ ions in "tetrahedral" environments. II. covalency and distortion in tetraethylammonium tetrachloronickelate(II), and bis(n-isopropylsalicylaldiminato)nickel(II). *J. Chem. Soc. (A)*, 6, p:1022–1028, **1969**.

[122] Liehr A.D. *J. Phys. Chem.*, 64, p:43–51, **1960**.

[123] Daul C. and Weber J. *Helv. Chim. Acta*, 65, p:2486, **1982**.

[124] Schreckenbach G. and Ziegler T. *J. Phys. Chem.* **A**, 101, p:3388, **1997**.

[125] Bruyndonckx R. *Density Functional Theory as a Practical Tool to Calculate Molecular Properties: EPR and Jahn-Teller parameters.* PhD thesis, University of Fribourg (Switzerland), **1999**.

[126] Belanzoni P., Baerends E.J., van Asselt S., and Langewen P.B. *J. Chem. Phys.*, 99, p:13094, **1995**.

[127] van Leeuwen R., van Lenthe E., Baerends E.J., and Snijders J.G. *J. Chem. Phys.*, 101, p:1272, **1994**.

[128] van Lenthe E., Baerends E.J., and Snijders J.G. *J. Chem. Phys.*, 101, p:9783, **1994**.

[129] van Lenthe E., Snijders J.G., and Baerends E.J. *J. Chem. Phys.*, 105, p:6505, **1996**.

[130] van Lenthe E., Wormer P.E.S., and van der Avoird A. *J. Chem. Phys.*, 107, p:2488, **1997**.

[131] Belanzoni P., Van Lenthe E., and Baerends E.J. *J. Chem. Phys.*, 114, p:4421, **2001**.

[132] van Lenthe E., van der Avoird A., and Wormer P.E.S. *J. Chem. Phys.*, 108, p:4783, **1998**.

[133] Calvin M. and Barkelew C. H. *J. Am. Chem. Soc.*, 68, p:2267, **1946**.

[134] Daul C., Schlaepfer C.W., and A. von Zelewsky. *Struct. Bond.*, 36, p:128, **1978**.

[135] Bencini A. and Gatteschi D. *J. Magn. Reson.*, 34, p:653, **1979**.

[136] Wertz J.E. and Bolton J.R. *Electron Spin Resonance, Elementary Theory and Practical Applications*. McGraw-Hill, New York, **1972**.

[137] Cariati F., Morazzoni F., Busetto C., Del Piero G., and Zazzetta A. *J. Chem. Soc., Dalton Trans.*, page 342, **1976**.

[138] Ceulemans A., Dendooven M., and Vanquickenborne L.G. *Inorg. Chem.*, 24, p:1153, **1985**.

[139] Ceulemans A., Dendooven M., and Vanquickenborne L.G. *Inorg. Chem.*, 24, p:1159, **1985**.

[140] Ceulemans A., Debuyst R., Dejehet F., King G.S.D., and Vanhecke M. *J. Phys. Chem.*, 94, p:105, **1990**.

[141] Orgel L.E. *J. Chem. Soc. (A)*, 6, p:3683, **1961**.

[142] Solomon E.I., Chen P., Metz M., Lee S.-K., and Palmer A.E. *Angew. Chem. Int. Ed. Engl.*, 40, p:4570, **2001**.

[143] Wesolowski T.A. and Weber J. *Chem. Phys. Lett.*, 248, p:71, **1996**.

[144] Welch B.B., Jones K., and Hobbs J. *Pratical programming in Tcl and Tk*. Prentice Hall PTR, 4 edition, **2003**.

[145] Rose M.E. *Elementary Theory of Angular Momentum*. Dover Publications, Inc., **1995**.

Appendix A

Mathematical background

A.1 Expansion of $1/r_{ij}$

The ligand field potential is expressed in function of $1/|\vec{R}-\vec{r}|$ where $\vec{R}$ defined the ligand position and $\vec{r}$ defined the electron position. The expansion of this term is analog to the expansion of $1/r_{ij}$ where i and j represent the positions of the electrons i and j respectively. We will proceed to the expansion of $1/|r_{ij}|$ in order to give the intrinsic details of ligand field theory. So the norm of $|r_{ij}|$ is equal to:

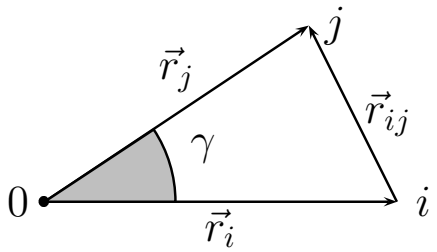

Figure A.1: *Position of the electrons i and j.*

$$|r_{ij}| = |\vec{r}_i - \vec{r}_j| = \sqrt{r_i^2 + r_j^2 - 2r_i r_j \cos\gamma} \qquad \text{(A.1)}$$

where γ is the angle between the two vectors. If we define $x = r_j/r_i$, Equation A.1 reads:

$$|\vec{r}_i - \vec{r}_j| = r_i\sqrt{1 + x^2 - 2x\cos\gamma} \qquad \text{(A.2)}$$

So if we consider the inverse and we expand it in terms of Legendre polynomials we get the relation A.3:

$$\begin{aligned}\frac{1}{|r_{ij}|} &= \frac{1}{r_i}\frac{1}{\sqrt{1 + x^2 - 2x\cos\gamma}} \\ &= \frac{1}{r_i}\sum_n a_n P_n(\cos\gamma)\end{aligned} \qquad \text{(A.3)}$$

If we square the both side of this equation and multiply by $\sin\gamma\, d\gamma$ and integrate over γ from 0 to π, we obtained

$$\frac{1}{x}\log\frac{1+x}{1-x} = \sum_n \frac{2}{2n+1}a_n^2 \qquad \text{(A.4)}$$

But, by an expansion, we have:

$$\frac{1}{x}\log\frac{1+x}{1-x} = \sum_n \frac{2}{2n+1}x^{2n} \qquad \text{(A.5)}$$

so we conclude that $a_n = x^n$ and the expansion of $1/|r_{ij}|$ in terms of $P_n(\cos\gamma)$ is:

$$\frac{1}{|r_{ij}|} = \frac{1}{r_i}\sum_n x^n P_n(\cos\gamma) \tag{A.6}$$

We must now express $P_n(\cos\gamma)$ as a function of θ's and ϕ's of two particles and we may expand it in terms of the orthogonal functions $P_l^{|m|}(cos\theta_i)e^{im\phi_i}$. $P_n(\cos\gamma)$ is a solution of the equation:

$$\frac{1}{\sin\theta_i}\frac{\partial}{\partial\theta_i}\left(\sin\theta_i\frac{\partial P_n}{\partial\theta_i}\right) + \frac{1}{\sin^2\theta_i}\frac{\partial^2 P_n}{\partial\phi_i^2} + n(n+1)P_n = 0 \tag{A.7}$$

since this equation remains unchanged under any rotation. The general solution of this equation is a linear combination of the functions $P_n^{|m|}(cos\theta_i)e^{im\phi_i}$, so that we may express $P_n(\cos\gamma)$ as:

$$P_n(\cos\gamma) = \sum_{m=-n}^{n} A_{nm}P_n^{|m|}(\cos\theta_i)e^{im\phi_i} \tag{A.8}$$

where

$$A_{nm} = \frac{2n+1}{4\pi}\frac{(n-|m|)!}{(n+|m|)!}\int P_n(\cos\gamma)P_n^{|m|}(\cos\theta_i)e^{im\phi_i}d\tau \tag{A.9}$$

we also can expand $P_n^{|m|}(\cos\theta_i)e^{im\phi_i}$ in terms of a function $P_n^{|k|}(\cos\gamma)e^{ik\phi}$

$$P_n^{|m|}(\cos\theta_i)e^{im\phi_i} = \sum_{k=-n}^{n} B_{nk}P_n^{|k|}(\cos\gamma)e^{ik\phi} \tag{A.10}$$

where

$$B_{nk} = \frac{2n+1}{4\pi}\frac{(n-|k|)!}{n+|k|)!}\int P_n^{|m|}(\cos\theta_i)e^{-im\phi_i}P_n^{|k|}(\cos\gamma)e^{ik\phi}d\tau \tag{A.11}$$

Equation A.10 must hold for $\gamma = 0$, that is, for $\theta_i = \theta_j$ and $\phi_i = \phi_j$. Then

$$P_n^{|m|}(\cos\theta_j)e^{-im\phi_j} = \sum_{k=-n}^{n} B_{nk}P_n^{|k|}(1)e^{ik\phi} = B_{n0}P_n^0(1) \tag{A.12}$$

since $P_n^k(1) = 0$ for $k \neq 0$. $P_n^0(1) = 1$ from Eq A.11 & A.12 we have:

$$\frac{2n+1}{4\pi}\int P_n^{|m|}(\cos\theta_i)e^{-im\phi_i}P_n(\cos\gamma)d\tau = P_n^{|m|}(\cos\theta_j)e^{-im\phi_i} \tag{A.13}$$

so that

$$A_{nm} = \frac{(n-|m|)!}{(n+|m|)!}P_n^{|m|}\cos(\theta_j)e^{-im\phi_j} \tag{A.14}$$

Combining Eqs A.6, A.9 & A.14, we have the final result:

$$\frac{1}{|r_{ij}|} = \sum_{n=0}^{\infty}\sum_{m=-n}^{n}\frac{(n-|m|)!}{(n+|m|)!}\frac{r_j^n}{r_i^{n+1}}P_n^{|m|}\cos(\theta_j)e^{im(\phi_i-\phi_j)} \tag{A.15}$$

Eq. A.15 may alternatively be expressed as:

$$\frac{1}{|r_{ij}|} = \sum_{n=0}^{\infty} \sum_{m=-n}^{n} \frac{4\pi}{2n+1} \frac{r_j^n}{r_i^{n+1}} Y_{n,m}(\theta_i, \phi_i) Y_{n,m}^*(\theta_j, \phi_j) \tag{A.16}$$

A.2 Spherical Harmonic Properties

For chemical problem, we are concerned by real potential quantities so it is more convenient to work with real spherical harmonics, $y_{l,m}$, which are defined in regards to complex spherical harmics as:

$$y_{l,m}(\theta,\phi) = \begin{cases} \frac{1}{\sqrt{2}} \left[Y_{l,m}(\theta,\phi) + Y_{l,m}^*(\theta,\phi) \right] & \text{if } m > 0 \\ Y_{l0}(\theta,\phi) & \text{if } m = 0 \\ -\frac{i}{\sqrt{2}} \left[Y_{l,|m|}(\theta,\phi) - Y_{l,|m|}^*(\theta,\phi) \right] & \text{if } m < 0 \end{cases} \tag{A.17}$$

Moreover, the real spherical harmonics can be also defined as:

$$y_{l,m}(\theta,\phi) = N P_{l,m}(\cos\theta) \begin{cases} \sin|m|\phi & \text{if } m < 0 \\ \cos m\phi & \text{if } m \geqslant 0 \end{cases} \tag{A.18}$$

with N such as $\iint y_{l,m}(\theta,\phi) = sqrt4\pi$. The complex spherical harmonics $Y_{l,m}$ and its complex conjugate $Y_{l,m}^*$ are linked by the following relation

$$Y_{l,m}^*(\theta,\phi) = (-1)^m Y_{l,-m}(\theta,\phi) \tag{A.19}$$

And the normalization of the real spherical harmonics $y_{l,m}$ is such that $\int y_{l,m}^2(\theta,\phi) d\tau = 1$. If we look at the d-wavefunctions, the real forms will be:

$$\begin{aligned} d_{z^2} &\rightarrow y_{2,0}(\theta,\phi) = Y_{2,0}(\theta,\phi) \\ d_{yz} &\rightarrow y_{2,-1}(\theta,\phi) = \frac{-i}{\sqrt{2}} \left[Y_{2,1}(\theta,\phi) + Y_{2,-1}(\theta,\phi) \right] \\ d_{xz} &\rightarrow y_{2,1}(\theta,\phi) = \frac{1}{\sqrt{2}} \left[Y_{2,1}(\theta,\phi) - Y_{2,-1}(\theta,\phi) \right] \\ d_{xy} &\rightarrow y_{2,-2}(\theta,\phi) = \frac{-i}{\sqrt{2}} \left[Y_{2,2}(\theta,\phi) - Y_{2,-2}(\theta,\phi) \right] \\ d_{x^2-y^2} &\rightarrow y_{2,2}(\theta,\phi) = \frac{1}{\sqrt{2}} \left[Y_{2,2}(\theta,\phi) + Y_{2,-2}(\theta,\phi) \right] \end{aligned} \tag{A.20}$$

A.3 Spherical Harmonic Addition Theorem

We will attempt to demonstrate the spherical harmonic theorem. For this, we have to recall the definition of a rotation:

$$\Psi(x',y',z') = R\Psi(x,y,z) \tag{A.21}$$

and more particulary a rotation through the Euler angles α, β and γ:

$$R\Psi_{jm} = \sum_{m'} D_{m'm}^j(\alpha\beta\gamma) \Psi_{jm'} \tag{A.22}$$

Now if we consider the expression:

$$g = \sum_m Y^*_{lm}(\theta_1, \phi_1) Y_{lm}(\theta_2, \phi_2) \tag{A.23}$$

where (θ_1, ϕ_1) and (θ_2, ϕ_2) are the spherical coordinates of two points P_1 and P_2 on the unit sphere and we rotate the coordinate system through the Euler angles, we can write:

$$g = \sum_m [R^{-1} Y^*_{lm}(\theta'_1, \phi'_1)] \times R^{-1} Y_{lm}(\theta'_2, \phi'_2) \tag{A.24}$$

where the primes indicates the spherical coordinates in the rotated frame. Because $D^j_{mm'}(\alpha\beta\gamma)$ is unitary, the Eq A.24 can be rewritten as

$$R^{-1}\Psi_{jm} = \sum_{m'} D^{j*}_{mm'}(\alpha, \beta, \gamma)\Psi_{jm'} \tag{A.25}$$

which means that:

$$g = \sum_{m_1}\sum_{m_2}\left[\sum_m D^{l*}_{mm_2} D^l_{mm_1}\right] Y^*_{lm_1}(\theta'_1, \phi'_1) Y_{lm_2}(\theta'_2, \phi'_2) \tag{A.26}$$

But the sum over m is, by the unitary nature of the rotation matrix, simply $\delta_{m_1 m_2}$. Therefore we have shown that g is independant of coordinate system:

$$g = \sum_m Y^*_{lm_1}(\theta_1, \phi_1) Y_{lm_2}(\theta_2, \phi_2) = \sum_m Y^*_{lm_1}(\theta'_1, \phi'_1) Y_{lm_2}(\theta'_2, \phi'_2) \tag{A.27}$$

i.e., g is invariant under rotations. We can evaluate g in any coordinate system, and the one we now choose is such that P_1 is on the z-axis and $\phi_2 = 0$; i.e., the xz-plane is defined as the plane containing P_1, P_2 and the origin. Thus $\theta_1 = 0$, and $\theta_2 = \theta$, $\phi_2 = 0$, θ being the angle between the radius vectors of the two points. Since:

$$Y_{lm}(\theta, \phi_1) = \delta_{m0}\left(\frac{2l+1}{4\pi}\right)^{1/2} \tag{A.28}$$

So

$$g = \left(\frac{2l+1}{4\pi}\right)^{1/2} Y_{l0}(\theta, 0) \tag{A.29}$$

Finally, the spherical harmonic addition theorem is obtained:

$$Y_{l0}(\theta, 0) = \left(\frac{4\pi}{2l+1}\right)^{1/2} \sum_m Y^*_{lm}(\theta_1, \phi_1) Y_{lm}(\theta_2, \phi_2) \tag{A.30}$$

But we use more often the expression:

$$Y_{l0}(\theta, 0) = \left(\frac{4\pi}{2l+1}\right)^{1/2} P_l(\cos\theta) \tag{A.31}$$

where P_l is the Legendre polynomial, and write the spherical harmonic addition theorem as:

$$\begin{aligned} P_l(\cos\theta) &= \frac{4\pi}{2l+1}\sum_{m=-l}^{l}(-1)^m Y_{l,m}(\theta_1,\phi_1)Y_{l,m}(\theta_2,\phi_2) \\ &= \frac{4\pi}{2l+1}\sum_{m=-l}^{l} Y_{l,m}(\theta_1,\phi_1)Y^*_{l,m}(\theta_2,\phi_2) \\ &= P_l(\cos\theta_1)P_l(\cos\theta_2) + 2\sum_{m=-l} l\frac{(l-m)!}{(l+m)!}P_l^m(\cos\theta_1)P_l^m(\cos\theta_2)\cos[m(\phi_1-\phi_2)] \end{aligned} \tag{A.32}$$

where θ is defined by:

$$\cos\theta \equiv \cos\theta_1\cos\theta_2 + \sin\theta_1\sin\theta_2\cos(\phi_1-\phi_2) \tag{A.33}$$

A.4 Wigner-Eckart Theorem

A theorem of fundamental importance in spectroscopy and angular momentum theory which provides both (1) an explicit form for the dependence of all matrix elements of irreducible tensors on the projection quantum numbers and (2) a formal expression of the conservation laws of angular momentum (Rose 1995). The theorem states that the dependence of the matrix element $\langle j'm'|T_{LM}|jm\rangle$ on the projection quantum numbers is entirely contained in the Wigner 3j-symbol (or, equivalently, the Clebsch-Gordan coefficient), given by:

$$\langle j'm'|T_{LM}|jm\rangle = C(jLj';mMm')\langle j'||T_L||j\rangle \tag{A.34}$$

where $C(jLj';mMm')$ is a Clebsch-Gordan coefficient and T_{LM} is a set of tensor operators. The quantity $\langle j'||T_L||j\rangle$ is called the reduced matrix element of the set of tensor operators T_{LM}.

A.5 Clebsch-Gordan Coefficient

Clebsch-Gordan coefficients are mathematical symbol used to integrate products of three spherical harmonics. Clebsch-Gordan coefficients commonly arise in applications involving the addition of angular momentum in quantum mechanics. If products of more than three spherical harmonics are desired, then a generalization known as Wigner 6j-symbols or Wigner 9j-symbols is used. The Clebsch-Gordan coefficients are variously written as $C^j_{m_1m_2}$, $C^{j_1j_2j}_{m_1m_2m}$, $(j_1j_2m_1m_2|j_1j_2jm)$, $\langle j_1j_2m_1m_2|j_1j_2jm\rangle$. The Clebsch-Gordon coefficients are defined by:

$$\Psi_{jm} = \sum_{m=m_1+m_2} C^j_{m_1m_2}\Psi_{m_1m_2} \tag{A.35}$$

where $j \equiv j_1 + j_2$ and satisfy

$$(j_1j_2m_1m_2|j_1j_2jm) = 0 \tag{A.36}$$

for $m_1 + m_2 \neq m$. The coefficients are subject to the restrictions that (j_1, j_2, j) be positive integers or half-integers, (m_1, m_2, m) be positive or negative integers or half-integers, and

$$\begin{aligned} j_1 + j_2 - j &\geqslant 0 \\ j_1 - j_2 + j &\geqslant 0 \\ -j_1 + j_2 + j &\geqslant 0 \\ j_1 + j_2 + j &\in \mathbb{N} \end{aligned} \tag{A.37}$$

and

$$\begin{aligned} -|j_1| \geqslant m_1 \geqslant |j_1| \\ -|j_2| \geqslant m_2 \geqslant |j_2| \\ -|j| \geqslant m \geqslant |j| \end{aligned} \tag{A.38}$$

A.6 Laplace Expansion

For a given matrix A, the determinant, $\det A$, is a scalar that depends upon the elements of A. Also the determinant is defined only for a square matrix. The Laplace expansion allow us to calculate the determinant of an order-N matrix as a weighted sum of N order-2 determinants which simplify its evaluation. At this level we have to introduce the notion of minor and cofactor. The minor M_{ij} of the element A_{ij} of an $N \times N$ matrix A is the determinant of the $(N-1) \times (N-1)$ matrix obtained by removing all the elements of the i^{th} row and the j^{th} column of A; the associated cofactor is found by multiplying the minor by $(-1)^{i+j}$. If we define the matrix A as:

$$A = \begin{pmatrix} A_{11} & A_{12} & A_{13} \\ A_{21} & A_{22} & A_{23} \\ A_{31} & A_{32} & A_{33} \end{pmatrix} \tag{A.39}$$

$\det A$ is then defined as:

$$\begin{aligned} \det A = |A| &= A_{21}C_{21} + A_{22}C_{22} + A_{23}C_{23} \\ &= A_{21}(-1)^{2+1}M_{21} + A_{22}(-1)^{2+2}M_{22} + A_{23}(-1)^{2+3}M_{23} \\ &= -A_{21}\begin{vmatrix} A_{12} & A_{13} \\ A_{32} & A_{33} \end{vmatrix} + A_{22}\begin{vmatrix} A_{11} & A_{13} \\ A_{31} & A_{33} \end{vmatrix} - A_{23}\begin{vmatrix} A_{11} & A_{12} \\ A_{31} & A_{32} \end{vmatrix} \end{aligned} \tag{A.40}$$

In the same way, the determinant of the 2×2 matrix can be calculate:

$$\begin{aligned} \begin{vmatrix} A_{12} & A_{13} \\ A_{32} & A_{33} \end{vmatrix} &= A_{12}(-1)^{1+1}|A_{33}| + A_{13}(-1)^{1+2}|A_{32}| \\ &= A_{12}A_{33} - A_{13}A_{32} \end{aligned} \tag{A.41}$$

Appendix B

LFDFT Scripts

B.1 Creation of the SD calculation input

The inputs for the geometry optimization or the AOC calculation correspond to a normal ADF input but for the SD calculation, we have to list all the Slater determinants in a specific order. I wrote a program which is a graphical interface (GUI) to generate the SD calculation inputs because as we can see in section 3.1.4 this input can be very long and it can be time consuming and source of errors to write it. This program is written in Tcl/Tk (Tool Command Language/Tool Kit)[144] and it calls a small Fortran program. I will describe here how to use it.
Under the create menu, two options are available, *full input* and *SD part*, the first option opens a window like in Figure B.1 while the second option opens a window corresponding to the part delimited by the black rectangle of Figure B.1. For the *full input* creation mode you need:

1. to precise the *xyz file*[a] of your compound. For this, you have to click on the *Load xyz file* button and a selector of file appears.

2. to precise the title you want to give to your calculation.

3. to give the charge of your compound.

4. you have to precise the kind of approximation you want to use: LDA or GGA.

5. in you choose GGA, you have to precise which functional you want to use (*cf.* Table 3.1 to have the full description of each name).

6. to precise which is the "TAPE21" file of the AOC calculations. For this, you have to click on the button "Precise which is the tape21 file of your AOC" and a selector of file appears.

As soon as you had entered all these data, you arrived to the part corresponding to the part delimited by the black rectangle in the Figure B.1 which is common for the two

[a]The *xyz file* is constructed in the following fashion: the first line contains the number of atoms in the compound, the second line is normally dedicated to the name of the compound and the following line gives (one line per atom) give the label of the atom and its x, y, z coordinates.

creation modes: *full input* and *SD part*. Thus the following description is valid for the two creation modes. Now the data you have to enter now refer to the SD part of the input, you need:

7. to precise the number of electrons on the *d*-shell.

8. to precise the total number of electrons in your compound.[b]

9. to precise the symmetry you use in the AOC calculation.

10. to precise, for each irrep, the number of time it appears with a full electronic configurations in the KS MO diagram of the average of configuration output.

11. to precise, for each of the five *d*-AO (since the TM has an open *d*-shell), which are the corresponding MO in the AOC calculation output. It means, for each *d*-AO, to select the MO which corresponds to the maximum contribution of this *d*-AO.

As soon as the user gives all the data, some routines check if the input is valid based on the total number of electrons, the number of electrons on the *d*-shell and the occupations of each irreps, and then if all data entered are valid, the program proposed to save the file with the desired filename. The advantage of the *full input* creation mode is that the input created can directly be executed by the ADF program.

B.2 Extraction of data

B.2.1 SD energies

The very short and very useful script *get.x* reads the *logfile* of the single determinant calculation and stores all the energies of SD in a new file *esd*. This new file contains only an array of numbers which is directly loadable by the LFDFT program. The command to run *get.x* is:

`get.x <` *aoc-file*`.logfile`

The source code of this script is contained in Figure B.2.

```
#! /bin/bash
# By Rauzy Cédrick
# this script is to generate the list of SD energies
# from a SD calculations logfile.
#
grep "GGA-XC" $1 | grep "eV" | awk '{print $5}' > esd
```

Figure B.2: *Source code of the script "get.x".*

[b] You can find it in the AOC calculation output under the section "S Y M M E T R Y , E L E C T R O N S" and then "Total". Since you use frozen-core approximation, this number is not equal to the sum of electron per "real" atom.

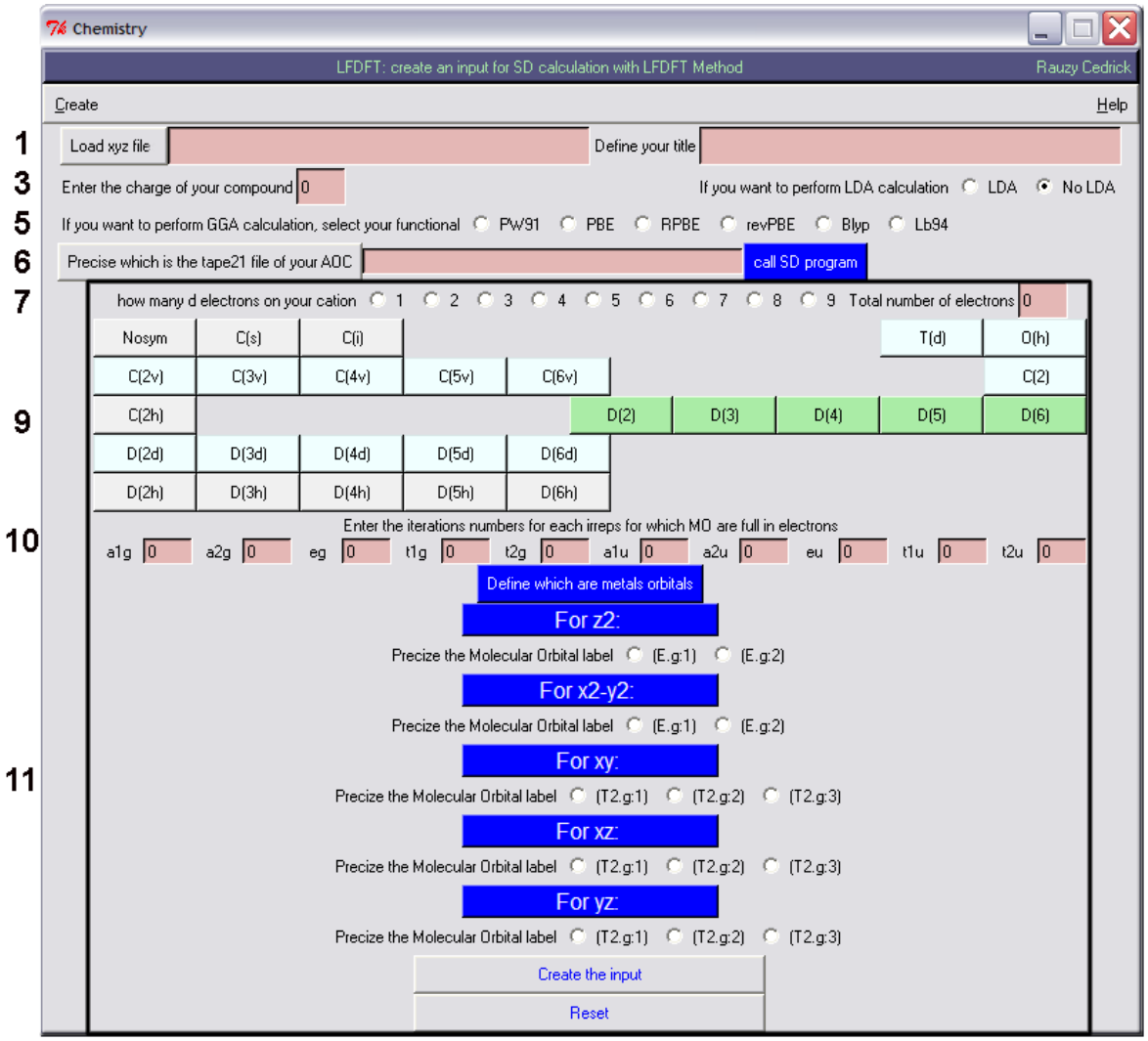

Figure B.1: *Snapshot of the program chem.x. The number on each side refer to the item number in the previous two lists.*

B.2.2 Eigenvalues of KS orbitals

The script to extract the eigenvalues of the MO's is not fully optimized, it works for cases where the compound has a high symmetry like T_d or O_h but for lower symmetry where there is mixing between d-AO in the MO's, this script does not work. A script valid for every symmetry can be written with a more complex code by including some line of code to compare the MO compositions. The source code of the actual version of *eigen.x* is presented in Figure B.3.

```
#! /bin/tcsh
# By Rauzy Cédrick
# ------
# This script is to run on the average of configuration
# with the command eigen.x aoc-calculation.OUT
# it gives the matrix of the eigen values of MO with
# dominant d-character. It act just on transition metal with d-orbitals
# and for a mono metallic compound
#
grep -A1000 "List of all MOs" $1 | grep "1 D:z2" | awk '{ if ($10 =="1")
print "L = [" $1 " 0.000 0.000 0.000 0.000 ;"}'
grep -A1000 "List of all MOs" $1 | grep "1 D:x2-y2" | awk '{ if ($10 =="1")
print " 0.000 " $1 " 0.000 0.000 0.000;"}'
grep -A1000 "List of all MOs" $1 | grep "1 D:xy" | awk '{ if ($10 =="1")
print " 0.000 0.000 " $1" 0.000 0.000;"}'
grep -A1000 "List of all MOs" $1 | grep "1 D:xz" | awk '{ if ($10 =="1")
print " 0.000 0.000 0.000 " $1" 0.000 ;"}'
grep -A1000 "List of all MOs" $1 | grep "1 D:yz" | awk '{ if ($10 =="1")
print " 0.000 0.000 0.000 0.000 " $1 "];"}'
```

Figure B.3: *Source code of the script "eigen.x".*

The command to run *eigen.x* is:

`eigen.x <` *aoc-file*`.OUT`

B.2.3 Eigenvectors of KS orbitals

There is no script written yet and the better way up to now to extract the eigenvectors is to do it manually as it is explained in Section 3.2.1.1.

B.2.4 Evaluation of Standard Deviation

The LFDFT method accuracy is evaluated through the calculation of the Standard deviation between the SD energies calculated by DFT and the SD energies from LFDFT: we use the Racah's parameters and the ligand field matrix determined by the LFDFT program in equation 3.2 to calculate these SD energies. Then to calculate the standard deviation, we use the Equation B.1:

$$StDev = \frac{\sqrt{\sum_{i=1}^{N_{SD}} (E_i(fit) - E_i(DFT))^2}}{(N_{SD} - 1)} \tag{B.1}$$

Appendix C

Gener_ln Functions

In this appendix, each functions of the "*Gener_ln*" program are given. First, "*GENERSD*" is depicted, then the functions to calculate matrix elements in the basis of spin-orbitals are presented, at the end, the "*ZAB*", "*LFAB*" and "*GAB*" functions which are corresponding to the Slater's rule applied to the one-electron operator for the two first ones and to the Slater's rule applied to the two-electron operator for the latter one. This structure of this appendix corresponds to the Figure 4.3.

C.1 GENERSD Function

This function is done to create a matrix, *ir*, which by associating one number to each spin orbitals, list all the configurations of each Slater determinants in a specific order. So the number of column in *ir* corresponds to the number of electron on the *d*-shell and the number of line to the number of SD for the given configuration.
If we have, for example, a d^3 configuration and we consider the first SD: we fix arbitrarily that the first electron is on the orbital $l = -2$ with spin down, the second on the obital $l = -2$ with spin up and the third on the orbital $l = -1$ whith spin down. So the first SD corresponds to the configuration $d^-_{xy}d^+_{xy}d^-_{yz}$, in the matrix *ir*, it corresponds to a line with the numbers 1 2 3. The second SD is 1 2 4, the third 1 2 5 and so on until 8 9 10 with the following correspondence: $1 \equiv d^-_{xy}$, $2 \equiv d^+_{xy}$, $3 \equiv d^-_{yz}$, $4 \equiv d^+_{yz}$ and so on up to 10 with m going from -2 to 2 and having the spin down before the spin up (the spin moving faster than the value of m).
This order is the same as the one used to generate the ADF SD calculation input. The Figure C.1 corresponds to the source code of the "*GENERSD*" function.

```
function ir=genersd(ne,ka,kb)
% generate ir corresponding to Slater determinants configuration
% ordered in a specific way.
nf=kb-ka+1;
nsd=factorial(nf)/factorial(nf-ne)/factorial(ne);
% initialize ir
nr=1;
ir(nr,:)=[ka:ka+ne-1];
% generate SD
for nr=2:nsd
  ir(nr,1:ne)=ir(nr-1,1:ne);
  loop=1;j=0;
  while loop==1 & j<=ne
    j=j+1;
    ip=ne-j+1;
    np=kb-j+1;
    if ir(nr,ip)<np
      ir0=ir(nr,ip)-ip+1;
      ir(nr,ip:ne)=[ir0+ip:ir0+ne];
      loop=0;
    end
  end
end
```

Figure C.1: *Source code of the* **GENERSD** *function.*

C.2 Function to Determine Matrix Elements in the Basis of Spin-Orbitals

C.2.1 GET2EI4A

This function calculates the non-redundant electrostatic 2-e integrals for atomic orbitals with angular momenta lq. The Slater-Condon parameter are ordered by: $F_k(lq_1lq_1|lq_1lq_1), F_k(lq_1lq_2|lq_1lq_1), \ldots, F_k(lq_1lq_n|lq_1lq_1), F_k(lq_2lq_1|lq_1lq_1), \ldots, F_k(lq_nlq_n|lq_nlq_n)$. The way to obtain the Slater condon parametererization is explained in Section 2.1.4.1 so the function can be easily understand; the source code is given in Figure C.3. First, the Clebsh Gordan coefficients are calculated in the *CGR* function and they are stored as $< lm|m_1m_2 >$, where:

$$
\begin{aligned}
abs(l_1 - l_2) \leqslant l \leqslant l_1 + l_2 \\
-l \leqslant m \leqslant l \\
-l_1 \leqslant m_1 \leqslant l_1 \\
-l_2 \leqslant m_2 \leqslant l_2
\end{aligned}
$$

Only even l values if $la + lb$ is even or odd l values if $la + lb$ is odd contribute. Then, the one-electrons product is calculated so the loop runs over $(2l + 1) \times ((2l + 1) + 1)/2 = 15$ elements for $l = 2$. Finally the two electrons products is achieved and the loop runs

over $(15 \times (15+1)/2$ elements. As the result, *iabcd* matrix contains the left hand of Table 2.1 where orbitals are represented by numbers as it is explained in Appendix C.1 and *vabcd* matrix contains the coefficients corresponding to the right hand of Table 2.1 but for Slater Condon parameterisation. One can remark at the end of the *Gener_ln* program that Racah's parameterization is obtained by linear transformation.

CGR

This function calculates the real Clebsch-Gordan coefficients, $\langle lm|m_1m_2\rangle$, of full rotation group. They are stored in a $((2l+1)\times(2l+1))^2$ matrix, v, where $\langle lm|$ corresponds to the lines and $\langle m_1m_2|$ corresponds to the columns. For $lq = 2$, the $\langle m_1m_2|$ values corresponding to the columns are ordered as: -2 -2, -2 -1, ..., -2 2, -1 -2, -1 -1, ... 2, 2, and the the $\langle lm|$ values corresponding to the lines are ordered as: 0 0, 1 -1, 1 0, 1 1, 2 -2, ..., 4 4. This function is equivalent to the Eq 2.49. We can see that Clebsch-Gordan coefficients represent an integration over the product of three spherical harmonics, thus we have first to calculate this three spherical harmonics. Depending on the value of l_1, l_2 and l, the function **YLM1** is called 1, 2 or 3 times. The spherical harmonic function are calculated numerically using a Lebedev grid which is chosen depending on the values of l_1 and l_2. The source code of the function is given in Figure C.4.

YLM1

```
function yl=ylm1(l,z,phi)
% get associated legendre function normalised to 1
plm=legendre(l,z,'sch');
plm(1,:)=plm(1,:)*sqrt(0.5*(l+l+1));
plm(2:l+1,:)=plm(2:l+1,:)*sqrt(0.25*(l+l+1));
% get azimuthal part
for m=-l:l
  if m<0, fm(l+m+1,:)=sin(-m*phi); end
  if m==0, fm(l+1,:)=0.70710678118655; end
  if m>0, fm(l+m+1,:)=cos(m*phi); end
end
fm=fm/sqrt(pi);
% multiply both to get yl(-l:l)
for m=-l:l
  yl(l+m+1,:)=plm(abs(m)+1,:).*fm(l+m+1,:);
end
```

Figure C.2: *Source code of the* **YLM1** *function.*

This function determine the values of the real spherical harmonic function, $y_{lm}(\theta,\phi)$, within a Lebedev grid.
The source code is given in Figure C.2. We have then to define the expression of $Y_l^m(\theta,\phi)$:

$$Y_{lm}(\theta,\phi) = (-1)^m \sqrt{\frac{2l+1}{4\pi}\frac{(l-m)!}{(l+m)!}} P_{lm}(\cos\theta) e^{im\phi} \tag{C.1}$$

In a first time, the Schmidt semi-normalized associated Legendre functions is computed

so we can define it in terms of the Legendre function defined by:

$$P_{nm}(x) = (-1)^m (1-x^2)^{m/2} \frac{d}{dx^m} P_n(x) \tag{C.2}$$

where $P_n(x)$ is the Legendre polynomial of degree n defined by:

$$P_n(x) = \frac{1}{2^n n!} \left[\frac{d^n}{dx} (x^2-1)^n \right] \tag{C.3}$$

The Schmidt seminormalized associated Legendre function are related to the normalized associated Legendre functions $P_n^m(x)$ by:

$$S_{lm}(x) = (-1)^m \sqrt{\frac{2(n-m)!}{(n+m)!}} P_{lm}(x) \tag{C.4}$$

Thus Eq C.1 read as:

$$Y_{lm}(\theta, \phi) = (-1)^m \sqrt{\frac{2l+1}{2\pi}} S_{lm}(\cos\theta) e^{im\phi} \tag{C.5}$$

As we consider real spherical harmonic, we can write:

$$y_{lm}(\theta, \phi) = (-1)^m \sqrt{\frac{2l+1}{2\pi}} S_{lm}(\cos\theta) \begin{cases} \sin|m|\phi & \text{if } m < 0 \\ \cos m\phi & \text{if } m \geqslant 0 \end{cases} \tag{C.6}$$

```
function [vabcd,iabcd]=get2ei4a(lq)
ndl=length(lq);   nf=0;
for kl=1:ndl
  for km=1:lq(kl)+lq(kl)+1
    nf=nf+1;   lf(nf)=lq(kl);   mf(nf)=km-lq(kl)-1;
  end
end
nvx=(2*max(lf)+1)^2;   v=zeros(nvx,nvx,ndl*(ndl+1)/2);   kk=0;
for k=1:ndl
  mulk=lq(k)+lq(k)+1;
  for kp=k:ndl
    mulkp=lq(kp)+lq(kp)+1;   kk=kk+1;
    nv(kk)=mulk*mulkp;
    v(1:nv(kk),1:nv(kk),kk)=CGR(lq(kp),lq(k));
    lab(kk,:)=[lq(kp) lq(k)];
  end
end
kkp=0;   ip0(1)=0;
for k=1:kk
  la=lab(k,1);   lb=lab(k,2);
  for kp=1:k
    lc=lab(kp,1);   ld=lab(k,2);
    k1=abs(la-lb):2:la+lb;   k2=abs(lc-ld):2:lc+ld;   k12=find(k1==k2);
    kx=k2(k12);   kkp=kkp+1;   ip0(kkp+1)=ip0(kkp)+length(kx);
  end
end   % 1-e products
nab=0;   k=0;
for ia=1:nf
  for ib=1:ia
    nab=nab+1;   iab(nab,:)=[ia ib];
    la=lf(ia);   lb=lf(ib);   ma=mf(ia);   mb=mf(ib);
    % get index of matrix where Clebsch-Gordan coeff. are stored
    lv(nab) = find( lab(:,1)==la & lab(:,2)==lb );
    % get column of matrix where Clebsch-Gordan coeff. are stored
    mv(nab)=(la+ma)*(lb+lb+1)+lb+mb+1;
  end
end   % non-redundant 2-e integrals
for j1=1:nab
  for j2=1:j1
    k=k+1;
    ia=iab(j1,1);   ib=iab(j1,2);   ic=iab(j2,1);   id=iab(j2,2);
    % iabcd contains the 4 indices of the non-redundant 2-e integrals
    iabcd(k,:)=[iab(j1,:) iab(j2,:)];
    la=lf(ia);   lb=lf(ib);   lc=lf(ic);   ld=lf(id);
    k1=abs(la-lb):2:la+lb;   k2=abs(lc-ld):2:lc+ld;
    k12=find(k1==k2);   kx=k2(k12);
    for ix=1:length(kx)
      mu1=(kx(ix)+1)^2-min(k1)^2;   mu2=(kx(ix)+1)^2-min(k2)^2;
      ml1=mu1-kx(ix)-kx(ix);   ml2=mu2-kx(ix)-kx(ix);
      a(ix)=sum( v(ml1:mu1,mv(j1),lv(j1)).*v(ml2:mu2,mv(j2),lv(j2)) );
    end
    ip0(lv(j1)*(lv(j1)-1)/2+lv(j2));
    vabcd(k,ip0(lv(j1)*(lv(j1)-1)/2+lv(j2))+1:ip0(lv(j1)*(lv(j1)-1)/2+lv(j2))+
    length(kx))=a(1:length(kx));
  end
end
```

Figure C.3: *Source code of the* **CET2EI4A** *function.*

```
function v=cgr(l1,l2)
% test if l1 + l2 are out of range
if l1+l2 > 29 ,
  disp('l1+l2 are out of range'),
  pause,
end
% get grid
load lebedev lmx=[1 3 5 7 9 11 15 17 19 23 29 35 41 47 53 59];
igrid=min(find(lmx>=2*(l1+l2)));
grid=LG(LLLG(igrid):ULLG(igrid),:);
x=grid(:,1);y=grid(:,2);z=grid(:,3);w=grid(:,4);
% get azimuthal angle phi
phi=atan2(y,x)';
% get yl1 and yl2
yl1=sqrt(4*pi)*YLM1(l1,z,phi);
if l1==l2,
  yl2=yl1;
else
  yl2=sqrt(4*pi)*YLM1(l2,z,phi);
end
% start quadrature loop
mu=0;
for l=abs(l1-l2):l1+l2
  % get yl
  if l==l1,
    yl=yl1;
  elseif l==l2,
    yl=yl2;
  else
    yl=sqrt(4*pi)*YLM1(l,z,phi);
  end
  % get < l m | l1 m1 , l2 m2 > as sum(Yl_m*Yl1_m1*Yl2_m2)
  for m=-l:l
    mu=mu+1;
    nu=0;
    for m1=-l1:l1
      for m2=-l2:l2
        nu=nu+1;
        v(mu,nu)=sum(w'.*yl(l+m+1,:).*yl1(l1+m1+1,:).*yl2(l2+m2+1,:));
      end
    end
  end
end
```

Figure C.4: *Source code of the* **CGR** *function.*

C.2.2 GETLS

This function creates the *lx, ly, lz, sx, sy, sz* and *ls* matrices in the basis of the spin-orbitals (10×10 matrix for $lq = 2$). We can devide this function in three parts. Firstly, the function *lmat* calculates the equivalent matrix operator of l_i in the basis of orbitals. Secondly, the function *getj* is called to calculate the Pauli matrices for the electron. And finally, the l_i and s_i matrices are transformed in the basis of spin orbitals. In this function, the spin-orbit coupling matrix is also calculated: $\langle l, m_l, s, m_s | l \cdot s | l, m_{l'}, s', m_{s'} >$. The order of the basis functions is:
$|m_l, m_s\rangle = |-l, -s\rangle, |-l, +s\rangle, |-l+1, -s\rangle, |-l+1, +s\rangle, ..., |l, -s\rangle, |l, +s\rangle$. The source code of the function is given in Figure C.6.

GETJ

J is the total angular momentum which is the vector sum of the spin angular momentum S and the orbital angular momentum L:

$$J \equiv S + L \tag{C.7}$$

This operator is quantized by two quantum numbers j and m_j and this function has the role to compute: $j_i(m : m') = \langle j, m_j | J_i | j, m'_j \rangle$ which in fact corresponds to the Pauli spin matrices. The complete description of the construction of these matrices can be found in the Rose's book.[145]

```
function [jx,jy,jz]=getj(j)% j=1/2
half=0.5;
mul=j+j+1;% mul=2
jx=zeros(mul,mul)+i*zeros(mul,mul);
jy=zeros(mul,mul)+i*zeros(mul,mul);
jz=zeros(mul,mul)+i*zeros(mul,mul);
% jz
mj=-j-1;
for k=1:mul
  mj=mj+1;
  jz(k,k)=jz(k,k)+mj;
end
% jx and jy
mj=-j-1;
for k=1:mul-1
  mj=mj+1;
  jx(k+1,k)=jx(k+1,k)+half*sqrt(j*(j+1)-mj*(mj+1));
  jx(k,k+1)=jx(k+1,k);
  jy(k+1,k)=jy(k+1,k)-half*i*sqrt(j*(j+1)-mj*(mj+1));
  jy(k,k+1)=conj(jy(k+1,k));
end
```

Figure C.5: *Source code of the* **GETJ** *function.*

```
function [alx,aly,alz,asx,asy,asz,ls]=getls(l,s)
nl=l+l+1;
lx=zeros(nl,nl)+i*zeros(nl,nl); ly=zeros(nl,nl)+i*zeros(nl,nl);
lz=zeros(nl,nl)+i*zeros(nl,nl);
% get l-matrices in basis of real spherical harmonics
for k=1:nl% 1 to 5 for lq=2
  ml=k-l-1;% ml going from -2 to 2 for lq=2
  mls=0;
  if ml<0
    mls=1;
  end
  for kp=1:nl
    mlp=kp-l-1;
    mlsp=0;
    if mlp<0
      mlsp=1;
    end
    lx(k,kp)=lx(k,kp)+i*LMAT(1,l,abs(ml),mls,l,abs(mlp),mlsp);
    ly(k,kp)=ly(k,kp)+i*LMAT(2,l,abs(ml),mls,l,abs(mlp),mlsp);
    lz(k,kp)=lz(k,kp)+i*LMAT(3,l,abs(ml),mls,l,abs(mlp),mlsp);
  end
end
% get s-matrices
[sx,sy,sz]=GETJ(s);
ns=s+s+1;
% get al=<ml,ms|l|mlp,msp> and as=<ml,ms|s|mlp,msp>
us=eye(ns,ns);
ul=eye(nl,nl);
for kl=1:nl
  for ks=1:ns
    for klp=1:nl
      for ksp=1:ns
        alx(ns*(kl-1)+ks,ns*(klp-1)+ksp)=lx(kl,klp)*us(ks,ksp);
        aly(ns*(kl-1)+ks,ns*(klp-1)+ksp)=ly(kl,klp)*us(ks,ksp);
        alz(ns*(kl-1)+ks,ns*(klp-1)+ksp)=lz(kl,klp)*us(ks,ksp);
        asx(ns*(kl-1)+ks,ns*(klp-1)+ksp)=ul(kl,klp)*sx(ks,ksp);
        asy(ns*(kl-1)+ks,ns*(klp-1)+ksp)=ul(kl,klp)*sy(ks,ksp);
        asz(ns*(kl-1)+ks,ns*(klp-1)+ksp)=ul(kl,klp)*sz(ks,ksp);
      end
    end
  end
end
ls=alx*asx+aly*asy+alz*asz;
```

Figure C.6: *Source code of the* **GETLS** *function.*

LMAT

The function "*LMAT*" calculates matrix elements of the angular momentum between atomic orbitals on one center. The angular momentum is defined by:

$$\hat{L} = -i\hbar(r \times \nabla) \tag{C.8}$$

Squaring the expression, we can write out the L_x component:

$$\hat{L}_x = -i\hbar\left(y\frac{\partial}{\partial z} - z\frac{\partial}{\partial y}\right) \tag{C.9}$$

By using spherical coordinates representations, Eq C.9 reads:

$$\hat{L}_x = -i\hbar\left(\sin\phi\frac{\partial}{\partial\theta} - \frac{\cos\phi}{\tan\theta}\frac{\partial}{\partial\phi}\right) \tag{C.10}$$

Then applying the angular momentum operator to atomic wavefunctions, the components of the angular momentum have the following expectation values:

$$\begin{aligned}
L_z|\phi_{nlm}\rangle &= m\hbar|\phi_{nlm}\rangle \\
L_x|\phi_{nlm}\rangle &= \frac{1}{2}\hbar\sqrt{(l-m)(l+m+1)}|\phi_{n,l,m+1}\rangle + \frac{1}{2}\hbar\sqrt{(l+m)(l-m+1)}|\phi_{n,l,m-1}\rangle \\
L_x|\phi_{nlm}\rangle &= -\frac{1}{2}\hbar\sqrt{(l-m)(l+m+1)}|\phi_{n,l,m+1}\rangle + \frac{1}{2}i\hbar\sqrt{(l+m)(l-m+1)}|\phi_{n,l,m-1}\rangle
\end{aligned} \tag{C.11}$$

And we have to realise that in fact when *lmat* is called, we compute:

$$\langle\phi_{n_2,l_2,m_2'}|L_i|\phi_{n_1,l_1,m_1'}\rangle \tag{C.12}$$

In the program the value of m' is decomposed in m and ms, respectively the m' absolute value and the m' sign so the atomic orbitals are defined with quantum numbers (l,m,ms) which corresponds to a real normalized combination of spherical harmonics Y(l,m) and Y(l,-m) (ms=0 is the cosine, ms=1 the sine). In the last line of this function, we can see the same expression than in equation C.11 for couple $(l2, m2, ms2; l1, m1, ms1)$ which are not vanishing (two wavefunctions which are not orthogonal). The source code of the function is given in Figure C.7

```
function al=lmat(ix,l2,m2,ms2,l1,m1,ms1)
%
mm=[1 1 0];
mms=[1 0 1];
m=mm(ix);
ms=mms(ix);
if (l2 =l1)|(abs(m2-m1) =m)|(abs(ms2-ms1) =ms),
  al=0;
else
  if m2 =m1,
    if m2<m1,
      msign=-1;
      ma=m2;
      msa=ms2;
    end
    if m2>m1,
      msign=1;
      ma=m1;
      msa=ms1;
    end
    if ma==0,
      sign=msign*(1-2*ms);
      squ=(l1)*(l1+1)/2;
      al=sign*sqrt(squ);
    else
      sign=msign*(1-2*ms*(1-msa));
      squ=(l1-ma)*(l1+ma+1);
      al=sign*sqrt(squ)/2;
    end
  else
    al=(1-2*ms1)*m1;
  end
end
```

Figure C.7: *Source code of the* **LMAT** *function.*

C.3 Functions corresponding to the Slater's rules

C.3.1 One-electron Slater's rule

Considering Eq 2.42 and using Laplace's expansion (*cf.* Appendix A.6) on SD, we get:

$$\langle\Psi|\mathscr{H}_0|\Psi'\rangle = \sum_{i=1}^{N}\sum_{j=1}^{N}(-1)^{i+j}\langle\chi_{k_i}|f|\chi_{k_j}\rangle S_{ij} \tag{C.13}$$

where:

$$S_{ij} = \sum_{\sigma}\int dt|\chi_{k_1}\chi_{k_2}\cdots\chi_{k_{i-1}}\chi_{k_{i+1}}\cdots\chi_{k_n}|^* \times |\chi_{k'_1}\chi_{k'_2}\cdots\chi_{k'_{j-1}}\chi_{k'_{j+1}}\cdots\chi_{k'_n}| \tag{C.14}$$

where $\sum_\sigma \int dt$ is carried out for electrons $2, 3, \ldots, N$. Then we can distinguish three cases:

$$\begin{aligned} \text{if } k_i = k'_i \text{ for all } i \Rightarrow &\quad \langle\Psi|\mathscr{H}_0|\Psi'\rangle = \sum_i \langle\chi_{k_i}|f|\chi_{k_i}\rangle \\ \text{if } k_i \neq k'_i \text{ for only one } i \Rightarrow &\quad \langle\Psi|\mathscr{H}_0|\Psi'\rangle = (-1)^P\langle\chi_{k_i}|f|\chi_{k_i}\rangle \\ \text{if } k_1 \neq k'_1,\ k_2 \neq k'_2 \Rightarrow &\quad \langle\Psi|\mathscr{H}_0|\Psi'\rangle = 0 \end{aligned} \tag{C.15}$$

where P is the number of permutations needed to put the functions of Ψ in the same order of those of Ψ'. Eq C.15 corresponds to the Slater rules for evaluating the matrix elements of one-electron operators between Slater determinants written in an orthonormal basis of orbitals.

C.3.1.1 ZAB

This subroutine is reponsible of the creation of the matrix "*lsdata*" which is the sin-orbit coupling matrix in the basis of the microstates. It uses the l_i, s_i and ls matrices in the basis of spin-orbitals to create one matrix containing the l_i, s_i and ls matrix element in the basis of μ-states. The function corresponds to the application of the Slater rules for the one-electron operator (*cf.* Section 2.1.3) to perform the transformation of basis. The matrix created has the size: $(nsd \times (nsd+1))/2 \times 7$ where the seven columns corresponds to $l_x, l_y, l_z, s_x, s_y, s_z, ls$ and the line corresponds to each element of the lower symmetric matrix. The source code of the function is given in Figure C.8

```
function z=zab(la,lb)
global lx ly lz sx sy sz ls
% Get <A|z(1)|jB>
ne=max(size(la));
ie=0;
id=0;
sgn=1;
for k=1:ne
  ld=find(la(k)==lb);
  if isempty(ld)
    id=id+1;
    kd(id)=la(k);
    if rem(k,2)==1,
      sgn=-sgn;
    end
  else
    ie=ie+1;
    ke(ie)=la(k);
  end
end
if id == 0
  z=zeros(1,7)+i*zeros(1,7);
  for k=1:ne
    z=z+[lx(ke(k),ke(k)) ly(ke(k),ke(k)) lz(ke(k),ke(k))
sx(ke(k),ke(k)) sy(ke(k),ke(k)) sz(ke(k),ke(k)) ls(ke(k),ke(k))];
  end
elseif id==1
  iv=0;
  for k=1:ne
    ld=find(lb(k)==la);
    if isempty(ld)
      iv=iv+1;
      kdp(iv)=lb(k);
      if rem(k,2)==1,
        sgn=-sgn;
      end
    end
  end
  z=sgn*[lx(kd(1),kdp(1)) ly(kd(1),kdp(1)) lz(kd(1),kdp(1))
sx(kd(1),kdp(1)) sy(kd(1),kdp(1)) sz(kd(1),kdp(1)) ls(kd(1),kdp(1))];
else
  z=zeros(1,7)+i*zeros(1,7);
end
```

Figure C.8: *Source code of the* **ZAB** *function.*

C.3.1.2 LFAB

The role of "*LFAB*" is to generate the ligand field matrix elements which are stored in *lfdata*. *lfdata* has a sized $(nsd(nsd+1)/2) \times (lq^2)$, it is in fact the lower ligand field diagonal matrix in the basis of microstates. The LFAB function uses the Slater rules for the one electron matrix (*cf.* Section 2.1.3). The diagonal elements of LF matrix, i.e. the lines $1, 3, 6, 10, 15, \ldots$ of *lfdata*, corresponds to the occupations of the corresponding SD in the basis of orbitals. The source code of the function is given in Figure C.10.

IWAB

The source code of this function is given in Figure C.9. The role of this function is just to determine the index *iw* in the basis of orbitals from the indexes of *i* and *ip* in the basis of spin orbitals.

```
function iw=iwab(i,ip)
% i and ip in the basis of spin orbitals
% ia and ib in the basis of orbitals
ia=fix((i+1)/2);
ib=fix((ip+1)/2);
%
if rem(i,2) =rem(ip,2)
  iw=0;
else
  if ia<=ib, iw=ia+ib*(ib-1)/2;end
  if ib<=ia, iw=ib+ia*(ia-1)/2;end
end
```

Figure C.9: *Source code of the* **IWAB** *function.*

```
function lf=lfab(la,lb)
global lq;
% Get <A|lf(1:(lq+lq+1)*(lq+1))|jB>
ne=max(size(la));
lf=zeros(1,(lq+lq+1)*(lq+1));
ie=0;
id=0;
sgn=1;
for k=1:ne
  ld=find(la(k)==lb);
  if isempty(ld)
    id=id+1;
    kd(id)=la(k);
    if rem(k,2)==1
      sgn=-sgn;
    end
  else
    ie=ie+1;
    ke(ie)=la(k);
  end
end
if id == 0
  for k=1:ne
    if IWAB(ke(k),ke(k))>0
      lf(IWAB(ke(k),ke(k)))=lf(IWAB(ke(k),ke(k)))+1;
    end
  end
elseif id==1
  iv=0;
  for k=1:ne
    ld=find(lb(k)==la);
    if isempty(ld)
      iv=iv+1;
      kdp(iv)=lb(k);
      if rem(k,2)==1
        sgn=-sgn;
      end
    end
  end
  if iwab(kd(1),kdp(1))>0,
    lf(iwab(kd(1),kdp(1)))=sgn;
  end
end
```

Figure C.10: *Source code of the* **LFAB** *function.*

C.3.2 Two-electrons Slater's rule

Considering Eq 2.43 and if we use Laplace expansion to write SD's in terms of two-dimensional SD's:

$$\begin{aligned}|\chi_{k_1}\chi_{k_2}\cdots\chi_{k_n}| = \frac{1}{\sqrt{[N(N-2)/2]}}\sum_{j=1} N(-1)^{i+j+3}\times|\chi_{k_i}\chi_{k_j}|_{(1,2)} \\ \times|\chi_{k_1}\chi_{k_2}\cdots\chi_{k_{i-1}}\chi_{k_{i+1}}\cdots\chi_{k_{j-1}}\chi_{k_{j+1}}\cdots\chi_{k_N}|_{(3,4,\ldots,N)}\end{aligned} \tag{C.16}$$

Therefore Eq 2.43 reads:

$$\langle\Psi|\mathscr{H}_1|\Psi'\rangle = \sum_{q>p=1}^{N}\sum_{s>r=1}^{N}(-1)^{p+q+r+s}\left[\langle\chi_{k_p}\chi_{k_q}|g|\chi_{k'_r}\chi_{k'_s}\rangle - \langle\chi_{k_p}\chi_{k_q}|g|\chi_{k'_s}\chi_{k'_r}\rangle\right]S_{pq,rs} \tag{C.17}$$

where:

$$\begin{aligned}S_{pq,rs} = \sum_{\sigma}\int dt|\chi_{k_1}\chi_{k_2}\cdots\chi_{k_{p-1}}\chi_{k_{p+1}}\cdots\chi_{k_{q-1}}\chi_{k_{q+1}}\cdots\chi_{k_N}|^* \\ \times|\chi_{k_1}\chi_{k_2}\cdots\chi_{k_{r-1}}\chi_{k_{r+1}}\cdots\chi_{k_{s-1}}\chi_{k_{s+1}}\cdots\chi_{k_N}|\end{aligned} \tag{C.18}$$

where $\sum_\sigma\int dt$ is carried out for electrons $3,4,\ldots,N$. Then we can distinguish four cases:

$$\begin{aligned}&\text{if } k_i = k'_i \text{ for all } i \Rightarrow \quad \langle\Psi|\mathscr{H}_1|\Psi'\rangle = \sum_{j>i=1}^{N}\left[\langle\chi_{k_i}\chi_{k_j}|g|\chi_{k_i}\chi_{k_j}\rangle - \langle\chi_{k_i}\chi_{k_j}|g|\chi_{k_j}\chi_{k_i}\rangle\right] \\ &\text{if } k_i \neq k'_i \text{ only for } i=1 \Rightarrow \quad \langle\Psi|\mathscr{H}_1|\Psi'\rangle = (-1)^P\sum_{j=2}^{N}\left[\langle\chi_{k_1}\chi_{k_j}|g|\chi_{k'_1}\chi_{k_j}\rangle - \langle\chi_{k_1}\chi_{k_j}|g|\chi_{k_j}\chi_{k'_1}\rangle\right] \\ &\text{if } k_i \neq k'_i \text{ only for } i\in\{1,2\} \Rightarrow \quad \langle\Psi|\mathscr{H}_1|\Psi'\rangle = (-1)^P\left[\langle\chi_{k_1}\chi_{k_2}|g|\chi_{k'_1}\chi_{k'_2}\rangle - \langle\chi_{k_1}\chi_{k_2}|g|\chi_{k'_2}\chi_{k'_1}\rangle\right] \\ &\text{if } k_i \neq k'_i \text{ for } i\in\{1,2,3\} \Rightarrow \quad \langle\Psi|\mathscr{H}_1|\Psi'\rangle = 0\end{aligned} \tag{C.19}$$

where P is the number of permutations needed to put the functions of Ψ in the same order of those of Ψ'. Eq C.19 corresponds to the Slater rule for evaluating the matrix elements of two-electrons operators between Slater determinants written in an orthonormal basis of orbitals.

GAB

The GAB function transforms the *gdata* matrix in the basis of SD's and corresponds to the Slater rule for a two electrons operator (Eq C.19). So it calculates the electrostatic repulsion matrix elements:

$$GAB = \langle la(1), la(2), ..., la(ne)|G|lb(1), lb(2), ..., lb(ne)\rangle$$

between two Slater determinantals. The resulting elements GAB are expressed as a sum of reduced two-electron integrals $p(ip) * \langle i,j||k,l\rangle$ expressed in terms of Slater-Condon's parameters. The source code of the function is given in Figure C.11.

```
function g=gab(ne,la,lb)
% get < A|G|B >
ie=0;   id=0;   sgn=1;
for k=1:ne
  if any(la(k)==lb),
    ie=ie+1;
    ke(ie)=la(k);
  else
    id=id+1;
    kd(id)=la(k);
    if mod(k,2)==1,
      sgn=-sgn;
    end
  end
end
if id==1 | id==2
  iv=0;
  for k=1:ne
    if  any(lb(k)==la),
      iv=iv+1;
      kdp(iv)=lb(k);
      if mod(k,2)==1,
        sgn=-sgn;
      end
    end
  end
end
% id>2, more than 2 spinorbitals differ
g=zeros(size(GIJKL(1,1,1,1)));
% id=2, 2 spinorbitals differ
if id==2
  g=sgn*GIJKL(kd(1),kd(2),kdp(1),kdp(2));
end
% id=1, 1 spinorbital differ
if id==1
  for k=1:ne
    g=g+sgn*GIJKL(kd(1),la(k),kdp(1),la(k));
  end
end
% id=0, no spinorbitals differ, i.e. la=lb
if id==0
  for k1=1:ne-1
    for k2=k1+1:ne
      g=g+GIJKL(ke(k1),ke(k2),ke(k1),ke(k2));
    end
  end
end
```

Figure C.11: *Source code of the* **GAB** *function.*

GIJKL

This function determine:

$$g = \langle i(1), j(2)|g|ip(1), jp(2)\rangle - \langle i(1), j(2)|g|jp(1), ip(2)\rangle$$

where g are the reduced 2-e integrals obtained in "*GET2EI4A*" and stored in the *vabcd* matrix. *IROW* being a function to find the good line in *vabcd*.

```
function g=gijkl(i,j,ip,jp)
global iabcd vabcd
% get orbital indices
ia=fix((i+1)/2);
ib=fix((ip+1)/2);
ic=fix((j+1)/2);
id=fix((jp+1)/2);
% initialise
g=zeros(size(vabcd(1,:)));
%
if mod(i,2)==mod(ip,2) & mod(j,2)==mod(jp,2)
  g=vabcd(IROW(ia,ib,ic,id),:);
end
if mod(i,2)==mod(jp,2) & mod(j,2)==mod(ip,2)
  g=g-vabcd(IROW(ia,id,ic,ib),:);
end
```

Figure C.12: *Source code of the* **GIJKL** *function.*

IROW

The source code of this function is given in Figure C.13. The role of this function is to determine the index of the line, k in the matrix *gdtata* in function of the values of ia, ib, ic and id which represent the orbitals considered for a bi-electronic integral.

```
function k=irow(ia,ib,ic,id)
global iabcd vabcd

if ia>=ib,   j1=ib+ia*(ia-1)/2;   end
if ia<ib,   j1=ia+ib*(ib-1)/2;   end
if ic>=id,   j2=id+ic*(ic-1)/2;   end
if ic<id,   j2=ic+id*(id-1)/2;   end
if j1>=j2,
  k =j2+j1*(j1-1)/2;
end
if j1<j2,
  k =j1+j2*(j2-1)/2;
end
```

Figure C.13: *Source code of the* **IROW** *function.*

Appendix D

SOC: supplement

D.1 Spin-orbit coupling elements in symmetry D_{2d}

In Eq D.1, the spin-orbit coupling elements in terms of reduced matrix elements for D_{2d} symmetry are given (the notations in square brakets refer to the tetrahedral e and t_2 species).

$$\begin{aligned}
\langle a_1[e]||\vec{su}(e)||e[t_2]\rangle &= \zeta^{e}_{a_1e} \\
\langle b_1[e]||\vec{su}(e)||e[t_2]\rangle &= \zeta^{e}_{b_1e} \\
\langle b_1[e]||\vec{su}(a_2)||b_2[t_2]\rangle &= \zeta^{a_2}_{b_1b_2} \\
\langle e[t_2]||\vec{su}(a_2)||e[t_2]\rangle &= \zeta^{a_2}_{ee} \\
\langle b_2[t_2]||\vec{su}(e)||e[t_2]\rangle &= \zeta^{e}_{b_2e}
\end{aligned} \tag{D.1}$$

Next, spin-orbit coupling elements are given in the basis of spin-orbitals, the symmetry notations for the real $3d$ orbitals in D_{2d} are written on the left hand side along with conventions for the e-components given in the ADF code.

		ζ^+	η^+	ξ^+	ε^+	θ^+	ζ^-	η^-	ξ^-	ε^-	θ^-
b_2^+	ζ^+				$i\zeta^{a_2}_{b_1b_2}$			$\frac{-i}{2}\zeta^{e}_{b_2e}$	$\frac{1}{2}\zeta^{e}_{b_2e}$		
$e:2^+$	η^+			$\frac{-i}{2}\zeta^{a_2}_{ee}$			$\frac{i}{2}\zeta^{e}_{b_2e}$			$\frac{-1}{2}\zeta^{e}_{b_1e}$	$\frac{\sqrt{3}}{2}\zeta^{e}_{a_1e}$
$e:1^+$	ξ^+		$\frac{i}{2}\zeta^{a_2}_{ee}$				$\frac{-1}{2}\zeta^{e}_{b_2e}$			$\frac{-i}{2}\zeta^{e}_{b_1e}$	$-\frac{\sqrt{3}}{2}i\zeta^{e}_{a_1e}$
b_1^+	ε^+	$-i\zeta^{a_2}_{b_1b_2}$						$\frac{1}{2}\zeta^{e}_{b_1e}$	$\frac{i}{2}\zeta^{e}_{b_1e}$		
a_1^+	θ^+							$-\frac{\sqrt{3}}{2}\zeta^{e}_{a_1e}$	$\frac{\sqrt{3}}{2}i\zeta^{e}_{a_1e}$		
b_2^-	ζ^-		$\frac{-i}{2}\zeta^{e}_{b_2e}$	$\frac{-1}{2}\zeta^{e}_{b_2e}$						$-i\zeta^{a_2}_{b_1b_2}$	
$e:2^-$	η^-	$\frac{i}{2}\zeta^{e}_{b_2e}$			$\frac{1}{2}\zeta^{e}_{b_1e}$	$-\frac{\sqrt{3}}{2}\zeta^{e}_{a_1e}$			$\frac{i}{2}\zeta^{a_2}_{ee}$		
$e:1^-$	ξ^-	$\frac{1}{2}\zeta^{e}_{b_2e}$			$-\frac{i}{2}\zeta^{e}_{b_1e}$	$-\frac{\sqrt{3}}{2}i\zeta^{e}_{a_1e}$		$-\frac{i}{2}\zeta^{a_2}_{ee}$			
b_1^-	ε^-		$-\frac{1}{2}\zeta^{e}_{b_1e}$	$\frac{i}{2}\zeta^{e}_{b_1e}$			$i\zeta^{a_2}_{b_1b_2}$				
a_1^-	θ^-		$\frac{\sqrt{3}}{2}\zeta^{e}_{a_1e}$	$\frac{\sqrt{3}}{2}i\zeta^{e}_{a_1e}$							

In Eq D.2, the spin-orbit coupling elements in terms of reduced matrix elements for T_d symmetry are given.

$$\begin{aligned}
\langle e||\vec{su}(t_1)||t_2\rangle &= \zeta^{t_1}_{et_2} = \zeta^{e}_{a_1e} = \zeta^{e}_{b_1e} = \zeta^{a_2}_{b_1b_2} \\
\langle t_2||\vec{su}(t_1)||t_2\rangle &= \zeta^{a_2}_{ee} = \zeta^{e}_{b_2e}
\end{aligned} \tag{D.2}$$

D.2 DFT treatment of JT activity in the case of mixing of electronic states

The Hamiltonian of the ${}^3T \otimes e$ Jahn-Teller problem in a linear approximation is:

$$H = (1/2)K_e(Q_\theta^2 + Q_\varepsilon^2).I + V_eQ_\theta.C_\theta + V_eQ_\varepsilon.C_\varepsilon \tag{D.3}$$

where I is the identity matrix and C_θ and C_ε are 3×3 matrices taken in the basis of the T_1 α, β and γ wave-functions:

$$C_\theta = \begin{bmatrix} \frac{1}{2} & 0 & 0 \\ 0 & \frac{1}{2} & 0 \\ 0 & 0 & -1 \end{bmatrix}; \quad C_\varepsilon = \begin{bmatrix} -\frac{\sqrt{3}}{2} & 0 & 0 \\ 0 & \frac{\sqrt{3}}{2} & 0 \\ 0 & 0 & 0 \end{bmatrix} \tag{D.4}$$

Q_θ and Q_ε are the higher and lower symmetric components of the e-vibration which distorts the tetrahedron into D_{2d} and D_2 geometries, respectively. If we restrict to distortions of Q_θ type and define Q_θ as being positive for tetragonal compression Eq D.3 simplifies to Eq D.5 for the non-degenerate ground state (${}^3A_2$ in D_{2d}) and to Eq D.6 for the degenerate higher energy state (${}^3E$).

$${}^3A_2 : E(T_1, \gamma) = (1/2)K_eQ_\theta^2 - V_eQ_\theta \tag{D.5}$$

$${}^3E : E(T_1, \alpha, \beta) = (1/2)K_eQ_\theta^2 + (1/2)V_eQ_\theta \tag{D.6}$$

Minimization of Eq D.5 with respect to Q_θ yields the equilibrium geometry Q_θ^o and the Jahn-Teller stabilization energy E_{JT}:

$$Q_\theta^o = V_e/K_e \tag{D.7}$$

$$E_{JT} = -(1/2)V_e^2/K_e \tag{D.8}$$

If we take θ (in ^{o}) to be the angle between the S_4 axis and the TM-ligand bond (for the tetrahedron we have $\theta_{Td} = 54.73^o$). Q_θ^o (in radians$\cdot\mathring{A}$) can be calculated from Eq D.9:

$$Q_\theta = R(\theta^o - \theta_{T_d})(\pi/180) \tag{D.9}$$

In tetrahedral NiX_4^{2-} complexes the ${}^3T_1$ wavefunction $\psi({}^3T_1)$ is given by:

$$\psi({}^3T_1) = c_1 \times \psi({}^3T_1, e^4t_2^4) + c_2 \times \psi({}^3T_1, e^3t_2^5) \tag{A.2.8}$$

where c_1 and c_2 (Table D.1) are given by the ground state eigenvector diagonalizing the matrix.

${}^3T^1(e^4t_2^4)$	${}^3T_1(e^3t_2^5)$	
0	$6B$	
$6B$	$9B + 10Dq$	

(A.2.9)

The ${}^3T_1(e^4t_2^4)$ and ${}^3T_1(e^3t_2^5)$ states, before the mixing, are described by single determinants and their equilibrium geometries (elongation, Table 5.3 and compression, Table D.1) and energies E_{JT} can be calculated from separate DFT geometry optimizations to yield corresponding parameters K_e and V_e (via Eqs D.7 & D.8). Let us denote these parameters by K_e', V_e' and K_e", V_e", respectively. Than K_e and V_e after mixing are given by:

$$K_e = c_1^2K_e' + c_2^2K_e'' \tag{A.2.10}$$

$$V_e = c_1^2 V_e^{'} + c_2^2 V_e^{''} \qquad (A.2.11)$$

Substitution into Eq. D.7 yields the equilibrium distortion Q_θ^o and utilizing Eq. D.9 we get the equilibrium angle θ^o. This is given in Table 5.3. Parameter values summarizing the logical steps of this procedure are listed in Table D.1.

Species	c_1	c_2	$\delta\theta$	E_{JT}	$K_e^{''}$	$V_e^{''}$	$K_e^{'}$	$V_e^{'}$	K_e	V_e
NiF_4^{2-}	-0.944	0.330	34.4	-8655	12792	14883	22234	-6049	21206	-3770
$NiCl_4^{2-}$	-0.953	0.303	15.5	-2599	13721	8447	10549	-2334	10840	-1344
$NiBr_4^{2-}$	-0.955	0.297	13.3	-1907	11948	6752	7686	-1747	8064	-998
NiI_4^{2-}	-0.956	0.292	10.1	-1247	11517	5360	2122	-453	2921	43

Table D.1: *Mixing coefficients c_1 and c_2 of $^3T_1(e^4t_2^4)$ and $^3T_1(e^3t_2^5)$ in the $^3T_1$ ground state function, DFT optimized angles $\delta\theta^o = \theta^o - \theta_{T_d}$ and E_{JT} values for $^3T_1(e^3t_2^5)$, force field constants and vibronic coupling parameters K_e", V_e"; K_e', V_e' and K_e, V_e of $^3T_1(e^3t_2^5)$; $^3T_1(e^4t_2^4)$ and the $^3T_1$ ground state (taking mixing into account) for NiX_4^{2-} (X=F^-, Cl^-, Br^-, I^-) . For values of $\delta\theta^o$ and E_{JT} for the $^3T_1(e^4t_2^4)$ DFT optimized single determinant energy, see the entries in Table 5.3. K_e, V_e and E_{JT} parameters have been expressed in $cm^{-1}/Å^2$, $cm^{-1}/Å$ and cm^{-1}, respectively, $\delta\theta$ in ^{o}.*

Appendix E

ESR: Programs

To calculate the $g-$ and $A-$tensors in Chapter 6, the two programs, Gener_ln and LF, have been modified and in this appendix the complete version of both are proposed.

E.1 Gener_ln pogram

Figures E.1& E.2 depict the source code of the modified *Gener_ln* program and the source code of the *HFAB* function, respectively. In the first time, we can see that three lines are added in the LF program to compute a_α :

$$a_\alpha = 4 * s_\alpha - ls * l_\alpha - l_\alpha * ls \tag{E.1}$$

which is the part of the hyperfine operator and in a second time, the $hfab$ function is called to apply the Slater rules to a_α in order to transform it from the basis of spin-orbitals to the basis of Slater determinants.

E.2 LF program

To calculate the g- and A-tensors, the LF program proposed in section 4.2.1 has been modified. The structure is pratically the same but we are obiged to introduce three constant: ζ, κ and P which are respectively the spin-orbit constant, the Fermi contact term and the hyperfine parameters. The determination of these paramameters is discussed in Chapter 6. Then in the source code, the parts which are added in the calculation are the determination of equivalent operator matrix elements of l_i and s_i for $i \in \{x, y, z\}$ and the calculation of the Zeeman and the HFS matrices determined according to the Equation 6.2 & Equation 6.7 respectively. Then the g- and A-tensors are determined respectively to Equation 6.3 & Equation 6.14. We can underline that the spin-orbit constant is determined by an atomic relativistic ZORA DFT calculation and is reduced by the orbital reduction factor, k, which should be equal to one if we don't want to take into account the reduction twice (since we already reduce the spin-orbit constant, ζ).

$$(k * l_\alpha - kappa * s_\alpha + \frac{1}{7} * a_\alpha) \tag{E.2}$$

The source code of this modified LF program is proposed in Figure E.3.

```
global lx ly lz sx sy sz ls ax ay az
t0=cputime;
%type de couche s, p, d(2) , f(3)
lq=[2];
ne=3;
% generate single determinants or microstates for lq^ne
ir=genersd(ne,1,2*sum(lq+lq+1));
% get ⟨ab|cd⟩ [vabcd,iabcd]=get2ei4a(lq);
% get l, s and l*s 1-e matrices: l=2 & s=1/2
[lx,ly,lz,sx,sy,sz,ls]=getls(lq,1/2);
% a_k (Griffith eq. 12.22)
ax=4*sx-ls*lx-lx*ls;
ay=4*sy-ls*ly-ly*ls;
az=4*sz-ls*lz-lz*ls;
nsd=length(ir);
ij=0;
for i=1:nsd
  for j=1:i
    ij=ij+1;
    lfdata(ij,:)=lfab(ir(i,:),ir(j,:));
    lsdata(ij,:)=zab(ir(i,:),ir(j,:));
    hfdata(ij,:)=hfab(ir(i,:),ir(j,:));
    gdata(ij,:)=gab(ne,ir(i,:),ir(j,:));
  end
end
gdata_racah(:,1)= gdata(:,1);
gdata_racah(:,2)= (49.0/5.0)*gdata(:,2);
gdata_racah(:,3)= (7.0/5.0) *(gdata(:,1)+gdata(:,2)+gdata(:,3));
Elapsed_time=cputime-t0
save data_d3 ir lfdata lsdata hfdata gdata gdata_racah
```

Figure E.1: *Source code of the* **Gener_ln** *program modified to enable us to calculate the g- and the A-tensors.*

```
function a=hfab(la,lb)
global ax ay az
% Get ⟨A|hf(1)|jB⟩ a part of hyperfine interaction (cf. Griffith eq.
12.22)
ne=max(size(la));
ie=0;
id=0;
sgn=1;
for k=1:ne
  ld=find(la(k)==lb);
  if isempty(ld)
    id=id+1;
    kd(id)=la(k);
    if rem(k,2)==1,
      sgn=-sgn;
    end
  else
    ie=ie+1;
    ke(ie)=la(k);
  end
end
if id == 0
  a=zeros(1,3)+i*zeros(1,3);
  for k=1:ne
    a=a+[ax(ke(k),ke(k)) ay(ke(k),ke(k)) az(ke(k),ke(k))];
  end
elseif id==1
  iv=0;
  for k=1:ne
    ld=find(lb(k)==la);
    if isempty(ld)
      iv=iv+1;
      kdp(iv)=lb(k);
      if rem(k,2)==1,
        sgn=-sgn;
      end
    end
  end
  a=sgn*[ax(kd(1),kdp(1)) ay(kd(1),kdp(1)) az(kd(1),kdp(1))];
else
  a=zeros(1,3)+i*zeros(1,3);
 end
```

Figure E.2: *Source code of the* **hfab** *function.*

```
load data
r=[0; B; C]; r=r./1000;
lfpar=[ h(1,1) ; h(2,1) ; h(2,2) ; h(3,1) ; h(3,2) ; h(3,3) ;
 h(4,1) ; h(4,2) ; h(4,3) ; h(4,4) ; h(5,1) ; h(5,2) ; h(5,3) ; h(5,4) ; h(5,5)];
lfpar=lfpar./1000;
zeta=...;   P=...;   kappa=... ;
ge=2.0023;   [nsd ne]=size(ir);   ij=0;
for i=1:nsd
  for j=1:i
    ij=ij+1;
    h(i,j)=gdata(ij,:)*r+lfdata(ij,:)*lfpar+lsdata(ij,7)*zeta; h(j,i)=conj(h(i,j));
    % Get orbital and spin angular momentum matrices
    lx(i,j)=lsdata(ij,1); sx(i,j)=lsdata(ij,4);  lx(j,i)=conj(lx(i,j));
sx(j,i)=conj(sx(i,j));
    ly(i,j)=lsdata(ij,2); sy(i,j)=lsdata(ij,5);  ly(j,i)=conj(ly(i,j));
sy(j,i)=conj(sy(i,j));
    lz(i,j)=lsdata(ij,3); sz(i,j)=lsdata(ij,6);  lz(j,i)=conj(lz(i,j));
sz(j,i)=conj(sz(i,j));
    kx(k,kp)=hfdata(kkp,1);kx(kp,k)=conj(kx(k,kp));
    ky(k,kp)=hfdata(kkp,2);ky(kp,k)=conj(ky(k,kp));
    kz(k,kp)=hfdata(kkp,3);kz(kp,k)=conj(kz(k,kp));
  end
end
[c,e]=eig(h); [e,ie]=sort(real(diag(e))); e(:)=e(:)-e(1); c=c(:,ie);
i0=1; i1=0;
for i=2:nsd
  if abs(e(i)-e(i-1))>0.001
    i1=i1+1; w(i1)=e(i-1); mul(i1)=i-i0; i0=i;
  end
end
fprintf('------------------------------ \n')
fprintf('(2S+1)*M(gamma) E \n')
fprintf('------------------------------ \n')
for i=1:i1, fprintf(' %3i %12.3f\n',mul(i),w(i)), end
fprintf('------------------------------ \n')
% Get Zeeman matrices
zx=c(:,1:2)'*(orf*lx+ge*sx)*c(:,1:2);zy=c(:,1:2)'*(orf*ly+ge*sy)*c(:,1:2);
zz=c(:,1:2)'*(orf*lz+ge*sz)*c(:,1:2);
% Get HFS matrices
ax=c(:,1:2)'*p*(orf*lx-kappa*sx+0.14285714285714*kx)*c(:,1:2);
ay=c(:,1:2)'*p*(orf*ly-kappa*sy+0.14285714285714*ky)*c(:,1:2);
az=c(:,1:2)'*p*(orf*lz-kappa*sz+0.14285714285714*kz)*c(:,1:2);
% Get g-tensor
g(1,3)=real(zx(1,1))-real(zx(2,2));g(2,3)=real(zy(1,1))-real(zy(2,2));
g(3,3)=real(zz(1,1))-real(zz(2,2));g(1,1)=real(zx(1,2))+real(zx(2,1));
g(2,1)=real(zy(1,2))+real(zy(2,1));g(3,1)=real(zz(1,2))+real(zz(2,1));
g(1,2)=imag(zx(1,2))-imag(zx(2,1));g(2,2)=imag(zy(1,2))-imag(zy(2,1));
g(3,2)=imag(zz(1,2))-imag(zz(2,1));
gg=g*g'; gtensor=sqrt(eig(gg))
% Get A-tensor
a(1,3)=real(ax(1,1))-real(ax(2,2));a(2,3)=real(ay(1,1))-real(ay(2,2));
a(3,3)=real(az(1,1))-real(az(2,2));a(1,1)=real(ax(1,2))+real(ax(2,1));
a(2,1)=real(ay(1,2))+real(ay(2,1));a(3,1)=real(az(1,2))+real(az(2,1));
a(1,2)=imag(ax(1,2))-imag(ax(2,1));a(2,2)=imag(ay(1,2))-imag(ay(2,1));
a(3,2)=imag(az(1,2))-imag(az(2,1));
A=a*a'; Atensor=sqrt(eig(A))
```

Figure E.3: *Source code of the* **LF** *program modified to enable us to calculate the g and the A-tensors.*

Curriculum Vitae

2001-04	Ph.D. in computational chemistry *University of Fribourg*
2000[a]	
1999	DEA Chemistry of atmospheric pollution and physics of environment (eq. Master) *University Paris 7 & University of Grenoble*
1998	Maîtrise (four year university degree) of chemistry *University of Toulouse*
1997	Licence (three year university degree) of chemistry *University of Toulouse*
1996	DEUG (two year university degree) in Life Sciences *University of Toulouse*
1994	Bac C (equivalent A-level) in mathematics and physics *Toulouse*

[a]Military service done from February to November 2000

List of publications

2002

1. *A Novel Density Functional Study of the Ground State Properties of a localized trinuclear Copper (II,II,III) Mixed-Valence System.*
Daul C., Fernandez-Ceballos S., Ciofini I., Rauzy C. and Schläpfer C. W.
Chem. Eur. J., **2002**, 8, 4392-4401.

2003

2. *New insights into the effects of covalency on the ligand field parameters : a DFT study.*
Atanasov M., Daul C. and Rauzy C.
Chem. Phys. Lett., **2003**, 367, 737-746.

3. *General chemistry for students enrolled in a life sciences curriculum.*
Bunzli J.-C. G., Fernandes E., Imbert D., Chauvin A.-S., Emmenegger F., Rauzy C., Piguet C., Ouali N., Koeller S., Suss-Fink G. and Cherioux F.
Chimia, **2003**, 57(3), 99-104.

2004

4. *A DFT Based Ligand Field Theory*
Atanasov M., Daul C.A. and Rauzy C.
Structure and Bonding, **2004**, 106, 97-125.

5. *Polytopal Rearrangement of [Ni(acac)$_2$(py)]: A New Square Pyramid $\rightleftharpoons$ Trigonal Bipyramid Twist Mechanism*
Daul C.A., Niketic S., Rauzy C. and Schläpfer C.W.
Chem. Eur. J., **2004**, 10, 721-727.

6. *Calculation of spin-orbit coupling within the LFDFT: applications to $[NiX_4]^{2-}$ ($X = F^-, Cl^-, Br^-, I^-$)*
Atanasov M., Rauzy C., Baettig P., Daul C.A.
Int. J. Quant. Chem., **2005**, 102, 119-131.

7. *A DFT study of mixed valent Mn(II/III) hexacyanide clusters*

Daul C.A., Rauzy C., Decurtins S., Franz P.
Int. J. Quant. Chem., **2004**, 101, 753-760.

8. *Influence of the ice growth rate on the incorporation of gaseous HCl*
Dominé F. and Rauzy C.
Atm. Chem. Phys., **2004**, 4, 2513-2519.

9. *The calculation of ESR parameters by density functional theory: the g- and A-tensors of Co(acacen)*
Atanasov M., Baerends E.J., Baettig P., Bruyndonckx R., Daul C., Rauzy C. and Zbiri M.
Chem. Phys. Lett., **2004**, 399(4-6), 433-439.

10. *DFT Study of Equilibrium Mo-Isotope Fractionations From Vibrational Spectroscopy*
Rauzy C., Wille M., Daul C. and Naegler T.
Chem. Phys. Lett., *to be submitted.*